TECHNISCHE UNIVERSITÄT MÜNCHEN

Fakultät für Medizin

Lehrstuhl für Biomolekulare Sensoren

AXONAL TRANSPORT IN ANIMAL MODELS OF AMYOTROPHIC LATERAL SCLEROSIS

Petar Marinković

Vollständiger Abdruck der von der Fakultät für Medizin der Technischen Universität München zur Erlangung des akademischen Grades eines

Doctor of Philosophy (Ph.D.)

genehmigten Dissertation.

Vorsitzende/r: apl. Prof. Dr. Helmuth Adelsberger

Prüfer der Dissertation:

1. Univ.-Prof. Dr. Thomas Misgeld

2. Univ.-Prof. Dr. Martin Kerschensteiner,

   Ludwig-Maximilians-Universität München

Die Dissertation wurde am 19.03. 2012 bei der Fakultät für Medizin der Technischen Universität München eingereicht und durch die Fakultät für Medizin am 23.03.2012 angenommen.

ACKNOWLEDMENTS

I would like to begin by thanking my PhD supervisor, Prof.Dr. Thomas Misgeld, who gave me the opportunity to work on the fascinating and exciting research project. Here, I would like to express my gratitude to Thomas for all the support, guidance and encouragement during the work on my PhD thesis. I learned a lot from you. Thanks.

Next, I would like to thank my co-supervisor Prof. Dr. Martin Kerschensteiner for all the insightful comments and valuable discussions. I also want to thank Prof. Dr. Hemuth Adelsberger for his help as a member of thesis commitee.

Working on my PhD thesis in the Misgled lab was an interesting and exciting journey. As it nears the end, it is a wonderful feeling to realize how many friends I made along. Now it is the moment to say thanks for all the support, help and great fun that we had over the years. Thanks Miriam, Sascha, Leanne, Yvonne, Cathy, Monika, Gabriela, Peter, Tatjana, Phil, Michael! Thanks to all members of the Kerschensteiner and Bareyre labs, especially to Ivana and Claudia who were there from the start. Thanks to all medical students in the lab. Many thanks to all members of Konnerth and Sakmann lab. Further, I would like to thank our technicians for fantastic work and great help: Manuela, Petra, Rosi, Anna, Christine, Ljiljana, Kristina, Sarah, Andy, Vlad, Werner and Stefan. Special thanks to Felix and Dietmar. I enjoyed working with you all!

My family was always there for me. My gratitude to my parents, Dragoslav and Lidija who continuously encouraged me to pursue my dreams. Thanks to my sister Mila, whose positive energy was always inspiring. Thanks to my little niece Lana for all the joy that she brought to my life.

Thanks to all my wonderful friends in Serbia, Germany and all around the world. Moji su drugovi biseri rasuti po celom svetu!

At the end, I would like to express my deep gratitude and love to my wife, Ljiljana. Through her love, patience, support and unwavering belief in me, I was able to finish this journey. Volim te zauvek!

ABSTRACT

Neurons use axonal transport to shuttle organelles and vesicles essential for their function and survival between soma and synapses. It thus appears logical that intact axonal transport is an important requirement for neuronal survival. Indeed, deficits in axonal transport have been shown in many neurodegenerative diseases including Alzheimer's disease, Huntington's disease and amyotrophic lateral sclerosis (ALS). The work in this PhD thesis was focused on the motor neuron disease ALS, because – in my view – the question if and how transport impairments are involved in ALS pathogenesis is still not settled. By imaging changes in axonal morphology and organelle transport over time in several animal models of ALS, I found that deficits in axonal transport of organelles (mitochondria and endosomes) and axon degeneration can evolve independently. This conclusion rests on the following results: (I) Axons can survive despite long-lasting transport deficits: In the SOD^{G93A} model of ALS, transport deficits are detected soon after birth, months before the onset of axon degeneration. (II) Transport deficits are not necessary for axon degeneration: In the SOD^{G85R} model of ALS, motor axons degenerate, but transport is unaffected. (III) Axon transport deficits are not sufficient to cause degeneration: In mice that over-express wild-type superoxide dismutase-1 (SOD^{WT}), axons show chronic transport deficits, but survive. Taken together these findings indicate that transport deficits are neither necessary nor sufficient to cause axon degeneration in these classical ALS models.

ABSTRACT

In Nervenzellen werden die für die Funktion der Zelle benötigten Organellen im Soma synthetisiert und anschließend mittels axonalem Transports bis in die Synapsen befördert. Es erscheint daher selbstverständlich, dass ein intakter axonaler Transport Grundvoraussetzung für das Überleben eines Neurons ist - in der Tat zeigt sich in zahlreiches neurodegenerativen Erkrankungen, wie bei Alzheimer, amyotropher Lateralsklerose oder Chorea Huntington ein Defizit im Organellentransport. Die Frage, wie genau eine Beeinträchtigung des axonalen Transportes in die Entstehung einer neurodegenerativen Erkrankung involviert ist, ist jedoch noch nicht vollständig geklärt. Mit Hilfe von bildgebenden Verfahren wurden in dieser Doktorarbeit der Transport von zellulären Organellen und Veränderungen der Axonmorphologie in mehreren Mausmodellen der amyotrophen Lateralsklerose, einer verheerenden Erkrankung des motorischen Nervensystems, untersucht. Dabei stellte sich jedoch heraus, dass Defizite im axonalem Transport verschiedener Organelle (Mitochondrien und Endosomen) und eine Degeneration der Axone unabhängig voneinander auftreten können. Diese Schlussfolgerung beruht auf folgenden Resultaten: (I) Axone können trotz langfristiger Transportdefizite überleben: Im SOD^{G93A}-Mausmodell der ALS können Störungen im axonalen Transport bereits kurz nach der Geburt nachgewiesen werden, viele Monate vor Beginn der Axondegeneration. (II) Transportdefizite sind nicht unbedingt notwendig für die Degeneration von Axonen: Im SOD^{G85R}-Modell der ALS degenerieren Motorneurone, obwohl ihr axonaler Transport unbeeinflusst ist. (III) Defizite in axonalem Transport sind nicht ausreichend um eine Degeneration auszulösen: In Mäusen, die die Wildtypform der Superoxid-Dismutase (SOD^{WT}) überexprimieren, zeigen die Axone chronische Transportdefizite, überleben jedoch. Diese Daten legen daher nahe, dass Beeinträchtigungen im Transport von Organellen kein notwendiger oder hinreichender Schritt dabei sind, eine Erkrankung der Motorneurone auszulösen.

1. Introduction 1

1.1. Axonal transport 2
1.1.1. Microtubules 3
1.1.2. Kinesins 4
1.1.3. Dynein 5
1.1.4. Axonal transport of mitochondria 6
1.1.4.1. Studying mitochondrial transport 6
1.1.4.2. Motor, adaptor and docking proteins 8
1.1.4.3. Regulation of mitochondrial transport 11
1.2. Amyotrophic lateral sclerosis 14
1.2.1. Signs and symptoms 14
1.2.2. Diagnosis of ALS; electrophysiological and histopathological changes in ALS 15
1.2.3. Treatment 17
1.2.4. Sporadic ALS 17
1.2.5. Familial ALS 18
1.2.6. SOD-mediated toxicity in ALS 22
1.1.6.1. Role of nonneuronal cells and excitotoxicity 23
1.1.6.2. Oxidative stress and copper toxicity 25
1.1.6.3. Protein aggregation 26
1.1.6.4. Mitochondrial dysfunction 26
1.1.6.5. Defects in axonal transport 29
1.2.7. SOD-based animal models of ALS 32

2. Materials and Methods 34

2.1. Animals 34
2.2. Mouse genotyping 35
2.3. qPCR quantification of SOD gene copy number 38
2.4. Generation of *Thy1-mitoKaede* mice 41
2.5. Behavioral testing 41
2.6. Staging of SOD^{G85R} mice 41
2.7. Explants preparation and transcardial perfusion of mice 42
2.8. Tissue preparation, immunohistochemistry and confocal microscopy 45
2.9. Imaging mitochondrial transport 47
2.10. Imaging transport of CTB-labeled vesicles 48
2.11. Axotomy 49
2.12. Image processing and analysis 49
2.13. Statistics 54
2.14. Buffers and solutions 55

3. Results 58

3.1. SOD copy number and expression levels in transgenic mouse lines 58

3.2. Axonal transport in *SOD*^{G93A} mice 60

3.2.1. Disease course clinical symptoms and denervation in *SOD*^{G93A} mice 60

3.2.2. Reduced mitochondrial density in axons and synapses of *SOD*^{G93A} mice 61

3.2.3. Reduced mitochondrial transport in motor axons of *SOD*^{G93A} mice 62

3.2.4. Mitochondrial transport is unaffected in saphenous nerve of *SOD*^{G93A} mice 64

3.2.5. Tibialis nerve composition 65

3.2.6. Single mitochondrion tracking using new mouse transgenic line *Thy1-MitoKaede* reveals changes in transport characteristics in *SOD*^{G93A} mice 67

3.2.7. Transport of synaptic vesicles precursors in *SOD*^{G93A} mice 70

3.2.8. Transport deficits precede disease onset in *SOD*^{G93A} mice 72

3.2.9. Mitochondrial density in intercostal axons over disease course in *SOD*^{G93A} mice 73

3.2.10. Anterograde transport deficits precede deficit in retrograde transport in individual axons in *SOD*^{G93A} mice 74

3.2.11. Axonal transport deficits affect all axons irrespective of their diameter 76
3.2.12. Early changes in mitochondrial morphology in *SOD^{G93A}* mice 77
3.2.13. Shape factor and volume of moving mitochondria in *SOD^{G93A}* mice 79
3.2.14. Motor neurons can support complex arbors despite transport deficits in *SOD^{G93A}* mice 80
3.2.15. Capacity to increase axonal transport is not exhausted in *SOD^{G93A}* mice 83
3.2.16. Sham operated animals do not show an increase in transport 87
3.2.17. Increase in transport after axotomy in SOD^{G93A} mice is accompanied by changes in transport characteristics of individual mitochondria 88
3.3. Axonal transport in *SOD^{G85A}* mice 89
3.3.1. Disease course, clinical symptoms and denervation in *SOD^{G85R}* mice 89
3.3.2. Axonal degeneration but no transport deficits are observed in *SOD^{G85R}* mice 90
3.3.3. Mitochondrial speed in *SOD^{G93A}, SOD^{G85R}* and *SOD^{WT}* mice 92
3.3.4. Time course of mitochondrial transport in *SOD^{G85R}* mice 92
3.3.5. Mitochondrial transport in *G85R SOD-YFP* mice 95

3.4. Axonal transport in *SOD*^{WT} mice 96
3.4.1. Disease course, clinical symptoms and denervation in *SOD*^{WT} mice 96
3.4.2. Axonal transport deficits are observed in *SOD*^{WT} mice 97

4. Discussion 100

4.1. Axonal transport deficits in *SOD*^{G93A} mice 102
4.2. Capacity of motor axons to increase transport in *SOD*^{G93A} mice is not exhausted 107
4.3. Changes of mitochondrial morphology in *SOD*^{G93A} mice 109
4.4. Axonal transport in *SOD*^{G85R} mice 110
4.5. Axonal transport in *SOD*^{WT} mice 112
4.6. General discussion 113

5. Publications 116

6. References 117

1. INTRODUCTION

Neurons use axonal transport to shuttle organelles and vesicles essential for their function and survival between soma and synapses (Hirokawa et al., 2010; Hollenbeck and Saxton, 2005). It thus appears logical that intact axonal transport is an important requirement for neuronal survival. Indeed, deficits in axonal transport have been shown in many neurodegenerative diseases including Alzheimer's disease, Huntington's disease and **a**myotrophic **l**ateral **s**clerosis (ALS) (Stokin et al., 2005; Bilsland et al., 2010; De Vos et al., 2007; Szebenyi et al., 2003). However, the exact relationship between axonal transport disturbances and motor axon degeneration remains unclear.

The aim of this PhD thesis was to investigate the role of axonal transport in the pathogenesis of the motor neuron disease, ALS. Therefore, in first part of this introduction, I will give an overview of the mechanisms that allow for axonal transport with special attention to mitochondrial transport – the latter being the transport cargo which my study is most concerned with. The second part of the introduction describes the clinical manifestations, pathology, genetics and treatment options for ALS and our current understanding of the pathogenic mechanisms that underlie this disease. Here it will become clear that axonal transport disturbances have been a favored mechanism in many attempts to explain the specific pathological characteristics of motor neuron diseases, including ALS.

1.1. Axonal transport

The unique morphology of neurons makes them very dependent on proper intracellular transport (Grafstein and Forman, 1980). Lipid, protein and RNA synthesis occurs almost exclusively in the cell body. Therefore these molecules need be actively transported to dendrites and axons. Similarly, the normal physiology of neurons depends critically on transport and intracellular distribution of various cell organelles, including mitochondria and peroxisomes. Lastly, signaling molecules taken up by synapses (such as neurotrophins and their receptors) are transported back to cell body allowing the cell to respond to changes in its environment. Transport in axons is classically divided into two categories; fast axonal transport of vesicles and organelles at rates of ~ 1μm/s and slow transport of cytoskeleton components, RNA and protein complexes at rate of ~ 1mm/day. It seems that the two categories of axonal transport share the same transport machinery (Wang et al., 2000; Terada et al., 2010), which I describe in detail in the following parts of this introduction.

Efficient transport is achieved in neurons by molecular motors that operate along the cytoskeleton. Three large super-families of molecular motors have been indentified – kinesins, dyneins and myosins (Hirokawa et al., 2010). Kinesins are using microtubules as rails to transport various cargoes and with few exceptions these motors are moving towards the plus end of microtubules. Dyneins are involved in transport towards the minus end of microtubules, while myosins in neurons use actin filament for short-range transport. As kinesin/dynein-mediated organelle transport along microtubules is most relevant to my study, I will give a detailed description of the structure, function and regulation of the molecules involved in this form of transport.

1.1.1. Microtubules

Microtubules are cytoskeletal filaments found in all eukaryotic cells which are involved in mitosis, cytokinesis, intracellular transport and maintenance of cell morphology. Microtubules are polarized polymers of α- and β-tubulin dimmers. The dimers form protofilaments thirteen of which are assembled into hollow cylinders to make one single microtubule of ~ 24 nanometers in diameter. In cells microtubules polymerize from templates made of gamma tubulin ring complexes, which as a result cap the minus end of microtubules. Thus further polymerization is only possible at the plus end. In neurons, microtubules are composed of tubulins of various isotypes with numerous different post-translational modifications, which can modulate polymerization rate and hence stability of microtubules (Conde and Caceres, 2009). In addition, microtubules interact with a large group of proteins called **m**icrotubule **a**ssociated **p**roteins (MAPs). Several types of MAPs are found in neurons, including structural MAPs (Halpain and Dehmelt, 2006), microtubule motors (Hirokawa et al., 2010) and plus-**t**ip **i**nteracting **p**roteins (+TIPs) (Galjart, 2010). +TIPs fused with fluorescent proteins are a tool for studying microtubule dynamics (Stepanova et al., 2003). It has been shown (Dixit et al., 2008) that MAP-microtubule interactions can impact the engagement of molecular motors to microtubules and hence organelle transport. Such a "road block" mechanism has, for instance, been suggested to explain the transport alterations induced by the dementia-associated MAP, tau.

In axons, microtubules are uniformly oriented with their plus end pointing away from the soma, while in dendrites microtubules show mixed orientation. Using microtubule depolymerising agents like nocodazole, two different populations of axonal microtubules were indentified: stable microtubules resistant to nocodazole with a half life of several hours and dynamic microtubules, which have turn-over rate of several minutes. How dynamic microtubules are recruited to the stable pool is still not entirely clear but it seems that post-translational modifications of tubulin like detyrosination and acetylation play an important role (Fukushima et al., 2009). Moreover, post-translational modifications can affect axonal transport. In that respect, a role of class 2 **h**istone **d**e**ac**etylaze **6** (HDAC6) is important (Hubbert et al., 2002). HDAC6 deacetylazes α-tubulin, inhibiting in that way binding of molecular motors to microtubules. Subsequent retardation of axonal transport

was shown to be a critical step in pathogenesis of sensory-motor neuropathies (d'Ydewalle et al., 2011). Blocking HDAC6 could therefore serve as a starting point for developing disease-modulating therapies that recuperate axonal transport.

1.1.2. Kinesins

Kinesin superfamily proteins (KIFs) are grouped into three main classes depending on the position of the motor domain in the molecule: N-terminal motor domains KIFs (N-KIFs), middle motor domain KIFs (M-KIFs) and C-terminal motor domains KIFs (C-KIFs). The motor domain is responsible for microtubule binding and ATP hydrolysis. Additionally, KIFs have so called “stalk” and “tail” domains. The majority of KIFs motors recognizes and binds cargoes with their “tail” domains. N-KIFs are the largest group within the kinesin superfamily and they generally move toward microtubule plus end while much rarer C-KIFs move toward minus end. By now more then 45 kinesin genes have been identified in mammals (Hirokawa et al., 2009). The first member of this gene family to be implicated in transport was Kinesin 1 (KIF5) indentified independently by two research groups (Vale et al., 1985; Brady, 1985) Most KIFs are structurally similar to KIF5. The KIF5 motor complex is a heteromer composed of two heavy (KIF1A, KIF1B, or KIF1C) and two light (KLC1 or KLC2) chains and it is binding directly to microtubules as revealed by electron microscopy (Hirokawa et al., 1989). KIF1B is expressed ubiquitously, while expression of KIF1A and KIF1C is neuron-specific.

KIFs evolved into a large group of structurally similar proteins which enabled them to recognize and bind various cargoes. Of interest for this study are KIFs that transport organelles and vesicles, but it was shown that the same KIFs are involved in slow axonal transport of proteins as well (Terada et al., 2010). KIFs transport cargos anterogradely such as synaptic vesicle precursors (KIF1A and KIF1Bβ), presynaptic membrane or active zone vesicles (KIF5), mitochondria (KIF1Bα/KIF5), amyloid precursor protein (APP)-containing vesicles (KIF5), APOER2 vesicles (KIF5), TrkB vesicles (KIF5), plasma membrane precursors (KIF3), and phosphatidylinositol 3,4,5-triphosphate (PIP3) vesicles (KIF13B) (Hirokawa et al., 2010). It seems that, at least for mitochondria, KIF5s bind

cargoes through direct interaction with adaptor proteins and independent of kinesins light chains (Glater et al., 2006; Cai et al., 2005).

It is of interest for this thesis to mention that mutations in KIF genes can cause neurodegenerative phenotypes. Mutations in KIF5 can cause heredity spastic paraplegia (Reid et al., 2002) and KIF1A is mutated in hereditary sensory and autonomic neuropathy type 2 (Riviere et al., 2011).

1.1.3. Dynein

The members of the dynein superfamily proteins comprise two major groups of proteins: cytoplasmic and cilliary dyneins. Cytoplasmatic dynein is a huge protein complex (1.5 megadaltons) which is driving transport towards the microtubule minus end. It consists two heavy chains, which have ATPase activity and generate moving force, two intermediate chains, four light intermediate chains and several light chains. Additionally, dynein interacts with the dynactin complex composed of seven to nine subunits including p150^{Glued}, dynamitin, **a**ctin **r**elated **p**rotein **1** (Arp1) and others. The dynactin complex seems to be very important for normal functioning of dynein. It increases processivity (i.e. the time that dynein is moving along the microtubules) of dynein and binds vesicular cargoes (Karki and Holzbaur, 1995; King and Schroer, 2000). In contrast to KIFs, which during evolution diverged into a big superfamily of proteins each of which directly recognizes and binds a specific set of cargoes, only a single cytoplasmatic dynein heavy chain (Dync1h1) is responsible for transport of different cargoes in axons and dendrites. Specific cargo recognition and binding is achieved by evolution of different isoforms of other subunits and recruitment of associated proteins such as dynactin. Cytoplasmic dynein transports signaling endosomes which contain **b**rain-**d**erived **n**eurotrophic **f**actor (BDNF) or **n**erve **g**rowth **f**actor (NGF) bound to their receptors TrkA and TrkB, respectively. The piccolo/bassoon complex, mitochondria and myosin V are also retrogradely transported in the axons by dynein (Hirokawa et al., 2010).

Similarly to mutations in KIFs, mutations in dynein and p150^{Glued} subunit of dynactin as well as disruption of the dynein/dynactin complex, can cause neurodegeneration, again

highlighting the importance of axonal transport for normal functioning of neurons (Puls et al., 2003; LaMonte et al., 2002; Hafezparast et al., 2003).

1.1.4. Axonal transport of mitochondria

Mitochondria are essential cellular organelles. Their main function is energy production in form of ATP through oxidative phosphorylation. Therefore, proper distribution and function of mitochondria is of great importance for neurons because of this cell's high metabolic demand. Moreover, mitochondria are buffering cellular calcium, which is essential for signaling in neurons. Finally, mitochondria have an important role in apoptosis, which occurs in developmental and degenerative processes in the nervous system.

It is believed that the majority of mitochondria is produced in the cell body (Davis and Clayton, 1996). Thus, distal compartments of neurons, such as synapses, are dependent on active transport of mitochondria. Mitochondria are also transported back to be degraded or possibly fused with mitochondria in the cell body (Cai et al., 2012; Detmer and Chan, 2007). Finally, axonal transport of mitochondria is not just delivering or retrieving mitochondria but it also serving to position and reposition them along the axon (Hollenbeck and Saxton, 2005). Accordingly, axonal transport of mitochondria is being intensively studied, and a number of different approaches have been devised to do so.

1.1.4.1. Studying mitochondrial transport

Mitochondrial dynamics in axons are classically studied in cultured neurons prepared from embryonic or early postnatal mice. To visualize mitochondria, cells can be loaded with mitochondrial dyes (MitoTracker) or transfected to express fluorescent proteins targeted to mitochondria. Culture systems provide a valuable tool to study cellular and molecular mechanism of transport. However, this approach is limited to developing neurons which have a different morphology in culture than *in vivo*. Furthermore, culture

systems cells do not provide a natural environment for cells and are not suitable for investigating transport over longer periods of time, i.e. over an entire disease course of a slowly progressing condition. Finally, supporting cells (such as myelin forming glia cells) can impact transport (Ohno et al., 2011) and are lacking in simple cell culture systems (but see Di Giorgio et al., 2007). To overcome these limitations, transgenic mice with fluorescently labeled mitochondria selectively in neurons ("*MitoMice*") were developed in the Lichtman lab at Harward University

(Misgeld et al., 2007) and in a number of other groups (Vande Velde et al., 2011; Wang et al., 2011c). These mice provide an excellent tool to study mitochondrial dynamics in single, fully matured neurons in their natural environment.

By using time-lapse microscopy *in vivo* or in acute nerve muscle explants from *MitoMice*, complex and interesting mitochondrial behavior in axons can be observed. It was shown that the majority of axonal mitochondria is stationary and that only around 20% are moving at any given time-point (Misgeld et al., 2007). Moving mitochondria are transported as individual organelles, which as a population are shorter than their stationary counterpart. The motility of moving mitochondria is characterized by frequent stops and re-starts. Almost double the number of mitochondria is being transported away from the cell body (anterograde) than transported back to the cell body (retrograde). Mitochondria are transported slightly slower in the anterograde direction; 0.8 µm/s - 1.0 µm/s compared to 1.1 µm/s - 1.4 µm/s in the retrograde direction (peak velocity; Misgeld et al., 2007 and present study). Although often reported in cell culture, changes in direction of mitochondrial movement and fusion/fission events are rarely seen *in vivo* and in acute explant preparations (Misgeld et al., 2007; Liu et al., 2009). Interestingly, very similar behavior of mitochondria as found in mice was also observed in Drosophila neuromuscular preparations implying conserved transport mechanisms across species (Pilling et al., 2006).

1.1.4.2. Motor, adaptor and docking proteins

Mitochondria move in axons through the action of molecular motors that operate along cytoskeletal filaments (**Figure 1.1**). Generally, KIFs are driving anterograde movement while dynein is responsible for retrograde transport along microtubules. So far three members of the KIF family have been implied in anterograde transport of mitochondria. It is known that mutations in KIF5 cause impairments in transport and accumulation of mitochondria in the cell body (Tanaka et al., 1998). In addition to KIF5, KIF1Ba is a monomeric protein, which colocalizes with mitochondria *in vivo* and moves them along microtubules *in vitro* (Nangaku et al., 1994). Recently, KLP6, a newly identified kinesin was found to regulate the morphology and transport of mitochondria in neuronal cells (Tanaka et al., 2011). However, the exact role of KIF1Ba and KLP6 in anterograde transport is still unclear. In contrast to anterograde transport, where a number of motors were identified, strong evidence suggest that cytoplasmatic dynein is the sole motor for retrograde transport of mitochondria. Mutations in dynein specifically inhibit retrograde transport without any effects on anterograde transport (Pilling et al., 2006).

Similar to other organelles, mitochondria also use adaptors proteins to bind to motor proteins (**Figure 1.1**). By linking mitochondria to specific adaptor proteins which in turn can only bind to specific motors, the direction of mitochondrial transport can be regulated. Recently, substantial progress has been made in indentifying mitochondrial adaptor proteins and their mechanism of action, even though some details remain a matter of active debate in the field. I will give a short overview of our current knowledge of mitochondrial adaptor proteins. More detailed descriptions are available in excellent reviews by Macaskill and Kittler, 2010 and by Cai et al., 2011.

The first adaptor protein complex that was described linking mitochondria to KIFs was the Miro-Milton complex, which the Schwarz lab identified in *Drosophila* (Glater et al., 2006). Using genetic screens, in these papers the authors showed that Milton mutants have mitochondria restricted to the cell body, while in axons and synapses mitochondria were absent, suggesting a transport defect. It seems that Milton is directly recruiting kinesin heavy chain (KHC, the KIF5 *Drosophila* homologue) to mitochondria independent of the kinesin light chain. Since the initial identification of Milton in Drosophila, two

mammalian kinesin binding orthologues, TRAK1 and TRAK2 (also known as OIP106 and OIP98/Grif-1, respectively), have been identified. However, while Milton in *Drosophila* is binding exclusively to mitochondria, TRAK1 and TRAK 2 are involved in transport of endosomes and other cargoes (Grishin et al., 2006; Kirk et al., 2006).

In *Drosophila*, Milton is binding to **mi**tochondrial **R**h**o**-GTPase (Miro), a mitochondrial outer membrane protein. In flies, mutations in Miro induced abnormal distribution of mitochondria, confining them in neuronal cell bodies and preventing their transport into neurites (Guo et al., 2005). The mammalian Miro orthologs are Miro 1 and 2. Orthologs were also found in several eukaryotic organisms, including *Saccharomyces cerevisiae* and *Caenorhabditis elegans* (Fransson et al., 2003). Structural analysis showed that Miro proteins have two GTPase domains, two Ca^{2+} binding EF-hands and a transmembrane domain. These domains have role in Ca^{2+} induced stopping of mitochondria at synapses which will be described in more details later.

Syntabulin is another adaptor protein which is capable of linking mitochondria to KIF5 (**Figure 1.1**; Cai et al., 2005). Syntabulin has a C- terminal domain anchored to the mitochondrial outer membrane and an N-terminal domain which can directly bind KIF5. Reducing syntabulin expression or blocking its interaction with KIF5 leads to a decrease in anterograde transport of mitochondria in cultured hippocampal neurons while retrograde transport remains unaffected.

Several other proteins have also been suggested as adaptors for KIF5 binding to mitochondria including **f**asciculation and **e**longation factor **z**eta-**1** (FEZ1) and **RAN**-**b**inding **p**rotein **2** (RANBP2) (Fujita et al., 2007; Cho et al., 2007). Their exact role and mechanism of action still need to be elucidated (**Figure 1.1**).

While there is clear evidence that mitochondria bind to the KIFs via several adaptors, in case of dynein it is not entirely clear which, if any, adaptors are involved. The candidates include dynactin and dynein light chain, Tctex1, which interacts with mitochondrial **v**oltage-**d**ependent **a**nion-selective **c**hannel (VDAC) (Schwarzer et al., 2002) but the prevailing view is that dynein is bound through direct interaction with mitochondria (**Figure 1.1**. Sheng and Cai, 2012).

Finally, transported mitochondria are supposed to be immobilized in certain places along the axon. Recent study identified syntaphilin as a protein specific to docked axonal mitochondria that mediates an interaction with microtubules. Accordingly, the deletion of syntaphilin results in an increased number of motile mitochondria and a reduced mitochondrial density in axons (Kang et al., 2008). The interaction between syntaphilin and microtubules appears to be regulated by the dynein light chain, LC8 (Chen et al., 2009). Here it is worth noting that there are strong evidences that mitochondria dock along other elements of cytoskeleton besides microtubules. First morphological evidence came from the fascinating work of Hirokawa which showed by electron microscopy that axonal mitochondria are connected to neurofilaments (Hirokawa, 1982) . Work by Chada and Hollenbeck, 2004, further suggested that mitochondria can also dock along actin filaments. However, the mechanisms of these interactions and the involved docking proteins still have to be identified.

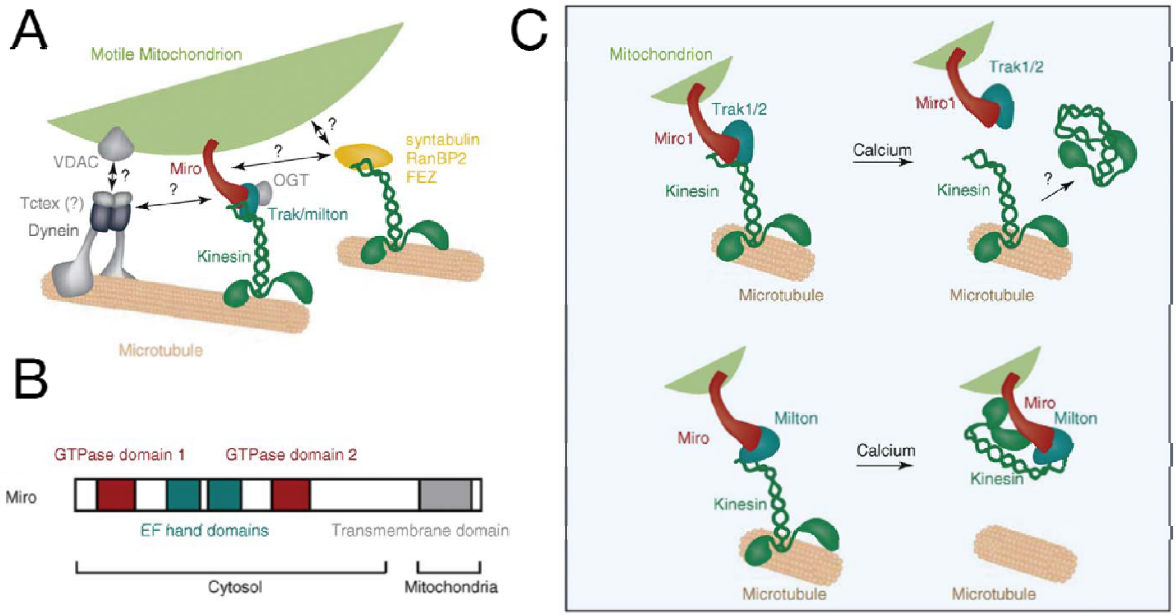

Figure 1.1 – Mitochondrial transport machinery (modified from Macaskill and Kittler, 2010)

A) Motor and adaptor proteins involved in mitochondrial transport. (**B**) Structure of the Miro protein. (**C**) Two models for Ca^{2+} induced mitochondrial arrest.

1.1.4.3. Regulation of mitochondrial transport

Mitochondrial mobility changes in regions such as synapses and nodes of Ranvier, where ATP consumption and demand for Ca^{2+} buffering are high. Mitochondrial transport can be regulated by numerous modifications of microtubules and their interaction with MAPs. In addition, a variety of motor, adaptor and docking proteins offers a number of levels at which mitochondrial mobility can be modulated. Taken all together, it is attractive to propose that this complex transport machinery evolved to allow neurons to regulate mitochondrial transport through separate mechanisms in response to different signals (Sheng and Cai, 2012). Here, I will address regulation of mitochondrial movement at synapses and nodes of Ranvier. Additionally, I will outline how some signaling pathways and MAPs might influence mitochondrial transport.

Local changes of ADP and Ca^{2+} can change mitochondrial motility and recruit mitochondria to metabolically active compartments such as synapses. An increase in ADP slows down the mitochondria, retaining them in the area where ATP production is needed (Mironov, 2007). How mitochondria sense changes in ADP/ATP concentration is unknown. In contrast, progress was made in understanding how mitochondrial movement is regulated by local Ca^{2+} levels (**Figure 1.1**). Three groups have independently shown that Ca^{2+} binding to the Miro promotes stopping of the mitochondria (Wang and Schwarz, 2009; Macaskill et al., 2009b; Macaskill et al., 2009a). However, two competing models have been proposed as to how this is accomplished mechanistically: In one model, proposed by Schwarz and Wang (2009), Ca^{2+} binding to Miro triggers uncoupling of kinesin from microtubules and subsequent binding of kinesin to Miro. In another model, Ca^{2+} binding detaches mitochondria and Miro from kinesin (Macaskill et al., 2009b).

Compared to synapses, less is known how mitochondrial mobility is regulated at nodes of Ranvier. During repetitive action potentials mitochondria are recruited to the nodes of Ranvier in PNS axons as shown by Zhang et al., (2010). These authors proposed a model, in which a local increase in Ca^{2+} and ATP depletion through action of the Na/K-ATPase are responsible for mitochondrial arrest (Zhang et al., 2010; Chiu, 2011). Similarly, in the CNS axons, increased electrical activity reduced mitochondrial transport and increased the stationary mitochondria pool in the nodal region (Ohno et al., 2011).

For a few signaling pathways it has already been shown that they can regulate mitochondrial transport. One of them is the NGF pathway. Mitochondria tend to accumulate close to a source of NGF, probably through increased transport and increased docking to actin filaments (Chada and Hollenbeck, 2004). The exact mechanism of this NGF effects is not clear, but the authors of the study suggested the glycogen-syntase kinase 3β (GsK3β) pathway as a possible regulator of mitochondrial transport. GsK3β can phosphorylate kinesin light chain and inhibit anterograde transport of membrane-bound organelles (Morfini et al., 2002). In later studies, it was shown that the GsK3β pathway can directly modulate transport of mitochondria (Chen et al., 2007; Chen et al., 2008). For example, serotonin (5-HT), acting through the 5-HT1A receptor subtype, promotes axonal transport of mitochondria in cultured hippocampal neurons by increasing Akt activity, and consequently decreasing GsK3β activity. Application of dopamine agonists had the opposing effect. Recently a link between GsK3β and HDAC6 emerged (Chen et al., 2010). This is of interest, since HDAC 6 activity plays a very important role in regulating mitochondrial transport and could promote pathogenesis in some neurodegenerative conditions (d'Ydewalle et al., 2011).

Another molecular regulator appears to be tau, a MAP. The main role of tau in axons is to stabilize microtubules. In addition, it can regulate axonal transport. Overexpression of tau blocks anterograde transport of organelles including mitochondria in cell culture (Stamer et al., 2002). The proposed mechanism was competition of tau with KIFs for binding sites on the microtubules (Trinczek et al., 1999). Interestingly, tau and HDAC 6 interact with each other establishing another cross-link between different pathways that regulate transport (Ding et al., 2008).

Finally, a critical role for the Parkin/PINK1 complex in regulating mitochondrial motility was demonstrated (Wang et al., 2011b). PINK1 phosphorylates Miro, which leads to proteasome-mediated degradation of Miro. Without Miro, the kinesin motor is detached from the mitochondrion which leads to mitochondrial arrest. This could be a regulatory mechanism, which would target damaged mitochondria. Once immobile they would undergo degradation. This new concept contrasts with previous views, where

incapacitated mitochondria would be retrogradely transported towards the soma for digestion, rather than locally degraded (Miller and Sheetz, 2004; Cai et al., 2012).

In summary, mitochondrial transport is driven by a very complex machinery and it can be changed and regulated in response to many physiological signals. Detailed knowledge of the underlying mechanisms would offer a possibility to manipulate mitochondrial transport. This could be a possible avenue for therapy in many neurodegenerative diseases, as for many diseases there is growing evidence that mitochondrial dysfunction and transport impairments are important pathological events. The work in this PhD thesis was focused on a devastating disease, ALS, because – in my view – the question, if and how mitochondrial dysfunction and transport impairments are involved in ALS pathogenesis is still not settled. ALS constitutes the one relatively common disorder, where the case for a "transport-o-pathy" has been made most forcefully. Moreover, motor neurons represent the neuron type, which due to size, bio-energetics and geometry, is believed to depend most critically on transport. Hence I believe pathology of this cell type can provide a "lackmus" test for the idea that transport disruptions might represent a final common pathway of "dying-back" type axonopathies.

1.2. Amyotrophic lateral sclerosis

Amyotrophic lateral sclerosis (ALS) is the most common adult motor neuron disease typically with an onset in middle-age. One to two out of 100.000 people develop ALS each year with men being affected slightly more often than women. In North America it is known as Lou Gehrig's disease after a famous baseball player, who was diagnosed with this in 1939. The main feature of the disease is progressive degeneration of motor neurons. This leads to denervation of muscle, which causes weakness, muscle atrophy, paralysis and ultimately death due to respiratory failure. First case reports of disorders resembling ALS were published during the first half of the 18th century. It was the French neurologist, Jean-Martin Charcot, who first linked the symptoms of the disease to the pathology in the lateral columns of the spinal cord that he observed during autopsies. In a paper from 1874, he described the symptoms and course of the disease and for the first time used the term, "amyotrophic lateral sclerosis" (Charcot J-M., 1874).

1.2.1. Signs and symptoms

Earliest signs of disease in ALS are muscle weakness and atrophy. Affected muscles show fasciculations, cramping and become rigid. Depending on which motor neurons degenerate first, muscles in different parts of the body can be affected. About 75% of patients experience so called "limb onset", i.e. muscle weakness in legs or arms, while around 25% have "bulbar onset", characterized by difficulties in speaking clearly and swallowing. As the disease progresses, muscle weakness and atrophy spread. Patients have problems with locomotion, swallowing and talking and with time are not able to stand, walk or eat on their own. Eventually they cannot breathe unassisted, as the respiratory muscles are denervated. ALS is usually fatal within five years of onset. ALS affects both corticospinal neurons (clinically called "upper" motor neurons) and spinal ("lower") motor neurons. Muscle spasticity and hyperreflexia, as well as an abnormal

Babinski's sign, suggest degeneration of "upper" motor neurons in the cortex, while muscle weakness and atrophy are the direct consequence of muscle denervation due to degeneration of spinal motor neurons. Also neurons outside the motor system can be affected in ALS. For example, in about half of the ALS patients some cognitive impairment can be observed, with 2-3% suffering from overt frontotemporal dementia (Ringholz et al., 2005).

1.2.2. Diagnosis of ALS; electrophysiological and histopathological changes in ALS

Definitive diagnosis of ALS is only possible post-mortem. The diagnosis in the patients is based on a combination of clinical signs, neurophysiological investigations and tests to rule out other diseases with similar symptoms. It is necessary to follow patients over longer periods of time and monitor progression by neurological examination. The El Escorial criteria (Brooks, 1994) revised in 1997 (Miller et al., 1999) use a combination of clinical symptoms to establish diagnostic certainty. However, these criteria are often criticized as stringent and restrictive, especially early in the disease process, when patients are likely to benefit from therapy.

The most commonly used neurophysiological examinations to diagnose ALS are nerve conduction velocity studies and electromyography (EMG). The nerve conduction velocity test is very useful in diagnosis because it could suggest that a patient suffers from some forms of peripheral neuropathy rather then ALS. For example, sensory nerve conduction is usually normal in ALS patients and therefore abnormalities in sensory conduction could point to a demyelinating neuropathy (Eisen and Swash, 2001). In the EMG, electrical activity of muscle is recorded which is often combined with muscle biopsies to confirm involvement of lower motor neurons. Muscles in ALS show complex traces in EMG with fibrillation potentials, positive sharp waves and late components (Hardiman et al., 2011). In other words, they show signs of ongoing denervation and reinnervation, which are processes typical for ALS. Fibrillation potentials and positive sharp waves are even detectable in muscles that look clinically normal, which is important for early diagnosis of

ALS. Having this in mind, it is clear why investigation of electrophysiological changes in ALS gained a lot of interest.

Motor neurons affected by ALS tend to fire spontaneously, causing muscle cramps and fasciculations. It is thought that the underlying mechanism of such ectopic motor neuron activity are changes in the electrophysiological properties. Changes in axonal ion channel function, such as reduction of slow and fast K^+ channel conductance, are described in familial and sporadic ALS patients (Vucic and Kiernan, 2006). The motor neurons from ALS animal models show increased **p**ersistent **i**nward **c**urrents (PICs). PICs are generated by voltage sensitive Na and Ca channels that inactivate slowly (Heckman et al., 2008). Motor neuron excitability and firing rate can be modulated by PICs and it is thought that increased PICs could lead to axon degeneration (Vucic and Kiernan, 2010).

While investigation of spinal motor neurons is relatively easy even in humans, degeneration of upper motor neurons is much more difficult to assess, especially in early phases of the disease. In search for signs of upper motor neurons involvement, techniques like diffusion tensor imaging, magnetization transfer imaging and functional magnetic resonance imaging are used (Wang et al., 2011a). Recently, researchers established a novel technique based on trans-cranial magnetic stimulation to record changes in cortical excitability, which would distinguish ALS from similar disorders (Vucic et al., 2011).

Denervation of muscle fibers is one of the hallmarks of ALS. Denervated muscle fibers get atrophic, which is clearly visible in muscle biopsies from ALS patients. The main neurohistopathological feature of sporadic and familial ALS is loss of both upper and lower motor neurons (Kato, 2008). Large motor neurons in ventral (anterior) horn are especially affected in ALS. In some cases of fALS including some caused by mutations in the **s**uper-**o**xide **d**ismutase 1 (SOD) gene, axons in dorsal (posterior) column are also affected. The surviving motor neurons show typical neurodegenerative changes: cytoplasmatic shrinkage, aggregation of lipofuscin granules and intracytoplamatic inclusions. Characteristic intracytoplasmatic inclusions for sporadic ALS are Bunina bodies, skein-like and round hyaline inclusions. Bunina bodies are also found in some cases of familial ALS. In familial SOD cases, presence of Lewy-body-like hyaline

inclusions, which show strong immunoreactivity for ubiquitin and SOD is common in motor neurons (Bruijn et al., 1998).

1.2.3. Treatment

Unfortunately, there is no treatment that can cure ALS. Only one drug, riluzole, is approved by the Food and Drug Administration in the United States for treatment of ALS. The use of riluzole is based on the "glutamate excitotoxicity" hypothesis of ALS (for details see “Nonneuronal cells and excitotoxicity” chapter, page 23). It is known that high levels of glutamate are toxic to neurons, and it is believed that glutamate excitotoxicity is one of the pathophysiological mechanisms contributing to motor neuron damage in ALS (Bogaert et al., 2010; Lau and Tymianski, 2010). Riluzole is blocking release of glutamate, but it might also be acting as an indirect antagonist of glutamate receptors or by inactivating neuronal voltage-gated Na^+ channels (Doble, 1996). However, the effects of riluzole in ALS are modest, prolonging life in patients for only a few months. All other treatments for ALS patients are palliative, i.e. designed to relive symptoms and improve quality of life.

1.2.4. Sporadic ALS

Most cases of ALS are sporadic (i.e. non-familial). It is not known what the cause of the disease in these patients is. Around 10% of ALS patients suffer from an inherited "familial" form of ALS (fALS). Sporadic and familial forms of ALS show very similar clinical pictures and affect the same motor neuron populations. Hence, it is hoped that studying fALS, which could be modeled in animals, might elucidate the pathophysiological mechanism underlying the sporadic form of the disease as well.

Several environmental factors were suggested to contribute to ALS susceptibility. Initial evidence came from the high incidence of ALS with dementia in the Chamorro people of Guam. In was found that Chamorro people were consuming seeds from cycad plants, which are rich in neurotoxins such as sterol glucosides and β-methylamino-L-alanine

(BMAA) (Khabazian et al., 2002). Neurotoxin exposure is also a plausible explanation for the high incidence of ALS in Gulf war veterans and in people, who occupationally come in contact with insecticides and pesticides (Horner et al., 2003; Qureshi et al., 2006). Interestingly excessive physical activity was also proposed as a risk factor, as high ALS incidence was observed among Italian professional football players (Chio et al., 2009).

Recently, it has been suggested that epigenetic factors are involved in causing several neurodegenerative diseases, including ALS (Santos-Reboucas and Pimentel, 2007). Epigenetic factors are altering gene expression without changes in DNA sequence (as opposed to genetic changes, i.e. mutations). This could explain the mechanism how certain environmental factors induce neurodegeneration. Environmental factors could, for example by DNA methylation, induce long-term changes in gene expression which would promote degenerative processes in cells.

1.2.5. Familial ALS

Using family-based linkage studies twelve genetic loci with mutations that cause ALS were identified. Additional genetic loci associated with ALS with fronto-temporal dementia (ALS-FTD1 and 2), and ALS-FTD coupled with Parkinson's disease (ALS-FTDP) were also identified (**Table 1.1**). For eight fALS loci the actual genes are known.

A major step forward in ALS research was made when it was discovered that mutations in the gene for SOD can cause ALS (Rosen et al., 1993). Around 1-2% of all ALS cases are due to mutations in SOD. SOD is a ubiquitously expressed enzyme that catalyzes conversion of superoxide radicals (O_2^-) to hydrogen peroxide (H_2O_2). SOD is located mostly in the cytosol, but also in the mitochondrial intermembrane space (Weisiger and Fridovich, 1973) and possibly in the nucleus and peroxisomes (Crapo et al., 1992). It is still not clear why and how mutated SOD causes degeneration, and why this is restricted to motor neurons. Transgenic overexpression of mutated human SOD is the basis of the most commonly used mouse models of fALS (SOD-mice) (Gurney et al., 1994) and a major part of what is known about the pathophysiological mechanisms of ALS comes from studies on SOD mice. Indeed, the experimental part of this PhD thesis

also focuses on SOD mice. Therefore SOD-mediated pathogenesis will be described in detail in a separate chapter.

ALS disease type	Chromosome	Gene (gene symbol)	Inheritance	Onset	Function	Refs
Mendelian genes						
ALS1	21q22.1	Superoxide dismutase 1 (SOD1)	AD	Adult	Detoxification enzyme	Rosen et al., 1993
ALS2	2q33	Amyotrophic lateral sclerosis 2 (ALS2)	AR	Juvenile	GEF signalling	Hadano et al., 2001
ALS4	9q34	Senataxin (SETX)	AD	Juvenile	DNA and RNA metabolism	Chen et al., 2004
ALS6	16q12	Fused in sarcoma (FUS)	AD/AR	Adult	RNA binding, exon splicing and DNA repair	Vance et al., 2009
ALS8	20q13.33	Vesicle associated membrane protein-associated protein B (VAPB)	AD	Adult	Vesicular trafficking	Nishimura et al., 2004
ALS9	14q11	Angiogenin (ANG)	AD	Adult	Neovascularization	Greenway et al., 2006
ALS10	1p36.22	TAR DNA-binding protein (TARDBP)	AD	Adult	RNA processing	Sreedharan et al 2008
ALS	2p13	Dynactin 1 (DCTN1)	AD	Adult	Axonal transport	Puls et al 2003
ALS-FTDP	17q21.1	Microtubule-associated protein tau (MAPT)	AD	Adult	Microtubule assembly and stability	Hutton et al., 1998
Mendelian loci						
ALS3	18q21	Unknown	AD	Adult	Unknown	Hand et al., 2002
ALS5	15q15.1-21.1	Unknown	AR	Juvenile	Unknown	Hentati et al., 1998
ALS7	20p13	Unknown	AD	Adult	Unknown	Sapp et al., 2003
ALS-X	Xcen	Unknown	XD	Adult	Unknown	Siddique et al., 1998
ALS-FTD1	9q21-22	Unknown	AD	Adult	Unknown	Hosler et al., 2000
ALS-FTD2	9p13.3-21.3	Unknown	AD	Adult	Unknown	Morita et al., 2006

AD, autosomal dominant; AR, autosomal recessive; GEF, guanine nucleotide excange factor; XD, X-linked dominant

Table 1.1 – Genetic loci associated with ALS (modified from Dion et al., 2009)

By now seven genes more in addition to SOD have been identified that are associated with fALS (**Table 1.1**). Especially interesting are the recent identification of mutations in the **TAR D**NA-**b**inding **p**rotein 43 (TARDBP) gene, which codes for TDP-43, and in the "fused in sarcoma" (FUS) gene (Kwiatkowski, Jr. et al., 2009; Sreedharan et al., 2008; Vance et al., 2009). These studies changed the general thinking about ALS pathogenesis, bringing attention to impairments in RNA processing, in which both TDP-43 and FUS are implicated. Specifically, it was found that ubiquinated and hyper-phosphorylated TDP-43 is a major constituent of inclusions in cell bodies and proximal axons of motor neurons in most ALS cases. TDP-43 was found in inclusions in patients with sporadic ALS, familial ALS and in patients with FTD. Only exception were fALS cases induced by SOD mutations (Mackenzie et al., 2007). This, on the one hand, suggests that neurodegeneration in SOD cases might be the result of a different mechanism than other

forms of ALS and, on the other hand, that TDP-43 could be a link between the majority of fALS cases and the sporadic form of the disease. Indeed, by now more then 30 mutations in the TARDBP gene have been described, accounting for 1-3% of ALS cases (Sreedharan et al., 2008). TDP-43 is a nuclear protein that is well conserved among species. It is a RNA/DNA-binding protein, which has been implicated in RNA splicing, stability and transcription (Buratti et al., 2005; Tollervey et al., 2011). Mutations are almost exclusively found in the C-terminal domain, with only one exception. This domain has a role in interactions with other heterogenous nuclear ribonucleoproteins (hnRNPs). Still, how TDP-43 mutations might lead to neurodegeneration or if the mutations are even necessary to cause neurodegeneration is not clear, as TARDBP mutations are not detected in the majority of ALS cases. One possible explanation could be that mutations might speed-up degenerative processes, which can also be initiated in the absence of the mutation as well. It is known that in ALS TDP-43 mislocalizes to the cytoplasm, where it forms protein aggregates. These aggregates could be toxic per se, i.e. a primary cause of degeneration, or solely the secondary by-product of an independent degenerative process. Some evidence for the latter scenario came from studies of TDP43-transgenic mouse models (Wegorzewska et al., 2009). In this study, the authors created a transgenic mouse, which expresses a mutant form of TDP-43 under control of the mouse prion protein promoter and shows ALS-like pathology. Interestingly, ubiquitin-positive but TDP-43 negative aggregates were detected in neurons that degenerated in this mouse. Later studies showed that overexpression of WT TDP-43 under the Thy1 or prion protein promoters is sufficient to cause ALS-like pathology with characteristics aggregates of TDP-43 leaving researchers with no definitive answer about the role of aggregates in TDP-43 models (Wils et al., 2010; Xu et al., 2010). In the context of this work, it is worth noting that also in the setting of TDP-43 based mouse models (as for SOD, see below) the situation is complicated by the fact that overexpression of the wild type protein alone suffices to induce toxicity, and the human disease-related mutations appear not to be necessary.

Following the reports about TDP-43, search and sequencing for other RNA/DNA binding proteins in genetic regions known to be implicated in ALS became very intense. It was already known that a genetic locus on chromosome 16 (ALS6, **Table 1.1**) was

implicated in ALS; however the responsible gene(s) had not been indentified. Sequencing led to the discovery of mutations in the FUS gene (Vance et al., 2009; Kwiatkowski, Jr. et al., 2009). Taking together results from both reports, mutations in FUS gene account for ~4% of familial ALS cases (0,4% of all ALS cases). Similar to TDP-43, FUS is also mainly localized in the nucleus. The described mutations lead to cytoplasmatic retention and aggregation of FUS protein, resembling the aggregation of TDP-43 or SOD in other forms of fALS. However, no FUS-positive cytoplasmatic inclusions were observed in patients with SOD or TDP-43 mutations. In converse, no TDP-43-positive inclusions were found in patients with FUS mutations, suggesting that pathogenesis induced by FUS mutations is independent from TDP-43 aggregation (Vance et al., 2009).

Finally, some more loci were implicated in ALS (**Table1.1**). Homozygous loss of function in ALS2 has been found to underlie a juvenile form of ALS (Hadano et al., 2001). Mutations in senataxin (SETX) are found in another atypical form of ALS with juvenile onset (Chen et al., 2004). A mutation in the **v**esicle-**a**ssociated membrane **p**rotein **B** (VAPB) was found in one Brazilian family with classical autosomal dominant ALS (Nishimura et al., 2004). Mutations in angiogenin (ANG) were associated with some familial ALS cases (Greenway et al., 2006). Most relevant to this thesis, a slowly progressing autosomal-dominant form of motor neuron disease is caused by mutations in the p150 subunit of dynactin 1, which is part of retrograde motor protein complex, dynein (Puls et al., 2003).

1.2.6. SOD-mediated toxicity in ALS

Cytosolic Cu/Zn **s**uper-**o**xide **d**ismutase 1 (SOD) is a metalloenzyme that is ubiquitously expressed and catalyzes conversion of superoxide radicals (O_2^-), a toxic by-product of mitochondrial oxidative phosphorylation, to hydrogen peroxide (H_2O_2). The SOD protein has 153 amino acids and functions as a homodimer, with each subunit binding a copper atom at its catalytic site. The SOD-catalyzed dismutation is a two step process, mediated by the copper atom, which is first reduced and then oxidized by superoxide. The first report about mutations in the SOD gene as a causative factor for fALS was published in 1993 (Rosen et al., 1993). By now, more the 100 mutations have been described (Gaudette et al., 2000) (a comprehensive and regularly updated list of ALS-related SOD-mutations can be found at http://alsod.iop.kcl.ac.uk). Soon after this initial report, transgenic mice overexpressing mutated forms of SOD were generated (Gurney et al., 1994). Using such mice, ALS pathogenesis has been intensively studied. These efforts revealed that neurodegeneration is caused by some novel property of mutated SOD (i.e. a “gain of function”). However, what this toxic property might be, and how it causes neurodegeneration, remains a topic of intense debate and study.

Many, not necessarily exclusive, hypotheses for ALS pathogenesis have been advanced, including oxidative stress, intracellular protein aggregates, and glutamate excitotoxicity (Rothstein, 2009). Recently, dysfunction of mitochondria and impairments in axonal transport in motor neurons were postulated as key events in ALS pathology (Manfredi and Xu, 2005; De Vos et al., 2008). Additionally, SOD toxicity in nonneuronal cells and their contribution to the disease is a subject of intensive investigation (Rothstein, 2009; Boillee et al., 2006a). A current view of how mutated SOD toxicity might lead to degeneration is schematically shown in **Figure 1.2.**

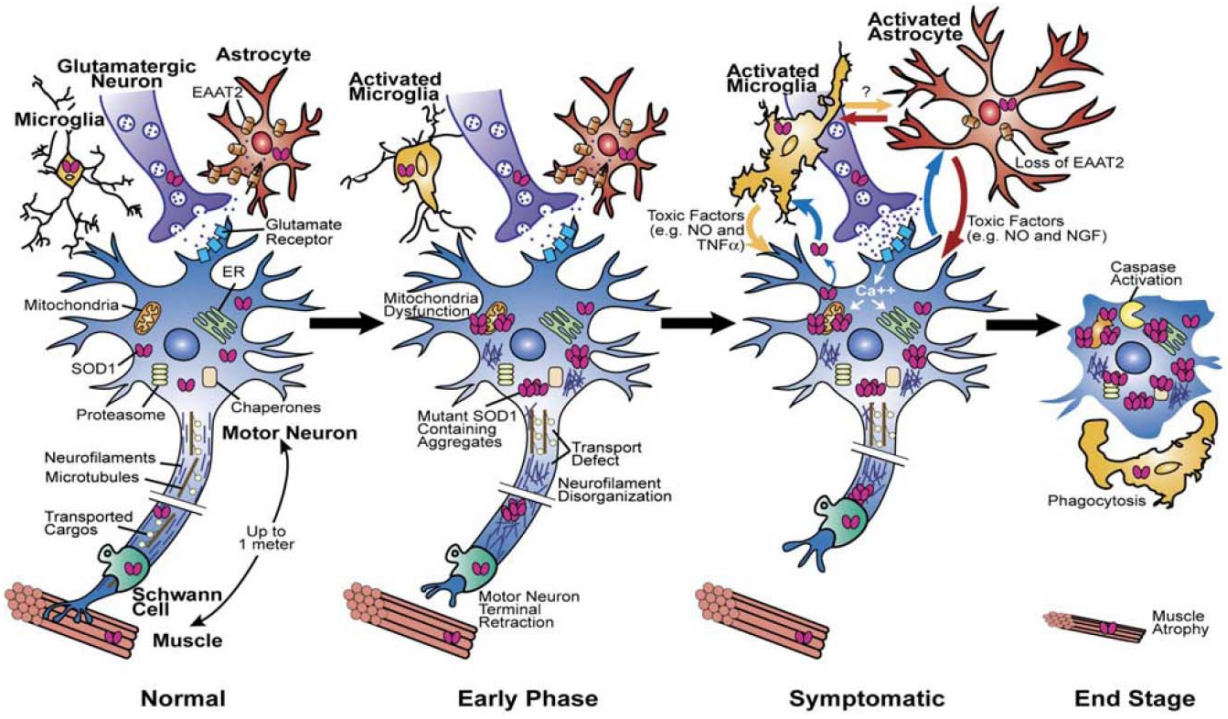

Figure 1.2 – Schematic of the evolution of motor neuron degeneration and glial activation during the course of mutant SOD-initiated ALS (from Boilee et al, 2006).

1.2.6.1. Role of nonneuronal cells and excitotoxicity

The hallmark of ALS is progressive degeneration of motor neurons. However, the familial cases of ALS are caused by mutations in ubiquitously expressed proteins, such as SOD. Hence, changes mediated by mutant SOD in non-neuronal cell types could contribute to disease onset and progression. A number of studies, mainly from the Cleveland lab, addressed this possibility. It became clear that ALS is non-cell autonomous disease, to which microglia and astrocytes make an important contribution and that SOD expression in motor neurons is necessary but not sufficient for full-blown disease (Boillee et al., 2006a). First evidence came for studies, where expression of mutant SOD was restricted to neurons (Pramatarova et al., 2001; Lino et al., 2002) and astrocytes (Gong et al., 2000). This was achieved by using cell type specific promoters like the GFAP promoter for astrocytes or the neurofilament light chain or Thy1.2. promoter for neurons. However, in these studies no degeneration of motor neurons was observed. Thy1.2. promoter was also used in later efforts which succeeded in producing disease

phenotype. This, however, was milder and progressed more slowly than the disease induced by expressing the same mutant protein ubiquitously (Jaarsma et al., 2008). Evidence for the involvement of the non-neuronal cells in ALS came also from studies with chimeric mice. It was shown that SOD mutant motor neurons survive longer when they are surrounded by non-mutated non-neuronal cells (Clement et al., 2003). To further dissect contribution of different cells to ALS pathology Boillee and colleagues made transgenic mice carrying a “floxed” mutant SOD (Boillee et al., 2006b). Thus they were able to delete mutant SOD in specific cell types. Excision of mutant SOD exclusively from motor neurons extended survival by slowing disease onset and early progression, while excision of mutant SOD from microglia and macrophages had almost no effect on disease onset by significantly slowed later disease progression. Similar results were obtained with experiments were myeloid cells in mutant mice were replaced by wild type cells by transplantation (Beers et al., 2006). It can be concluded from these studies that SOD-mediated damage of motor neurons determines the disease onset, while the speed of disease progression is determined by SOD action in microglial cells.

Astrocytes are providing trophic support to neurons and they are involved in neurotransmitter recycling after release into the synaptic cleft through action of the glial glutamate transporter, EEAT2 (Oberheim et al., 2012). The main excitatory neurotransmitter involved in signaling to motor neurons is glutamate. Excessive glutamate in the synaptic cleft can lead to repetitive firing, which can induce damage in the postsynaptic cell due to excesive levels of calcium. This phenomenon is known as "excitotoxicity". Motor neurons might be inherently sensitive to excitotoxicity. Their AMPA glutamate receptors have a low proportion of the GluR2 subunit, a subunit which reduces Ca^{2+} permeability of the receptor. It seems that astrocytes can regulate expression of this subunit in motor neurons (Hollmann et al., 1991; Van Damme et al., 2002; Van Damme et al., 2007). Both in sporadic ALS and in familial ALS patients evidence for impaired glutamate handling and reduced levels of EAAT2 were found (Rothstein et al., 1992; Rothstein et al., 1995). Taken together with the fact that riluzole, which might plausibly act as a glutamate receptor blocker, shows moderate effect in ALS treatment it seems that glutamate induced-excitotoxicity contributes to ALS pathogenesis.

What could be the mechanisms by which mutant SOD is involved in excitotoxicity? In the model proposed by Boillee et al., 2006, mutant SOD within astrocytes would promote loss of the EAAT2 glutamate transporter, reducing rapid recovery of synaptic glutamate and driving an excitotoxic response (**Figure 1.2**). Moreover, mutant SOD in astrocytes changes their ability to regulate GluR2 subunit expression in motor neurons thus further increasing their vulnerability to excitotoxicity (Van Damme et al., 2007).

1.2.6.2. Oxidative stress and copper toxicity

Initial reports suggested that mutations in SOD might cause a reduction in enzyme activity. Thus motor neuron degeneration could be triggered by oxidative stress (Rosen et al., 1993). However, knock-out mice lacking SOD do not develop any signs of motor neuron degeneration, while mice overexpressing SOD^{G85R}, a mutated but dismutase-inactive form of SOD, do develop motor neuron disease (Bruijn et al., 1997). Indeed, the existence of dismutase-inactive human SOD mutations strongly indicates that the ALS-relevant activity of mutated SOD is not its catalytic activity, giving the G85R mutation a special value in testing any effect seen with active mutations for a spurious effect of dismutase activity. SOD activity is dependent on catalytic copper. Free copper itself is highly toxic and reactive. Copper is loaded into the SOD enzyme by a separate protein, known as copper chaperone (CCS). Hence another hypothesis was that the changed conformation of mutant SOD could lead to inappropriate copper loading and handling. This hypothesis was tested by using mice with mutated CCS, which were crossed with SOD mutants expressing active or inactive form of SOD. No changes in disease course and progressing were observed (Subramaniam et al., 2002). Moreover mice, where all four histidines crucial for copper handling are eliminated from a SOD protein (SOD^{Quad}) still develop ALS-like motor neuron degeneration (Wang et al., 2003). Taking these results together, it is clear that the toxic properties of the mutated SOD protein are independent of its dismutase and copper-binding properties.

1.2.6.3. Protein aggregation

Protein aggregates are common feature in neurodegenerative diseases. Aggregates of tau and beta amyloid proteins are hallmarks of Alzheimer's disease (Alzheimer 1907, Haass, 2010). Huntingtin aggregates are found in Huntington's disease (Steffan et al., 2004). Similarly, a major component of Lewy bodies found in Parkinson's disease is misfolded α-synuclein (Spillantini et al., 1998; Spillantini et al., 1998; Bandopadhyay and de Belleroche, 2010). Protein inclusions are also found in sporadic and familial human ALS cases and in SOD-based mouse models of ALS (Watanabe et al., 2001). These aggregates are highly immunoreactive for SOD and ubiquitin. The ability to form aggregates in cell cultures was only seen in motor neurons, while they were absent in dorsal root ganglion (DRG) or hippocampal neurons expressing similar levels of mutated SOD (Durham et al., 1997). Similar to the case of TDP-43 aggregates in ALS, the contribution of protein aggregates to degeneration of motor neurons is still unclear. For example, it is unknown whether aggregates are toxic *per se*, or alternatively, whether they simply are a "downstream" product of the degenerative process. Several hypotheses have been proposed to explain how aggregates could cause degeneration (**Figure 1.2**). Co-aggregation of essential proteins with SOD would be one of the possibilities. Alternatively, aggregates could block the proteasome machinery or deplete chaperon supply leading to misfolding of other proteins (Tummala et al., 2005). Finally, it was proposed that aggregates could interfere with the function of cellular organelles, such as mitochondria and peroxisomes (Boilee et al., 2006).

1.2.6.4. Mitochondrial dysfunction

Characterization of the first SOD transgenic mice revealed early vacuolar degeneration of neurons and their processes in the anterior horns of the spinal cord (Gurney et al., 1994). Ultrastructural analysis showed that these vacuolar changes are the light microscopic equivalent of distended endoplasmatic reticulum, Golgi apparatus and especially mitochondria (Dal Canto and Gurney, 1995; **Figure 1.3**), suggesting that mitochondria may be a primary targets for SOD-induced toxicity. Even in early disease

stages, mitochondrial cristae already appear swollen. With disease progression separation and fragmentation of cristae, accompanied by breaking and splitting of the outer mitochondrial membrane, take place. Interestingly, mitochondria in neighboring interneurons appear normal, suggesting that the degenerative processes in mitochondria are specific for motor neurons. However, similar pathological changes were seen in mice expressing high levels of non-mutated SOD^{WT}, while being absent in mice expressing dismutase inactive forms of the SOD enzyme (Jaarsma et al., 2000; Bruijn et al., 1997). Taking these results together, it seems that vacuolation is a consequence of high expression of SOD in transgenic mice, and probably not a primary cause of motor neuron degeneration.

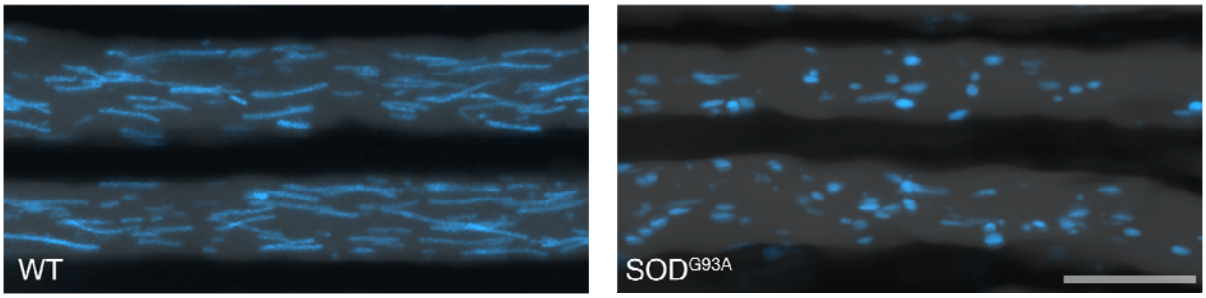

Figure 1.3 – Mitochondrial pathology in SOD^{G93A} mouse model of ALS

Intercostal axons (grey) in 4 months old WT and *SOD^{G93A}* mice. In *SOD^{G93A}* mice, mitochondria (cyan) are shorter and appear swollen. In addition, mitochondrial density is reduced in intercostal axons in *SOD^{G93A}* mice at 4 months of age. Scale bar, 10 μm

Another finding that links SOD with mitochondria is the fact that SOD protein that derives from a mutated gene, but not wild-type SOD, associates with mitochondria in the spinal cord of both mice and humans (Liu et al., 2004). This association correlates with disease progression. Ultractructural analysis revealed that mutant SOD molecules aggregate on the cytoplasmatic side of spinal mitochondria and get imported into the intramembrane space. The current model suggests that such aggregation impairs the mitochondrial import machinery leading to organelle dysfunction (Liu et al., 2004; Igoudjil et al., 2011).

Finally, mitochondria are a plausible target for SOD-induced toxicity because they are "gate-keepers" for apoptotic cell death. It is believed that the process of the motor neuron death is executed by apoptotic molecular machinery. Indeed, survival can be extended in SOD mice by increasing the levels of the apoptosis inhibitor, Bcl-2 (Kostić et al., 1997; Vukosavić et al., 2000). In accordance with this, increased levels of Bcl-2 delay activation of caspase-1 and caspase-3 in the spinal cords of SOD mice (Vukosavić et al., 2000).

1.2.6.5. Defects in axonal transport

Loss of neuromuscular junctions (NMJ) in ALS happens long before disease onset and precedes motor neuron death (**Figure 1.4**). This suggested that motor neuron pathology begins distally and then proceeds backwards, in a “dying back” pattern (Fischer et al., 2004; Schaefer et al., 2005). Hence, ALS could be considered a distal axonopathy. Furthermore, different types of motor neurons that innervate specific subgroups of muscle fibers show variable susceptibility to SOD toxicity (Pun et al., 2006). Synapses of so called "fast-fatiguable" neurons are lost first, followed by denervation of muscle fibers innervated by "fast-fatiguable resistant" neurons. "Slow" motor neurons are most resistant to SOD toxicity.

Motor neurons have one of the most fascinating geometries of all cells. Motor neuron cell bodies are located in the spinal cord, with their axons extending over distances as long as one meter in humans, before they reach their target muscle. In muscle, axon branch and innervate numerous muscle fibers (the so called "motor unit"). These long axons and their complex arbors are supplied by means of axonal transport with structural components, organelles, enzymes etc.

Having in mind this peculiar geometry of motor neurons and the dying back pathology seen in ALS, it is reasonable to propose that disturbances in axonal transport could be an initial step leading to axon degeneration in ALS. In this view, disturbances in axonal transport lead to inadequate support of distal arbors causing dying-back degeneration. Supporting evidence for this hypothesis is also coming from that the insight that

mutations in transport-related genes can result in motor neuron degeneration in mice and humans (Puls et al., 2003; Hafezparast et al., 2003). A reduced density of organelles is found in SOD and TDP-43 mouse models of ALS, further suggesting axonal transport deficit (Pun et al., 2006; Shan et al., 2010). Initial studies in SOD mice models showed deficits of slow axonal transport at very early stages of disease (Williamson and Cleveland, 1999).

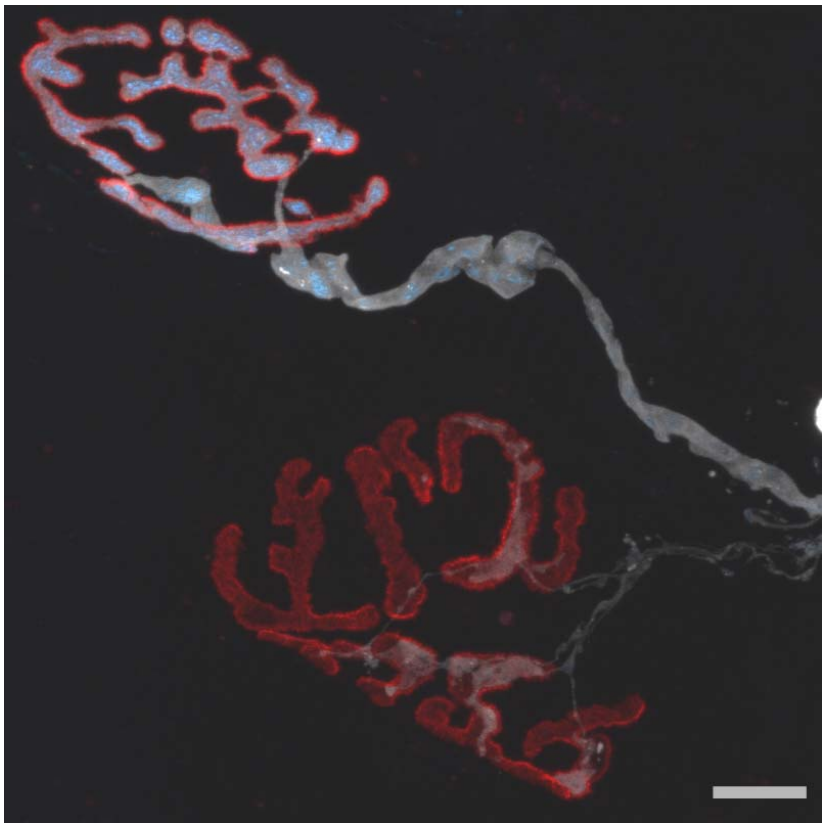

Figure 1.4 –Dying-back pathology in ALS

Confocal image of two NMJs in the triangularis muscle of a 4 months old *SOD*^{G93A} mouse. The upper synapse (stained with Alexa594-conjugated α-bungarotoxin, red) is fully covered by presynaptic axons (gray) filled with mitochondria (cyan). The lower synapse is only partially covered by axon indicating ongoing denervation-and reinnervation. Scale bar, 10 µm

Thus far, studies on fast axonal transport in the context of ALS were mostly done in cell culture systems, usually using primary motor neurons derived from transgenic mice or embryonic rat cortical neurons transfected with plasmids carrying human mutant SOD (Kieran et al., 2005; De Vos et al., 2007). Kieran et al. studied retrograde transport of endosomes labeled with tetanus toxin coupled with a fluorescent dye in cultured primary

motor neurons. It is known that the C-terminal fragment of tetanus toxin binds with high affinity to the neuronal plasma membrane and enters endocytic carriers containing neurotrophins and their receptors. In this study, using *in vitro* assay, the authors showed a retrograde transport deficit in SOD^{G93A} and *Loa* motor neurons Further, the authors crossed SOD^{G93A} mice with Loa mice, which carry a mutation in the dynein heavy chain gene and develop motor neuron degeneration (Hafezparast et al., 2003). Contrary to the expectation, crossing SOD^{G93A} into *Loa* mice delays disease progression and significantly increases life span. Authors also reported a full recovery of axonal transport in motor neurons from *Loa* x SOD^{G93A} mice *in vitro*, concluding that the recovery of the transport is the main cause of disease amelioration in *Loa* x SOD^{G93A} mice. De Vos et al., 2007 showed that mutant SOD^{G93A} damages in vitro transport of both mitochondria and other membrane bound organelles, but in a direction specific manner. While transport of membrane bound organelles was affected both in anterograde and retrograde direction, mitochondrial transport was selectively reduced in the anterograde direction. Furthermore, they showed reduced velocity and run length of transported mitochondria, as well as reduced mitochondrial density in axons of cultured SOD^{G93A} motor neurons. Expanding these results for SOD^{G93A} motor neurons, the authors showed similar effect of other ALS-causing mutations by transfecting various SOD constructs (G37R, G85R and A4V) into isolated rat cortical neurons.

Recently, a study done on SOD^{G93A} transgenic mice *in vivo* showed reduced velocity of retrogradely transported endosomes in sciatic nerve axons long before disease onset (Bilsland et al., 2010). This study also addressed mitochondrial transport using the transgenic approach developed in our lab (Misgeld et al., 2007). The authors reported no changes in flux rate of mobile mitochondria, but a higher percentage of mitochondria that paused in axons of SOD^{G93A} mice. A recent paper from Cleveland lab reported pathological changes in mitochondrial shape and volume (Vande Velde et al., 2011). These changes could affect mitochondrial axonal transport, as an “early and possibly central aspect of disease pathogenesis” as proposed by the authors. Finally, *in vitro* studies from the Manfredi lab done on primary motor neurons suggested altered mitochondrial fusion and transport as an important step in emergence of motor neuron degeneration observed in SOD mice (Magrane and Manfredi, 2009; Magrane et al., 2012)

Together, these studies corroborated the prevailing hypothesis that axonal transport deficits are early and central pathological features in SOD-caused fALS. In all these studies, the authors suggested that the described deficits in axonal transport are the immediate and key cause of axon degeneration.

However, there are also arguments to the contrary. A first hint that maybe axonal transport and motor neuron degeneration are not as closely coupled as widely assumed came from a seminal study by the Holzbaur lab (Perlson et al., 2009). These researchers studied retrograde transport of quantum dots conjugated with neuronal growth factor (NGF) in different models of neurodegenerative diseases including SOD^{G93A} mice. Their results showed quantitatively comparable deficits in transport in *Loa*, $Tg^{dynamitin}$ (mice that overexpress dynamitin, which interferes with transport) and SOD^{G93A} mice. However, Loa and $Tg^{dynamitin}$ develop only mild neurodegenerative disease, while SOD^{G93A} mice exhibit rapidly progressive neurodegeneration. Thus, according to these authors, slowing of retrograde transport alone leads only to mild degeneration and hence in isolation cannot explain ALS etiology. Instead, Perlson and colleagues suggested that qualitative changes in cargo composition and not quantitative changes in transport rates could be responsible for degeneration. They base this conclusion on a switch in retrograde signaling from survival to stress signals that they observed when analyzing the retrograde cargos in SOD^{G93A} neurons. Along the same vein, a recent study showed that increasing mitochondrial transport does not change the disease course in SOD^{G93A} mice, arguing that a central prediction of the "transport hypothesis" does not pan out (Zhu and Sheng, 2011).

In summary, it is clear from this overview of the literature that the role of axonal transport in ALS pathogenesis is still not resolved. A study is needed that would follow transport in mature, fully developed axons over the disease course, comparing various SOD ALS models. This was exactly the main aim of this PhD thesis. In my view, using comparative approach with various SOD mouse models and proper controls is very important for the design of such a study. Next chapter gives an overview of available SOD transgenic lines, which although different in many features, all show similar ALS like pathology.

1.2.7. SOD-based animal models of ALS

Since first report that mutations in SOD gene are causing ALS in humans, researchers tried to model ALS pathology in mice by making transgenic animals carrying different mutant human SOD genes. By now, there is a variety of SOD transgenic lines available (SOD mice). In most of these models, expression of mutant SOD is driven by endogenous promoter in various cell types and tissues. However, degeneration is observed only in motor neurons indicating selective vulnerability of this cell type since expression levels in some other tissues (i.e. in liver) are even higher then in motor neurons (Jonsson et al., 2006).

SOD mice show ALS-like clinical features that are inherited in an autosomal dominant fashion. The three most commonly used SOD mouse lines are: SOD^{G93A}, SOD^{G37R}, and SOD^{G85R} mice (Gurney et al., 1994; Wong et al., 1995; Bruijn et al., 1997). Mice expressing human non-mutated SOD protein (SOD^{WT}) are often used as controls (Gurney et al., 1994). Due to different transgene copy numbers inserted into the mouse genome, SOD mouse lines have different expression levels of the SOD gene, which seems to determine disease onset (**Table 2**). In SOD^{G85R} mice, the mutated protein is expressed to levels equal to the endogenous protein. In contrast, in SOD^{WT}, SOD^{G93A}, and SOD^{G37R} mice, the human protein is overexpressed to levels several times higher than the endogenous protein. Another variable in SOD mice lines is the enzymatic activity of the mutated protein. The transgenic lines could be divided in two groups: one with enzymatically active mutant SOD (SOD^{G93A}, SOD^{G37R},) and a second one which has enzymatically inactive protein (SOD^{G85R}). Detailed biochemical analysis revealed that mutants differ in activity due to different Cu-charging, which is critical for proper enzymatic action (Jonsson et al., 2006). Finally some mutated forms are very stable (SOD^{G93A}) while other have a short half-life time (SOD^{G85R}). Having in mind the variety of mutant SOD characteristics in available transgenic lines it is critical to use several different lines in any study. Our lab is proposing the use of one active and one inactive mutant as minimum and preferably of lines with lower expression levels. Further, mice expressing non-mutated SOD should be use as controls. In that way, it is possible to search for patterns and alternation common to different SOD mutants which induce essentially the same ALS-like phenotype.

In order to elucidate the role and contribution of different cell types to ALS pathology mouse lines with cell specific expression of mutated SOD were made. These mice have SOD expression restricted to specific cell types such as astrocytes (Gong et al., 2000) or strictly to neurons (Pramatarova et al., 2001; Lino et al., 2002; Jaarsma et al., 2008). This is achieved by using cell type specific promoters like GFAP promoter for astrocytes or neurofilament light chain and Thy1.2 promoters for neuronal cells. First attempts with expression solely in neurons (Pramatarova et al., 2001; Lino et al., 2002) and astrocytes failed to reproduce ALS-like pathology in mice. However in later attempts with higher expression levels, motor neuron degeneration is observed but not as severe as in lines when SOD was ubiquitously expressed (Jaarsma et al., 2008).

Many SOD mouse lines can be commercially obtained through Jackson Laboratory. An overview of different SOD lines is given in **Table 1.2**.

mutation	Line (transgene copy number)	SOD1 activity in CNS relative to control	Onset (months old)	Reference
hG37R	42	14.5	3.5-4	Wong et al., 1995
	9	9.0	5-6	Wong et al., 1995
	106	7.2	5.5-7.5	Wong et al., 1995
	29	7	6-8	Wong et al., 1995
hG85R	148	1.0	8	Bruijn et al., 1997
mG86R	M1	1.0	3-4	Ripps et al., 1995
hD90A	hetero	slightly increased	4-5	Brännström et al., 2000
	homo	markedly increased	N.D.	Brännström et al., 2000
hG93A	G1H/+(25)	N.D.	3	Gurney et al., 1994
	G1L/+(18)	4.2	4	Gurney et al., 1994
	G5/G5(10)	~50% of G1	10	Del Canto et al., 1997
	G93A^{dl}(8)	N.D.	6	Jaarsma et al., 2008
hWT	N1029(7)	3.6	N.A.	Gurney et al., 1994

h, human; m, mouse; N.D., not described; N.A. not applicable

Table 1.2 – Overview of SOD-based transgenic mouse lines (modified from Shibata, 2001).

2. MATERIALS AND METHODS

2.1. Animals

Transgenic mice carrying human wild-type (WT) or mutated SOD genes were obtained from Jackson Laboratory. The following strains were used (Jackson Laboratory strain designation):

SOD^{WT}	(Tg(SOD)2Gur/J)
SOD^{G93A}	(Tg(SOD-G93A)1Gur/J)
SOD^{G37R}	(Tg(SOD*G37R)42Dpr/J)
SOD^{G85R}	(Tg(SOD*G85R)148Dwc/J)

To study mitochondrial transport, density and morphology in ALS, males from these strains were crossed with *Thy1-mitoCFP^{C}* (Tg(Thy1-CFP/COX8A)C1Lich/J), and - in selected cases - *Thy1-mitoCFP^{S}* (Tg(Thy1-CFP/COX8A)S2Lich/J) or *Thy1-mitoCFP^{K}* females (Misgeld et al., 2007). *Thy1-mitoKaede* were generated and crossed with SOD mice as described below. Double transgenic mice were identified by PCR from tail biopsies (for details see below). As *Thy1-mitoCFP* and *Thy1-mitoKaede* animals were maintained on a mixed genetic background, SOD-negative, mitoCFP or mitoKaede-positive littermates were used as wild-type controls. For studying denervation and reconstructing motor units, SOD-mutant mice were crossed with *Thy1-YFP^{16}* (Tg(Thy1-YFP)16Jrs/J) and *Thy1-YFP^{H}* (Tg(Thy1-YFPH)2Jrs/J) mice, respectively (Feng et al., 2000). To study transport of synaptic vesicles precursors, *SOD^{G93A}* mice were crossed with *Thy1-synaptophysin7-YFP* mice (Umemori et al., 2004). *G85R SOD-YFP* mice were kindly provided by Dr. Arthur Horwich (Yale University; Wang et al., 2009) as part of a collaboration. All animal work conformed to institutional guidelines and was approved by the Animal Study Committee of the Regierung von Oberbayern.

2.2. Mouse genotyping

The mice were genotyped by PCR from tail biopsies. The labeling of animals and tail sniping was done in our animal facility by our animal caretakers: Manuela Budak, Petra Apostolopoulos and Ljiljana Marinković. The DNA isolation, PCR and gel electrophoresis were done by our technical assistants Anna Thomer and Kristina Wullimann.

DNA isolation: The mouse tails were collected in 1.5 mL tubes and DNA was isolated using a standard protocol:

Standard protocol for DNA isolation:

- Add 0.3 mL of lysis buffer with Proteinase K (Sigma, #P2308; 1µL Proteinase K per mL lysis buffer)
- Incubate at 55 °C 60-90 min in Thermomixer at 400 rpm (Thermomixer comfort, Eppendorf)
- Centrifuge for 5 min at 16 000 relative centrifuge force (rcf; Eppendorf 5415D)
- Prepare new tubes with 250 µL of isopropanol (ROTH, #6752.1.)
- transfer 250 µL of supernatant to the tubes with isopropanol and mix immediately
- Centrifuge for 5 min at 16 000 rcf (Eppendorf 5415D)
- Carefully discard the supernatant
- Wash the pellets with 0.7 mL 70% (vol/vol) ethanol
- Centrifuge for 5 min at 16 000 rcf (Eppendorf 5415D)
- Carefully discard the supernatant
- Centrifuge 1 min at 16 000 rcf (Eppendorf 5415D)
- Completely remove ethanol
- Incubate the pellets for 5 min at 65 °C in Thermomixer (400 rpm)
- Dissolve the DNA in 200 µL 10 mM TRIS pH 8.5; incubate for 20 min at 65 °C in Thermomixer (400 rpm)
- Store the DNA at 4°C
- Before PCR, incubate the DNA for 5 min at 65 °C in Thermomixer

PCR: The mice were genotyped for the expression of fluorescent proteins and different SOD mutated proteins. The primers for SOD mutants were designed to recognize all different forms of human SOD gene (SOD^{WT}, SOD^{G93A}, SOD^{G85R} and SOD^{G37R}). The following primers and protocols were used.

SOD:

SOD-F: 5´-CATCAGCCCTAATCCATCTGA-3´

SOD-R: 5´-CGCGACTAACAATCAAAGTGA-3´

Mito:

Mito-F: 5´-CGC CAA GAT CCA TTC GTT-3´

EYFP-R: 5´-GAA CTT CAG GGT CAG CTT GC-3´

YFP:

GFP-F: 5´-CACATGAAGCAGCACGACTT-3´

GFP-R: 5´-TGCTCAGGTAGTGGTTGTCG-3

Mito (181bp)		
Reagent	Quantity (for 1 reaction)	PCR program (Mito)
Total volume for one reaction	23.5 µl	94°C 2 min
H_2O	18.375 µl	
10 x Puffer S (PeqLab) ≡ 1,5mM $MgCl_2$	2.5 µl	94°C 30 sec
Mito-F (10pmol/µl)	1 µl	57°C 30 sec 35x
EYFP-R (10pmol/µl)	1 µl	72°C 30 sec
dNTPs (10mM)	0.5 µl	
Taq-Polymerase (PeqLab) 5U/µl	0.125 µl	72°C 5 min
DNA	1.5 µl	4° C ∞

YFP		
Reagent	Quantity (for 1 reaction)	PCR program (YFP)
Total volume for one reaction	23.5 µl	94°C 2 min
H_2O	18.375 µl	
10 x Puffer S (PeqLab) ≡ 1,5mM $MgCl_2$	2.5 µl	94°C 30 sec
GFP-F (10pmol/µl)	1 µl	58°C 30 sec 30x
GFP-R (10pmol/µl)	1 µl	72°C 1 min
dNTPs (10mM)	0.5 µl	
Taq-Polymerase (PeqLab) 5U/µl	0.125 µl	72°C 5 min
DNA	1.5 µl	4°C ∞

SOD (235bp)		
Reagent	Quantity (for 1 reaction)	PCR program (SOD)
Total volume for one reaction	23.5 µl	94°C 4 min
H_2O	18.375 µl	
10 x Puffer S (PeqLab) ≡ 1,5mM $MgCl_2$	2.5 µl	94°C 5 sec 63°C 45 sec 30x
SOD-F (10pmol/µl)	1µl	72°C 45 sec
SOD-R (10pmol/µl)	1µl	
dNTPs (10mM)	0.5 µl	72°C 2 min
Taq-Polymerase (PeqLab) 5U/µl	0.125 µl	4° C ∞
DNA	1.5 µl	

DNA electrophoresis on agarose gels: DNA electrophoresis was performed in horizontal gel chambers, DNA Pocket Block-UV (Biozym Diagnostik). For gels, buffers and solutions see recipes section below. Analytical gels with ethidium-bromide were prepared in order to visualize DNA. After the agarose gel solution preparation, gels were loaded with 15 µL mixes of probes and 10% (v/v) DNA-load buffer mix. Additionally, 7.5-10µl of DNA ladder solution was loaded into separate well (New England Biolabs, #N0469S). The electrophoresis was performed usually at a voltage of 70mV in 1 × TEA running buffer. Separated DNA bands in the gels were visualized under UV-light (312nm) and printed on Gel Doc 2000 (Biorad).

2.3. qPCR quantification of SOD gene copy number

The qPCR experiments were performed by Dr. Monika Brill in our laboratory. DNA was isolated from tail biopsies using DNeasy Blood & Tissue Kit (Qiagen, #69504) and diluted with 10 mM Tris pH 8.0. The following primers were used:

Mouse interleukin 2 (product: 139bp)
mIL2-F: 5´-CCT TTA CAG AGG ACA GGG AGT G-3´
mIL2-R: 5´-TTC TGT GGC CTA GAG GAG TAA TAA G-3´

human SOD (product: 152bp)
hSOD-F: 5´-CCG ATG TGT CTA TTG AAG ATT CTG-3´
hSOD-R: 5´-CCG CGA CTA ACA ATC AAA GTG-3´

The mastermix was prepared using Qiagen,QuantiTect Sybr Green PCR Kit, #204143.

Mastermix for qPCR	
Reagent	Quantity (for 1 reaction)
H_2O	6 µl
Forward primer (10pmol/µl)	1 µl
Reverse primer (10pmol/µl)	1 µl
Sybr	10 µl
DNA	2 µl

The following program was used for the PCR reaction:

LightCycler™ (Roche)			
program	**Temperature target (°C)**	**Hold time (sec)**	**Acquisition mode**
denaturation	95	900	none
amplification	94	15	none
	55	30	none
	72	20	single
final elongation	95	0	none
melting	95	0	none
	65	15	none
	95	0	continous
cool	40	30	none

qPCR reaction: A PCR reaction consists of three phases. In the first, so called "background" phase, the signal form PCR product is lower than the background signal. When enough of the PCR product is accumulated, signal becomes higher than background signal and the amplification is exponential (exponential phase). The Ct value is defined as the cycle in which there is a significant increase in signal above the threshold. This is the cycle in which the curve crosses the threshold. The Ct value is related to the initial amount of DNA. The Ct value shows also the sensitivity of the assay and it is used for relative quantification of qPCR. Within exponential phase it is also possible to define a point in the amplification curve that represents the same amount of PCR product in every curve. This point is called crossing point and it is defined by cycle number and identical copy numbers in all reactions. It is used in absolute quantification of qPCR. In the last phase PCR reactions enters plateau with low efficiency of the reaction.

qPCR quantification: The transgene copy number were evaluated using real time quantitative PCR by determining the difference in threshold cycle (ΔCt) between the transgene (human SOD) and a reference gene. For the reference gene, mouse interleukin 2 (IL2) was used, previously shown to be reliable control for human SOD gene copy number measurements (Alexander et al., 2004). The number of copies of the human SOD gene can be calculated using the previously reported copy number for the *SOD^{G93A}* mice (25±1.5; Gurney et al 1994) and following formula: $N*2^{(\Delta Ctx-\Delta CtG93A)}$, where N is known copy number and ΔCtx is the ΔCt of the gene for which copy number is calculated. Results showed following ΔCT values SOD^{G93A} 7.1; SOD^{G85R} 5.8; SOD^{WT} 6.2. Copy number calculations based on SOD^{G93A} value gave following results: 10 copies in SOD^{G85R} and 13 copies in SOD^{WT}. While the calculated value for SOD^{G85R} is within expected range (Bruijn et al 1997), the value for SOD^{WT} is higher than values previously reported in the literature (7.2 ± 2.4; Gurney et al 1994).

2.4. Generation of *Thy1-mitoKaede* mice

Thy1-mitoKaede transgenic mice used in this study were generated by Dr. Leanne Godinho from our lab in collaboration with Dr. Jae Song in Jeff Lichtman's lab at Harvard University by using standard procedures (Marinković et al., 2011). Briefly, an N-terminal in-frame fusion was created between the coding sequence of Kaede (MBL International Corporation) and the mitochondrial targeting sequence from subunit VIII of the human cytochrome c oxidase gene (Clontech). This fusion was then cloned downstream of the Thy1-promoter (Caroni, 1997); kindly provided by Dr. J.R. Sanes, Harvard University). Transgenic mice were generated by standard pronuclear injection in the transgenesis facility of Harvard University, and several founder lines were screened by Dr. Song to establish the transgenic mouse strain used here.

2.5. Behavioral testing

Animals were tested and weighed every 3-4 days. The grid test was a binary modification of a previously described test (Kraemer et al., 2010). Briefly, each mouse was placed onto a metal grid, which was positioned ~30 cm above a soft surface. The grid was inverted to determine whether an animal could support itself for more than 30s. For each animal three trials were performed with a 5 min rest period in between. The test was scored "normal" if the animal could hold itself for more than 30 s in at least one trial. In the figures, a “survival” curve of the percentage of animals which showed a normal test at a given time is presented.

2.6. Staging of *SOD^{G85R}* mice

For staging of *SOD^{G85R}* mice I deviated from a purely age-based classification, as clinical manifestation at a given age varied considerably given the long preclinical period and fast disease progression once the disease started. I therefore considered animals that had lost 10% of their peak body weight and showed an abnormal grid test as “preterminal” and used these animals - which would be expected to die within 2-3 weeks

- as the latest stage in my experiments. The mean ages of animals in these categories were: preterminal – 302±8 days; terminal – 311±11 days.

2.7. Explants preparation and transcardial perfusion of mice

The initial steps in preparing the triangularis sterni explant and in transcardial perfusion of mice are comprised of same dissection steps. Namely, the mice were first lethally anesthetized with isoflurane, and fixed with the needles to Styrofoam plate. Using large medical scissors (Fine Science Tools, #14108-09) I made a midline incision of the skin over the sternum and two incisions parallel to the lower edge of the rip cage. Next, I opened the abdominal wall and made incisions parallel to the rib cage all the way to the vertebral column. I cut the diaphragm open just below the xiphoideum cartilage and then dissected the diaphragm off along its costal insertions. While holding the rib cage onto the xiphoid process using forceps (Dumostar, Dumont #3, Fine Science Tools, #11293-00), I cut right and left ribs off the vertebral column, as close as possible to their insertions. Two cuts converged above the heart level to the manubrium sternii. At this point protocol for explantation and perfusion diverge. However, it is possible to continue with both in parallel if needed (see below).

Triangularis sterni explant preparation: In the case of the explant preparation I have cut the whole anterior thoracic wall off and transfer it into the dish with cooled 95% O_2 /5% CO_2 -bubbled Ringer's solution (for recipe see below). After this step it is possible to proceed with perfusion of the mouse (see below). However, total time that explant is kept in cooled 95% O_2 /5% CO_2 -bubbled Ringer's solution should be < 10 min. Therefore, until necessary experience in preparation is obtained, it is recommended to ask for assistance from a colleague. All further steps were done under the dissection microscope with cold-light illumination (Olympus SZ51 equipped with Schott KL 1500 LCD). I used small angled spring scissors (Fine Science Tools, #15033-09) to remove the remnants of thymus, pleura, diaphragm (inside) and pectoral muscles (outside). To fit the explant to the 3.5-cm dish, I dissected off all the ribs that do not insert to the sternum. This is best done using small angled spring scissors and cutting the tissue in between ribs. Finally, I pinned down the triangularis sterni explant into the Sylgard-coated 3.5 cm dish filled with 95% O_2 5%

CO_2-bubbled Ringer's solution using minutien pins (Fine Science tools, #26002-20, shortened to < 4 mm). Standard approach to do this is to put two pins through cartilaginous (white) parts of the sternum and at least two pins through the ribs both on left and right side of the explant aiming for the softer cartilaginous parts and avoiding the ribs under or close to the triangularis muscle.

Transcardial perfusion of mice: In case when fixing of triangularis sterni muscle in addition to perfusion was needed, I have cut the whole anterior thoracic wall off and submerged it into 4% paraformaldehyde (PFA; wt/vol, for recipe see below) for 2h. Subsequently I washed the thoracic wall three times in 1x PBS. If no fixation of the triangularis sterni was needed, I folded the anterior thoracic wall back, and pinned it down with a hypodermic needle—to reveal the heart. While holding the heart with Russian organ-holding forceps (Fine Science Tools, #11026-15), I carefully inserted the hypodermic needle attached to the perfusion pump tubing into the left ventricle. The left ventricle comprises the cardiac apex and can be recognized by its lighter color (compared with the dark red of the right ventricle). Next, I opened the right atrium with spring scissors and started the perfusion pump (Ismatec, ISM796B). I perfused the animal with 1x PBS (for recipe see below) at ~5 mL/min for approximately 1 min (until the liver turned from dark red to clay-like brown). Then I turned the pump off, put the tubing end in the tube with 4% PFA and restarted the pump perfusing at the same speed as above. After perfusing the mouse with ~25 mL of 4% PFA in 1x PBS, I removed the needle from the heart, and flushed the perfusion system with water. I cut the skin off of the animal and post-fixed the tissue in the 50mL tubes. To ensure access of the PFA to CNS tissue during post-fixation I made a transverse scissor cut between two vertebrae, and opened the cranium with a rostral cut. After the post-fixation period of 48h, I rinsed the tissues three times with 1x PBS. The tissue was stored in 0.01% NaN_3 (#13412, Riedel de Häen) in 1x PBS.

Saphenous nerve explant preparation: As the surgery for explanting the nerve is complicated and it lasts ~ 20min, mice were not lethally anesthetized but kept alive under ketamine-xylazine (KX; 1.5% ketamine, 0.1% xylazine) anesthesia. In that way better viability of the nerve is achieved. Additionally, during the surgery mice were kept on the heated metal plate ~30 °C and the exposed tissue was regularly manually superfused

with 95% O_2 5% CO_2-bubbled Ringer's solution using Pasteur pipette. The pure sensory saphenous nerve is located on the inner side of the tie. Therefore, it is necessary to shave the fur to get better visibility and prevent hair release during skin incisions. To explant the saphenous nerve I made a longitudinal skin incision along the tie trying to avoid the femoral artery which is visible through the skin. The saphenous nerve is immediately visible after the incision. I transected the saphenous nerve on the distal side the nerve just above the branching point using spring scissors. While holding the distal part of the nerve with fine forceps (Dumostar, Dumont #5, Fine Science Tools, #11295-00), I have dissected off the saphenous nerve with hypodermic needle. Finally, I made a transverse cut on the proximal side of the nerve to release the nerve and transferred the nerve into Sylgard-coated 3.5-cm dish, filled with 95% O_2 5% CO_2-bubbled Ringer's solution. I pinned down the nerve using minutien pins (Fine Science Tools, #26002-10, diameter 0.1mm, shortened to < 4 mm). After nerve explantation mice were sacrificed according to the animal protocol.

Tibialis nerve explant preparation: Similar like in the case of saphenous nerve preparation, surgery for explanting the tibialis nerve is complicated and it lasts ~ 20min. Therefore, mice were not lethally anesthetized but kept alive under KX anesthesia. Additionally, during the surgery mice were kept on the heated metal plate ~30 °C. To approach the tibialis nerve, I made skin incision using large medical scissors (Fine Science Tools, #14108-09) on posterior side of one of the hind limbs. The incision is made along the hind limb starting just below the knee joint and ending close to the vertebral column. The sciatic nerve which gives rise to the tibialis nerve is visible through the muscle tissue after the skin cut. Next, I exposed the sciatic nerve to the branching point in the knee joint. Using spring scissors, I made transverse cuts on the common peroneal branch and the tibialis branch. The tibialis branch is cut as close as possible to the entrance into the gastrocnemius muscle. Finally I cut the sciatic nerve on the proximal side I close as possible to the vertebral column. To make these cuts, extra-attention is needed to avoid cutting major blood vessels which would immediately obscure the visibility during the surgery and would be fatal for the mouse. After explanting, I transferred the nerve into Sylgard-coated 3.5-cm dish, filled with 95% O_2 5% CO_2-bubbled Ringer's solution. I pinned down the nerve using minutien pins (Fine Science

tools 26002-10, diameter 0.1mm, shortened to < 4 mm). After nerve explantation mice were sacrificed according to the animal protocol.

2.8. Tissue preparation, immunohistochemistry and confocal microscopy

Triangularis sterni muscles were fixed by dissection and submersion of the whole anterior thoracic wall in 4% PFA in 1×PBS for 2h as described above. Gastrocnemius muscles were fixed by transcardial perfusion with 4% PFA in 1×PBS as described above. The muscles were incubated in 50 µM solution of Alexa594-conjugated α-bungarotoxin (Invitrogen, #B-13423) diluted in 1× PBS, whole-mounted on glass slides with anti-fading medium (Vectashield, Vector Laboratories) and cover-slipped. Cover-slipped slides were gently squeezed between small magnets and a metal plate to flatten the tissue. Subsequently, high-resolution image stacks of fixed samples were obtained on an Olympus FV1000 confocal microscope equipped with standard filter sets and a ×60/ N.A. 1.42 oil objective (**Figure 2.1**).

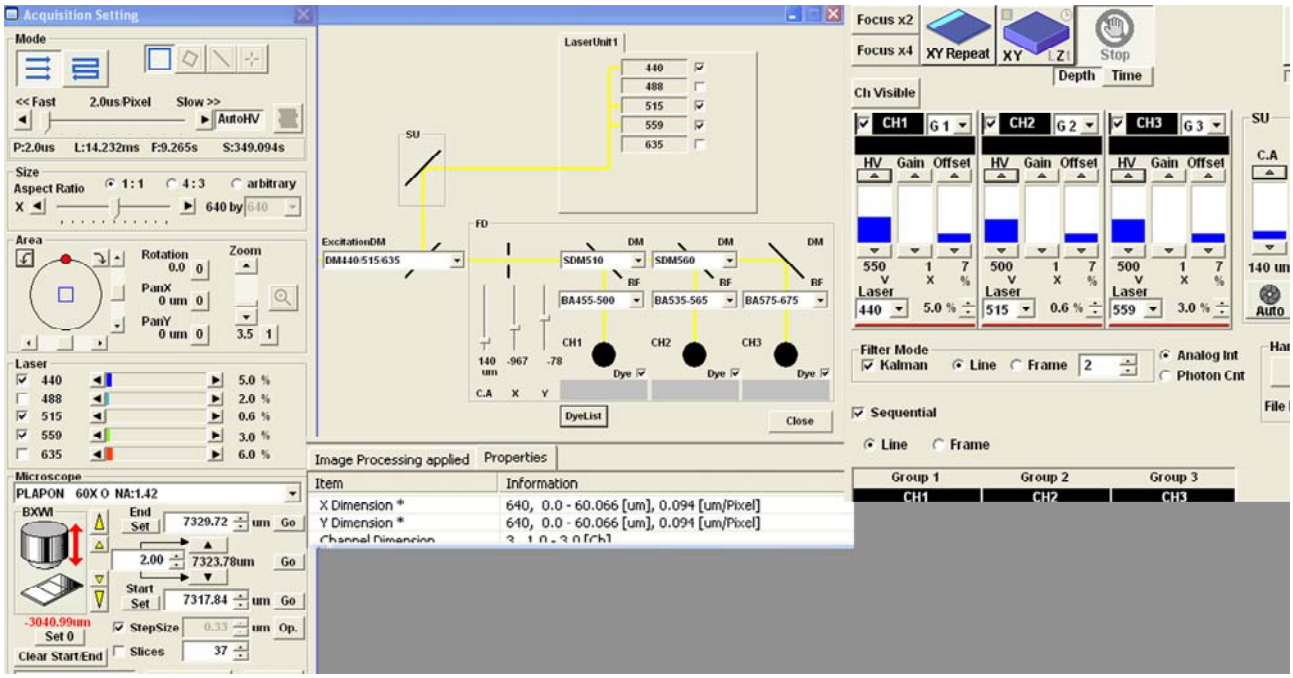

Figure 2.1 – Microscope settings for acquisition of high resolution NMJs images

A screen shot of Fluoview software (Olympus) with settings used for acquisition of NMJs images. The images obtained in this way were used for mitochondrial density and denervation index measurements.

For immunohistochemistry of motor neurons (these experiments were performed together with Dr. Monika Brill in our laboratory), mice were lethally anesthetized with isoflurane and transcardially perfused with 4% PFA in 1×PBS as described above. The tissue blocks consisting of the vertebral column and the head were dissected off and post-fixed for 48h in 4% PFA in 1×PBS. After post fixation the spinal cords were isolated and washed three times with 1×PBS. Next, I cryo-protected the spinal cords in 30% (wt/vol) sucrose in 1×PBS. After cryo-protection the tissue was embedded in "Tissue-Tek" medium (Sakura) and snap-frozen in 2-methyl butane (#M32631, Sigma) cooled down to -80°C. 50 µm spinal cord cross-sections were cut using cryostat (Leica, CM 1850 UV) and mounted to the "superfrost" glass slides (VWR Germany). The sections were stained overnight at 4°C with primary antibody against human SOD (#16831 and #13498; Abcam) diluted in 1×PBS containing 0,5% Triton X-100, 10% normal goat serum and 1% bovine serum albumin. Following antibody dilutions were used: 1:250 for #13498 and 1:1000 for #16831. Secondary, goat anti-rabbit antibody coupled with Alexa-594 (1:2000, #A-11012, Invitrogen) were used to visualize antibody staining. The staining was controlled for non-specific binding of the secondary antibody by omitting the primary antibody. The tibialis nerve-cross sections were prepared in similar way and stained with neuron-specific βIII tubulin antibody (1:250; BD Pharmigen, #560339). High-resolution stacks were obtained on an Olympus FV1000 confocal microscope using a ×60/ N.A. 1.42 oil objective. The quantification of SOD expression was done on single plane images in ImageJ/Fiji software. Regions of interest in motor neuron cytoplasm and nucleus (for background correction) were outlined using "line" tool in ImageJ and mean fluorescence intensity was measured using "measure" function in ImageJ. Around 25 motor neurons per mouse were measured.

2.9. Imaging mitochondrial transport

Transport of mitochondria was measured as previously described (Misgeld et al., 2007; Kerschensteiner et al., 2008). Preparation of triangularis sterni was done as described above. Briefly, the anterior thoracic wall (with the attached triangularis sterni muscle and its innervating intercostal nerves) was isolated by cutting ribs close to the vertebral column. The explant was pinned down on a Sylgard-coated 3.5cm plastic Petri dish using minutien pins (Fine Science tools). After excision, explants were kept in 95% O_2 5% CO_2-bubbled Ringer's solution oxygenated Ringer's solution at all times. During imaging, explants were kept in the heating ring for 3.5-cm dishes (Warner Instruments, #64-0110 DH-35), maintaing the temperature in the dish between 32°C and 34°C. Additionally, the explant was superfused with slow (~1.75 mL/min) and steady flow of warmed and oxygenated Ringer's solution. An in-line heater (Warner Instruments, #SC-20) was used for pre-warming. Preparation of triangularis sterni muscles from *Thy1-mitoKaede* mice was done under red light to prevent accidental photo-conversion. In addition to intercostal nerves, mitochondrial transport in saphenous and tibialis nerves was studied using acutely explanted nerves as described above.

Imaging setup and acquisition: Mitochondria were imaged using an Olympus BX51WL microscope equipped with a ×4/ N.A. 0.13 air objective and ×20/ N.A. 0.5 and ×100/ N.A. 1.0 water-immersion dipping cone objectives (Olympus), an automated filter wheel (Sutter) and a cooled CCD camera (Retiga EXi; Qimaging) and controlled by µManager, an open source microscopy software (Edelstein et al., 2010; **Figure 2.2**). The microscope is equipped with following filter sets for fluorescent proteins: ET F46-001 for CFP, ET F46-003 for YFP and ET F46-008 for TxRED all from AHF Analysentechnik, Germany. Neutral density filters (U25ND25 and U25ND6, Olympus) in the light path were used to prevent photo-toxicity and photo-bleaching. To follow mitochondrial movement, images were acquired at 1 Hz using an exposure time of 500 ms for 5 min. Transport characteristics of individual mitochondria were measured in explants from *Thy1-mitoKaede* mice. To highlight individual mitochondria I exposed intercostal nerves to short (~ 5 s) localized exposure of 405nm light from an LED light source (LED405E, Thorlabs) coupled into the microscope's excitation light path and manually controlled using LED driver (LEDD1,

Thorlabs). By moving the observation site proximally or distally from the photo-converted spot along the same nerve, I could use the red channel to track individual mitochondria.

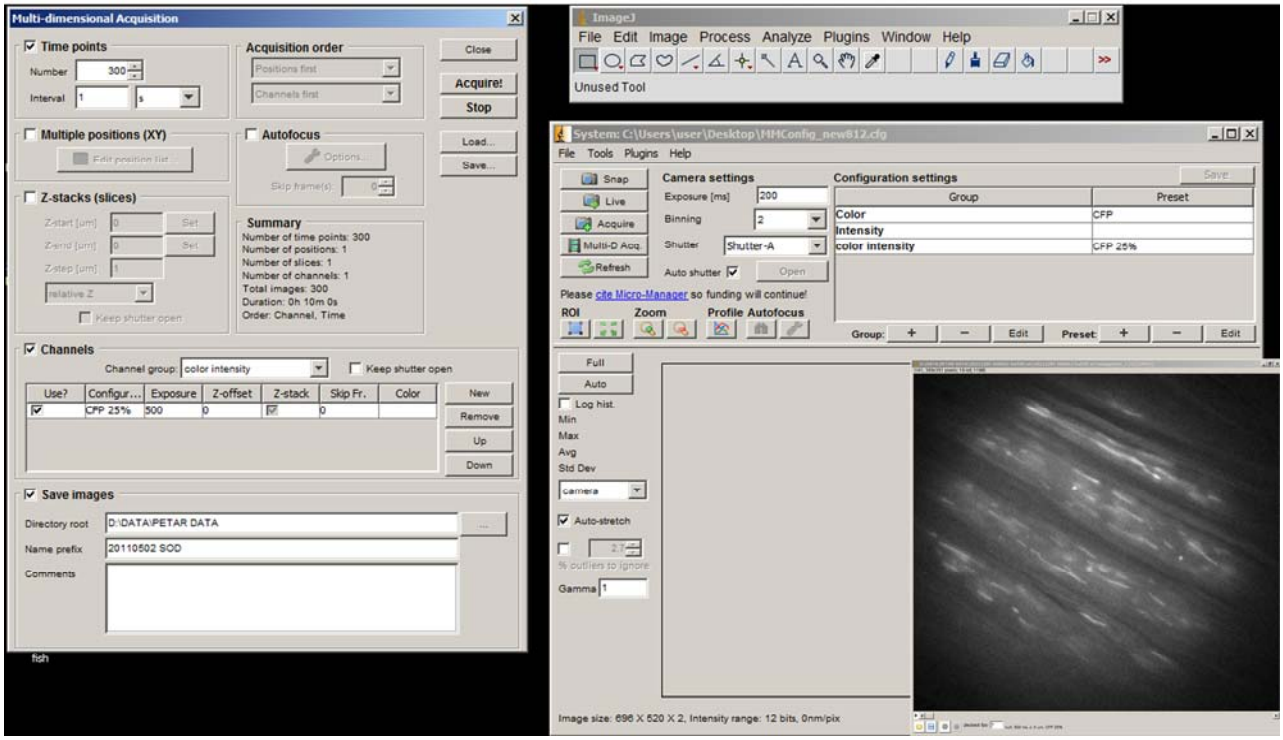

Figure 2.2 – Time-lapse imaging of the mitochondrial transport

A screen shot of Micro Manager software with settings used for acquisition of time-lapse movies of mitochondrial transport.

2.10. Imaging transport of CTB-labeled vesicles

To study transport of endosomal vesicles, I injected CTB-conjugated with Alexa Fluor 594 (#C-34777, Invitrogen) into the triangularis sterni muscle using a 5 µm micro syringe (#7634-01, Hamilton, see Mantilla et al., 2009). Mice were anesthetized with KX (1.5% ketamine, 0.1% xylazine). I made two injections of 0.05% CTB in 1×PBS between the 2nd and 3rd, and the 3rd and 4th ribs. I closed the injection site surgically and placed the mice in a heated recovery chamber. In order to label tibialis nerve, I anesthetized mice with KX and exposed the gastrocnemius muscle by making a skin incision on one of the hind limbs. I made 3-4 injections (to increase labeling probability) of 0.05% CTB in 1×PBS into gastrocnemius muscle. Axonal transport of CTB-labeled endosomes was then imaged

24h after injection in an acute triangularis sterni or tibialis nerve explant preparation as described above. CTB-labeled endosomes were imaged using same imaging setup as for mitochondrial transport (see above). To follow CTB-labeled endosomes movement, images were acquired at 1 Hz using an exposure time of 500 ms for 5 min.

2.11. Axotomy

To study changes in mitochondrial transport after axotomy, I transected one of the intercostal nerves innervating the triangularis sterni muscle *in vivo.* Briefly, mice were anesthetized with KX (1,5% ketamine, 0,1% xylazine) and immobilized on a heated metal plate. I used Puralube Vet Ointment (Fougera) to prevent the eyes from drying during the surgery. Using a surgical blade (Heinz Herenz, #1110911), I made a longitudinal skin incision on one side of the thorax, and approached the rib cage. Using spring scissors (Fine Science Tools, #15003-08), I exposed one intercostal nerve (usually, the nerve running parallel with the 3rd or 4th rib) by cutting the intercostal muscle close to the bone-cartilage transition of the corresponding rib. Next, I made a complete nerve transection using spring scissors (Fine Science Tools, #15003-08). The wound was surgically closed with surgical suture (Resorba, #5142) and mice were placed in a heated recovery chamber. In the sham-operated group, an intercostal nerve was exposed and the wound was closed with the nerve intact. Axonal transport of mitochondria was studied at 24h and 7 days after surgery in acutely explanted preparations as described above. Transport was measured in the intercostal nerve above the lesion (cut), the neighboring intercostal nerve (neighbor) and in the contra-lateral intercostal nerve (uncut).

2.12. Image analysis and processing

Denervation: In order to score muscles for denervation, confocal high-resolution image stacks were processed using ImageJ/Fiji software to generate maximum intensity projections. NMJs (>100 per muscle) were categorized either as “innervated” (if the

axonal marker – cytoplasmic YFP or mitochondrial CFP – covered the end plate) or "denervated".

Transport rates: The number of anterogradely and retrogradely transported mitochondria ("transport flux") was determined in explants from *Thy1-mitoCFP* mice as the number of fluorescent mitochondria per minute that crossed a vertical line placed across the axon (**Figure 2.3A**). For this purpose, time-lapse movies were obtained. The obtained movies were auto-aligned using the "StackReg" algorithm (Thevenaz et al., 1998) and manually scored for anterograde and retrograde transport.

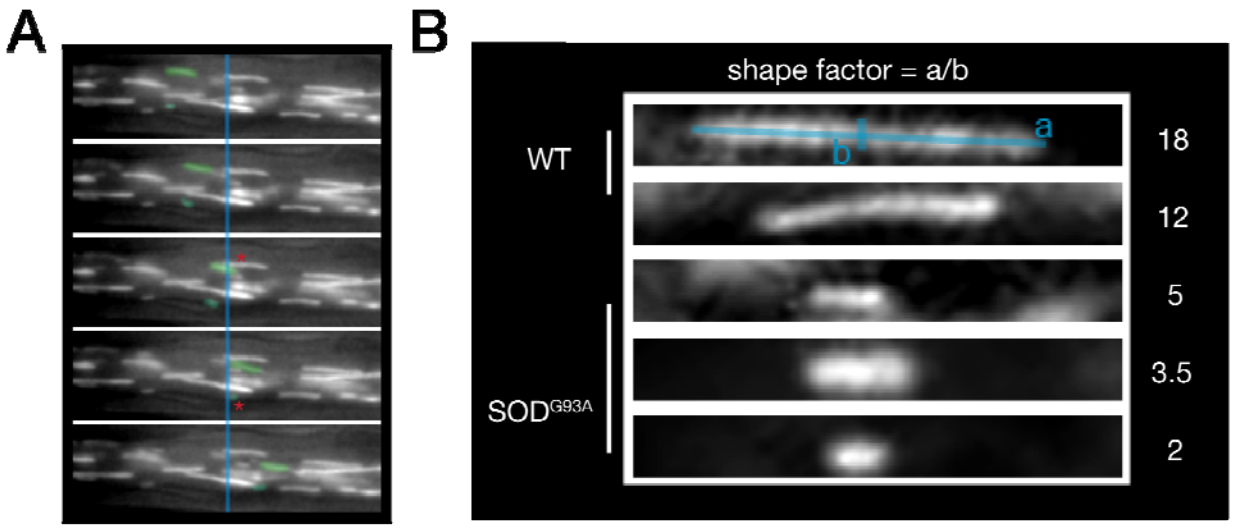

Figure 2.3 – Transport rate and shape factor measurements

(**A**) Transport measurements from wide-field movies. A sequence from a time-lapse movie showing two moving mitochondria (pseudo-green) crossing (red asterisk) the arbitrary line (blue).

(**B**) Shape factor measurements on single frames from wide-field movies obtained for transport measurements. Individual stationary mitochondria from WT and *SOD^{G93A}* mice and their shape factors values.

Shape factor measurements: Shape factor measurements were done on single frames from wide-field microscopy movies obtained for transport rates measurements (**Figure 2.3B**). Mitochondrial length and width were outlined using "line" tool in ImageJ and measured using "measure" function in ImageJ. Shape factor was calculated by dividing the length of the mitochondria by the width of the mitochondria.

Mitochondrial density: The mitochondrial density in axons was measured in single wide-field microscopy frames as the number of mitochondria per μm^2 of axonal area (as determined by the outline of the axon visible due to light scatter in myelin). As individual mitochondria cannot be resolved within synapses, mitochondrial density in synapses was measured as the area covered by mitochondria in the BTX-labeled area (in %; **Figure 2.4**). I first obtained high resolution confocal image stacks of NMJs. Maximum intensity projections were then generated using ImageJ/Fiji software. BTX channel image was processed using median filter (radius 2) in ImageJ/Fiji software. Next, all images were set to following grey values: 0 for minimum and 1000 for maximum and converted into 8 bit images. Finally, the images were converted into binary images using the "Otsu" auto-thresholding algorithm in ImageJ/Fiji. The ratio of labeled areas in the mitochondria and BTX channels was measured, restricted to regions of interest where the NMJ lay flat in the xy-plane.

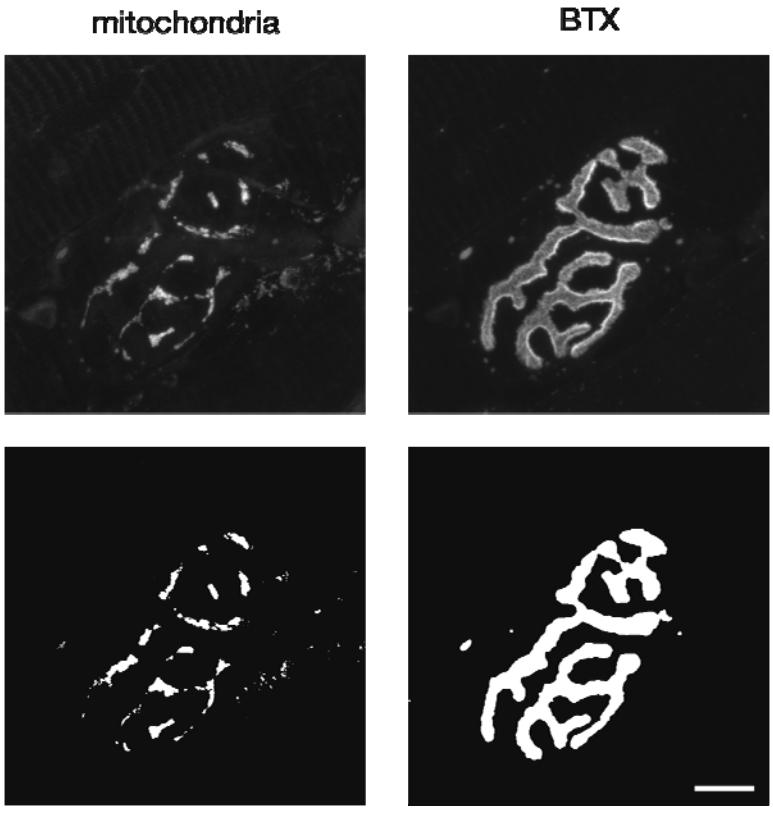

Figure 2.4 – **Mitochondrial density measurements in the synapses**

Images obtained on the confocal microscope for mitochondria and α-bungarotoxin staining of NMJs in the triangularis sterni (**upper panel**). Same images processed for mitochondrial coverage measurements using ImageJ/Fiji software (**lower panel**). Scale bar 10 μm.

Motor unit reconstruction: To analyse motor units, I first obtained triangularis sterni explants from *SOD^{G93A}, Thy1-MitoCFP*, *Thy1-YFP^{H}* triple-transgenic mice, measured transport in YFP-labeled single axons and reconstructed motor axons after fixation; axonal transport was found to be unaffected by YFP-expression in WT-controls at the ages examined here i.e. 4 months; however, beyond 6 months of age, transport was found to be selectively reduced in YFP-overexpressing axons, precluding use of these mice in later-onset *SOD^{G85R}* mice (see **Figure 3.17**; page 82). After transport measurements, I documented the imaging sites as well as complete motor unit by taking images with a ×4/ N.A. 0.13 air objective and a ×20/ N.A. 0.5 water-immersion dipping objective. The problematic places, where it was not easy to follow axon (axon branch points or sites where two or more YFP-overexpressing axons were intersecting), I documented additionally by taking images with ×100/ N.A. 1.0 water-immersion dipping objective. After imaging I fixed whole explant preparation by submersion in 4% PFA in 1×PBS for 2h. Subsequently I dissected the fixed muscle with the attached intercostal nerves from the thorax, mounted it in anti-fading agent on a slide and obtained tiled image series to cover the entire motor unit using a confocal microscope (FV-1000, Olympus) with a x20/ N.A. 0.85 oil objective (**Figure 2.5**). Individual NMJs within the motor unit were then scanned at full resolution (Nyquist limited pixel size of <100nm) using a x60/ N.A. 1.42 oil objective. I converted the individual image stacks into maximum intensity projections, montaged them to seamless panoramas using Photoshop software (Adobe) (Keller-Peck et al., 2001). I manually traced the axons to obtain “camera lucida”-like representations and scored the NMJs within the motor unit as “denervated” or “fully innervated” as described above.. Gamma was adjusted non-linearly to show low-intensity objects, and a “despeckle” filter was used to suppress detector noise.

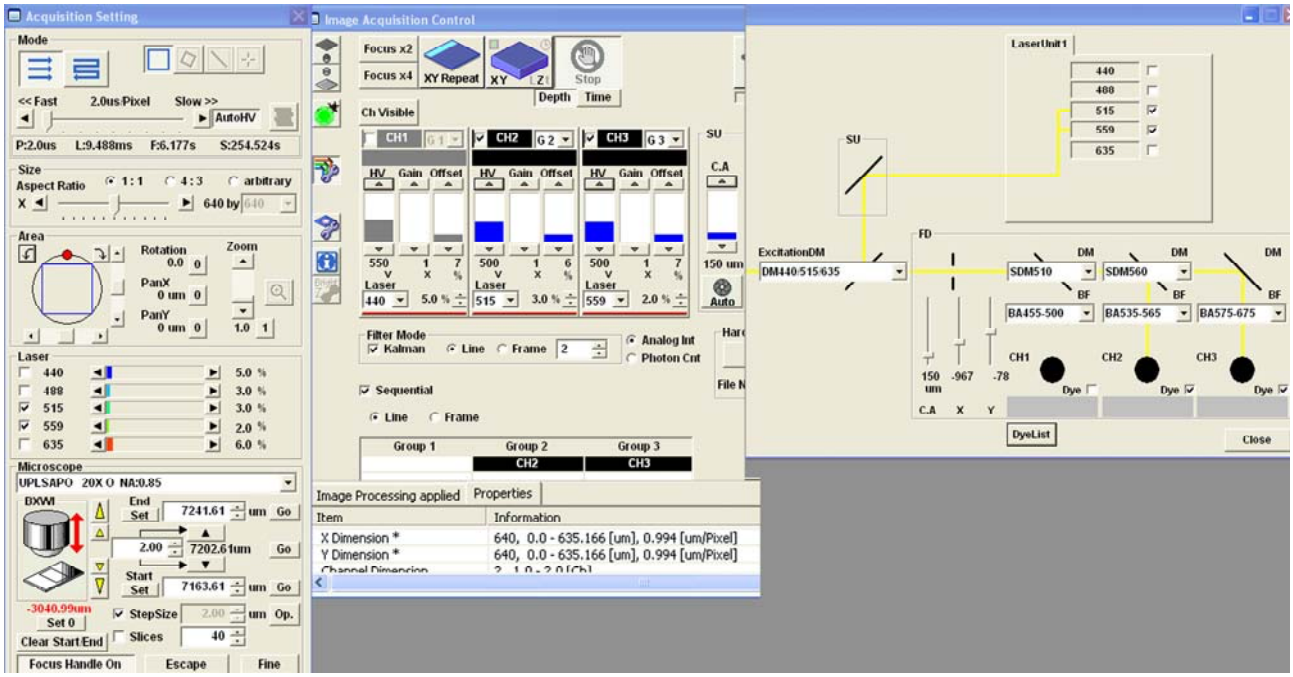

Figure 2.5 – Microscope settings for acquisition of motor unit reconstruction images

A screen shot of Fluoview software (Olympus) with settings used for acquisition of motor unit images. The images obtained in this way were used for motor unit reconstruction.

Single cargo analysis: Transport characteristics of individual photo-converted mitochondria and CTB-labeled vesicles were analyzed using MTrackJ ImageJ/Fiji plug-in (Fiji; developed by E. Meijering, Biomedical Imaging Group, Erasmus Medical Center, Rotterdam). A particle was considered to have paused if it moved al less than 2 pixels per s (0.25 μm^{-1}), which we estimate to be the precision limit of our measurements – periods between pauses were considered "runs". The following transport characteristics were measured: average speed (total displacement divided by the observation time), average moving speed (displacement during uninterrupted runs divided by the duration of the run), stop frequency (number of stops during an observation period divided by the duration of that period) and average stop length (averaged length of stops during an observation period). I included only mitochondria that could be tracked for at least 20s. Similarly, CTB-labeled vesicles (which move faster) were only considered when I could track them for 10s. Transport of synaptic vesicle precursors was quantified as total number of moving YFP positive objects per minute per µm of axon length.

2.13. Statistics

Significance was tested using t-tests (Excel software, Microsoft). * indicates $P<0.05$. Graphs indicate mean ± S.E.M unless stated otherwise.

2.14. Buffers and solutions

Agarose gel (2%)	
Reagent	Quantity for 50 mL of gel
Agarose	1 g
TAE (× 50) buffer	1 mL
H_2O	49 mL
Ethidium Bromide (0,1%)	25 µL

Add agarose into 50 mL 1 × TAE buffer, boil shortly, add 25 µL Ethidium Bromid (0,1%)

TAE (× 50)	
Reagent	Quantity for 500 mL of buffer
Tris BASE (MM 121g)	242 g
EDTA (0.5M; pH 8.0)	50 mL
Acetic acid	~ 50 mL

adjust pH to 8.0. with acetic acid at room temperature

Ethidium Bromide (0.1%)	
Reagent	Quantity for 500 mL of buffer
Ethidium Bromide (1%; #2218.1, ROTH)	60 µL
H_2O	540 mL

TBE (× 10)	
Reagent	Quantity for 500 mL of buffer
Tris BASE (MM 121g)	54 g
Boric acid	27.5 g
EDTA (0.5M; pH 8.0)	20 mL
H_2O	up to 500 mL

Autoclave the solution

DNA loading buffer	
Reagent	Quantity for 10 mL of buffer
Glicerol (80%;)	5 mL
Xylene-Cyanol FF (#38505.01, Serva)	25 mg
Bromphenolblue (Na)	25 mg
H_2O	up to 10 mL

PFA (4%)	
Reagent	Quantity for 1 L of buffer
PFA	40 g
H_2O	800 mL
NaOH (2N)	125 µL
PBS (10 ×)	100 mL

Mix PFA, H_2O and NaOH on heating plate (max 60°C) until the solution gets clear. Then, add PBS and adjust pH 7.2 – 7.5. Filter and aliquot. Store at -20°C

Blocking solutions	
Reagent	Quantity for 100 mL of solution
Goat serum (#G9023, Sigma)	10 mL
bovine serum albumin (#A3912, Sigma)	1g
Triton X-100 (#T9284, Sigma)	0.5 mL
NaN_3 (20% stock; Riedel de Häen,#13412)	50 µL
PBS (1 ×)	up to 100 mL

Ketamine-xylazine (KX)	
Reagent	Quantity for 20 mL of solution
Ketamine (#K2753, Sigma)	300 mg
Xylazine (#1251, Sigma)	20 mg
H_2O	up to 20 mL

Mix well, filter and aliquot the solution

Sucrose (30%)		
Reagent	Quantity (g for 1L)	Final concentration (mM)
Sucrose	30g	876.42
H_2O	up to 100mL	

adjust the pH to 7.4 using NaOH or HCl as necessary.

Phosphate-Buffered Saline (PBS) (10 ×)		
Reagent	Quantity (g for 1L)	Final concentration (mM)
NaH_2PO_4	2.56	18.6
Na_2HPO_4	11.94	84.1
NaCl	102.2	1750

Adjust the pH to 7.4 using NaOH or HCl as necessary, Optional: add 500 µL of 20% NaN_3

Ringer's solution (10 ×)		
Reagent	Quantity (g for 1L)	Final concentration (mM)
$NaHCO_3$	21.84	260
NaH_2PO_4* H_2O	1.72	12.5
KCL	1.86	25
NaCL	73.05	1.2
H_2O	to 1L	

Ringer's solution (1×)		
Reagent	Quantity (ml for 1L)	Final concentration (mM)
$CaCl_2$, 1M	2	2
H_2O	900	
$MgCl_2$, 1M	1	1
Ringer's solution (10 ×)	100	20
Glucose	3.6g	

$CaCl_2$ and $MgCl_2$ are prepared monthly as 1M stock solutions. Reagents are mixed on the day of the experiment in the order listed. Ringer's solution (1 ×) was bubbled with 95% O_2 5% CO_2 for at least 30min before use. Without 95% O_2 5% CO_2 pH of the 1 × Ringer's solution should be 7.8 and 7.3 after 30 min of bubbling with 95% O_2 /5% CO_2.

3. RESULTS

3.1. SOD copy number and expression levels in transgenic mouse lines

In this study I used transgenic mice lines which carry mutated (*SOD^{G93A}*, *SOD^{G37R}* and *SOD^{G885R})* or non-mutated (*SOD^{WT}*) form of human SOD gene. These lines carry different number of transgene copies inserted into the genome, which can cause different expression levels of SOD protein. Mice that were used in this study were purchased from Jackson laboratory and therefore should have the number of copies previously reported (Gurney et al., 1994; Bruijn et al., 1997; Wong et al., 1995). However, it is known that during colony breeding spontaneous changes of copy number can happen due to recombination events during meiosis (Alexander et al., 2004). To confirm that the animals used in this study had expected copy number, quantitative PCR was kindly performed by my colleague Dr. Monika Brill. Results showed following ΔCT values SOD^{G93A} 7.1; SOD^{G85R} 5.8; SOD^{WT} 6.2, which is within expected range. Copy number calculations based on SOD^{G93A} value gave following results: 10 copies in SOD^{G85R} and 13 copies in SOD^{WT}. While the calculated value for SOD^{G85R} is within expected range (Bruijn et al., 1997), the value for SODWT is higher than values previously reported in the literature (7.2 ± 2.4; Gurney et al., 1994).

Further, Dr. Monika Brill quantified SOD expression levels by immunohistochemistry in the motor neurons of the cervical-thoracic spinal cord (**Figure 3.1**).This is the region where the motor neurons which innervate the triangularis sterni muscle are located (confirmed by retrograde tracing in a previous experiment that I performed). The measurements showed, as expected, that SODG93A mice have the highest expression of human SOD protein. However the levels of the expression in SODG885R and SODWT mice appear to be very similar. This result is contrast to what is reported in the literature (Gurney et al., 1994; Bruijn et al., 1997). In previous studies, measurements were done on whole brain or spinal cord homogenates. Here we perform direct measurements in the cells of interest. The staining pattern also differs between the lines. In *SOD^{G93A}* mice

staining shows SOD positive punctae in cytoplasm implying aggregation of human SOD. In contrast, In *SOD*^{G885R} and *SOD*^{WT} mice staining pattern is uniform across the cytoplasm.

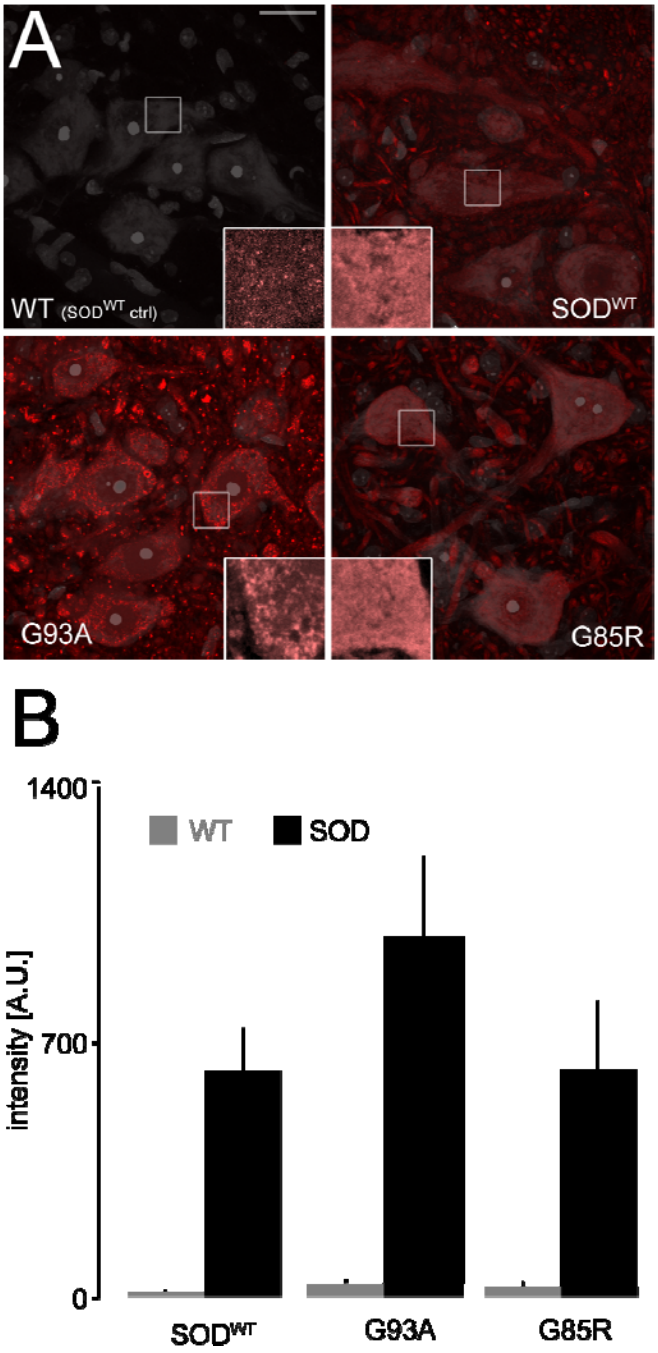

Figure 3.1 – SOD expression in different transgenic lines (figure courtesy Dr. Brill)

(**A**) Motor neurons in cervical-thoracic spinal cord stained against human SOD in different SOD lines.

(**B**) SOD expression levels quantified by measuring fluorescence intensities in arbitrary units (A.U.) in motor neurons of different SOD lines (n > 2 mice per phenotype, > 25 cells per animal).

3.2. Axonal transport in *SOD*^{G93A} mice

3.2.1. Disease course, clinical symptoms and denervation in *SOD*^{G93A} mice

I first investigated the most commonly used ALS animal model, the *SOD*^{G93A} mice. In this model, mutant mice start to develop clinical symptoms of disease (weight loss and muscle weakness) around 3-4 months of age (**Figure 3.2A**). During the same time period, denervation of neuromuscular junctions (NMJs) becomes apparent in various muscles, including the gastrocnemius and triangularis sterni muscles (**Figure 3.2B).** Denervation occurs earlier and it is more profound in the gastrocnemius muscle (**Figure 3.2B)**.

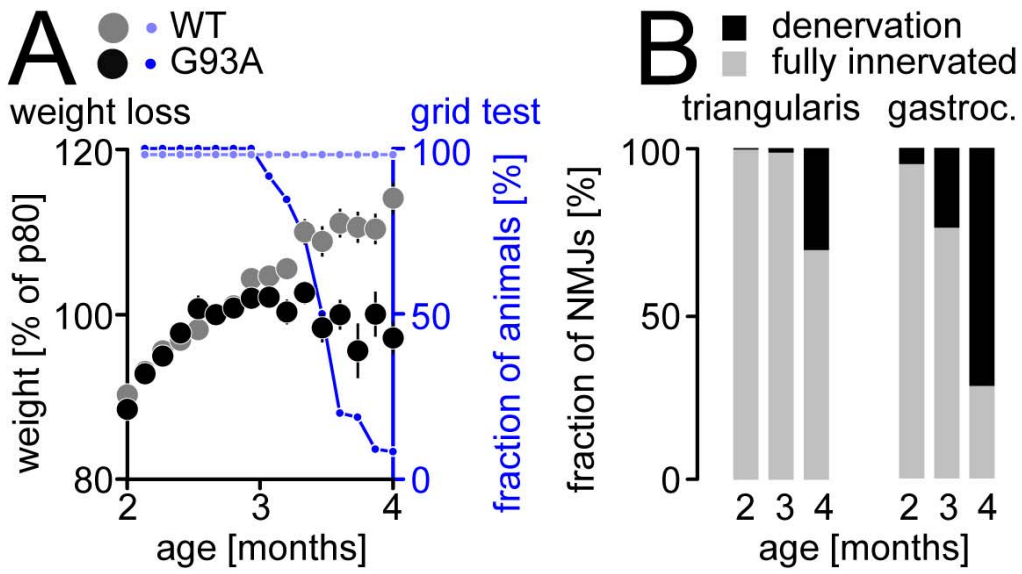

Figure 3.2 – Time-course of clinical symptoms and denervation in *SOD*^{G93A} *mice*

(**A**) Time-course of body weight (in % of weight at P80, mean ± S.E.M) and grid test performance (expressed as % of tested mice) of *SOD*^{G93A} and wild-type (WT) mice (n > 10 mice per genotype and time-point).

(**B**) Time-course of denervation in triangularis sterni and gastrocnemius muscles of *SOD*^{G93A} mice (n > 5 mice, > 1500 synapses).

3.2.2. Reduced mitochondrial density in axons and synapses of *SOD*^{G93A} mice

SOD^{G93A} mice showed a reduced density of mitochondria in axons and NMJs in the triangularis muscle at 4 months of age (postnatal (P) day 120) (**Figure 3.3A, B**). A reduced density was also observed in motor axons in the intercostal and tibialis nerves, but not in ALS-resistant sensory axons in the saphenous nerve (**Figure 3.3B**). Similar changes were observed in NMJs of the gastrocnemius muscle (35.7 ± 1.3 % mitochondrial coverage in control mice vs. 18.8 ± 1.0 in *SOD*^{G93A} mice; mean ± SEM; $p < 0.05$).

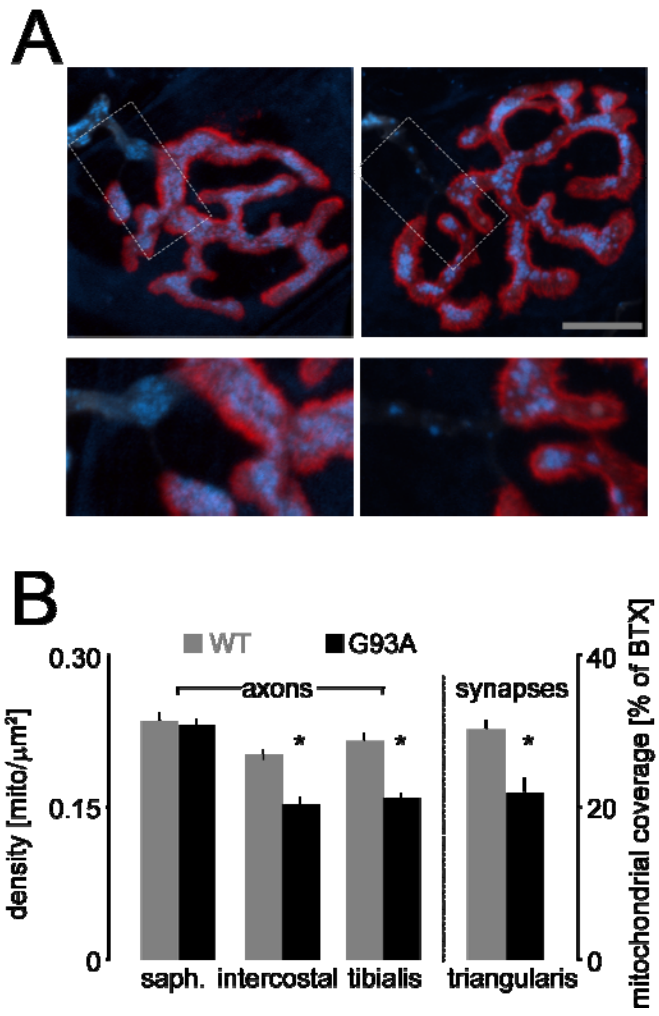

Figure 3.3

Reduced mitochondrial density in axons and synapses of *SOD*^{G93A} mice

(**A**) Confocal images of mitochondria (cyan) contained in presynaptic axons (gray), which overlie synaptic sites (stained with Alexa594-conjugated α-bungarotoxin, red) in triangularis sterni muscles of wild-type (WT, **left**) and *SOD*^{G93A} (G93A, **right**) mice fixed 4 months after birth.

(**B**) Quantification of mitochondrial density in intercostal nerve axons (n > 35 axons, n = 4-6 mice for each condition), saphenous (saph.) nerve axons (n > 45 axons, n = 8 mice), tibialis nerve axons (n > 40 axons, n = 4 mice) and of mitochondrial coverage in triangularis sterni synapses (n > 125 NMJs, n = 4-5 mice) of *SOD*^{G93A} and WT mice fixed 4 months after birth.

Scale bar, 10µm in (**A**). *, $P < 0.001$.

3.2.3. Reduced mitochondrial transport in motor axons of *SOD^{G93A}* mice

To investigate underlying mechanism of neurodegeneration observed in *SOD^{G93A}*, I measured axonal transport of mitochondria in nerve that innervated affected muscles. Measurements of mitochondrial transport revealed reduction in number of transported mitochondria (transport flux; mito/min) in motor axons of *SOD^{G93A}* mice at 4 months of age (**Figure 3.4A**). A reduction in anterograde and retrograde transport was observed in motor axons of intercostal and tibialis nerve (**Figure 3.4B).** Changes in mitochondrial morphology are also evident in motor axons. Mitochondria in motor axons of *SOD^{G93A}* mice appeared shorter and swollen in contrast to WT axons, where mitochondria have an elongated morphology (**Figure 3.4A**).

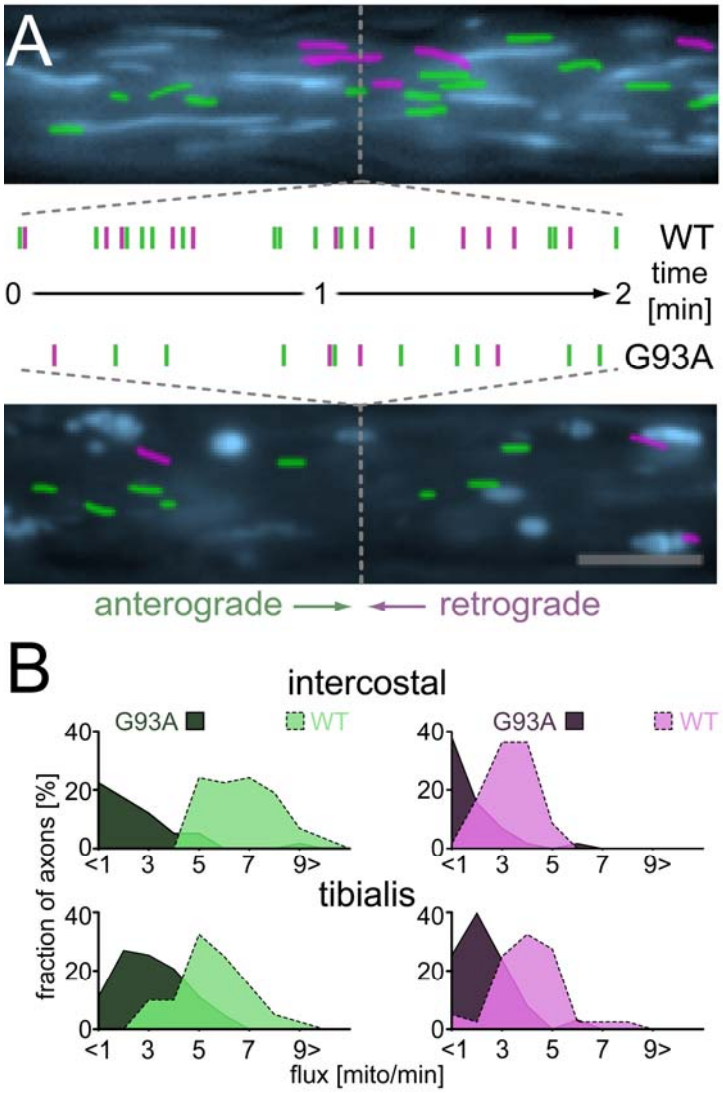

Figure 3.4 – Reduced mitochondrial transport in motor axons of *SOD^{G93A}* mice

(**A**) Wide-field images of intercostal axons in *SOD^{G93A}* and WT mice generated by averaging 50 frames of a time-lapse movie. Stationary mitochondria, cyan. Moving mitochondria from the 1st, 25th and 50th frames of the movie are superimposed as pseudo-coloured masks (green, anterograde moving mitochondria and magenta, retrograde moving mitochondria). **Middle panel**, "event diagram" indicating the time when moving mitochondria crossed an arbitrarily placed line (dashed gray) over 2 minutes of time-lapse imaging (green, anterograde movement; magenta, retrograde movement).

(**B**) Frequency distribution of anterograde and retrograde mitochondrial flux in axons of intercostal (**upper panel**) and tibialis nerves (**lower panel**) from *SOD^{G93A}* (n > 40 axons, n = 4 mice) and WT mice (n > 50 axons, n = 6 mice)

Scale bar, 5μm in (**A**).

3.2.4. Mitochondrial transport is unaffected in saphenous nerve of *SOD*^{G93A} mice

To investigate if transport deficits are specific for motor axons as it would be expected for the motor neuron disease ALS, I measured mitochondrial transport in pure sensory saphenous nerve. Measurements revealed normal transport fluxes in sensory axons of saphenous nerve of *SOD*^{G93A} mice at 4 months of age (**Figure 3.5A**).

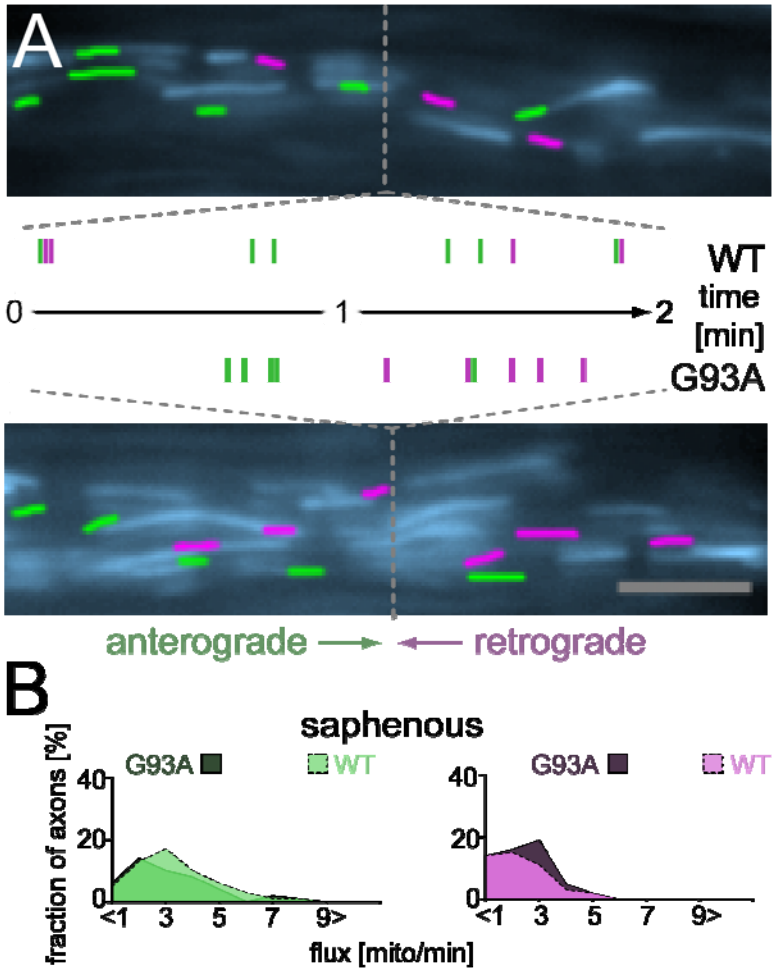

Figure 3.5 – Mitochondrial transport is unaffected in sensory axons of saphenous nerve in *SOD*^{G93A} mice

(**A**) Wide-field image of saphenous axons generated and labelled as described for **Fig. 3.4A**

(**B**) Frequency distribution of anterograde and retrograde mitochondrial flux in axons of saphenous nerve from *SOD*^{G93A} (n = 56 axons, n = 8 mice) and WT mice (n =45 axons, n = 8 mice)

Scale bar, 5µm in (**A**).

3.2.5. Tibialis nerve composition

The tibialis nerve comprises sensory and motor axons. To assess the contribution of the sensory component and a possible sensory "contamination" of my results, I performed two sets of experiments. First I looked at tibialis nerves of crosses between *Chat-cre* transgenic and *Rosa-tdTomato* reporter mice (**Figure 3.6A**) obtained from the Jackson Laboratory (Madisen et al., 2010). I found that the cholinergic (motor) component of the nerve is only about 50% (47 ± 6%, mean ± S.E.M., n = 4 nerves), However, the motor axons tend to be at the surface of the nerve. Further, I placed such a nerve into the recording chamber in the usual orientation used for transport measurements (**Figure 3.6B**). In this setting, I determined the percentage of tdTomato$^+$ axons (and hence cholinergic motor axons) of all myelinated axons as seen by oblique illumination. I found that ~75% of all axons that I could image are cholinergic, a clear enrichment over the nerve's composition (**Figure 3.6B**).

Second, I determined the size distribution of axons that I included into mitochondrial flux measurements (usually I image thick axons, as the *Thy1*-promotor biases for such axons) and compared this to the diameter distribution of superficial sensory axons as labeled by anterograde tracing by virus injection into the L4 dorsal root ganglion (kindly performed and provided by Anne Ladwig) (**Figure 3.6C**). This showed that the axon population measured for the transport assays was on average much thicker (5.4 ± 0.1µm) than sensory axons (2.3±0.3µm) further reducing any sensory "contamination" in my measurements (**Figure 3.6C**).

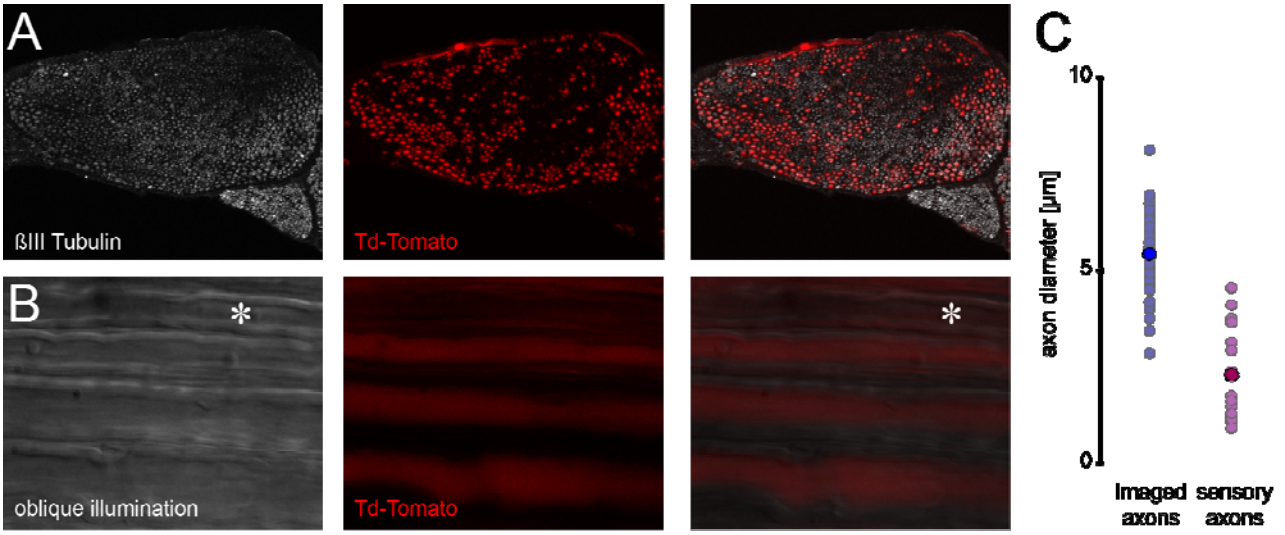

Figure 3.6 – Tibialis nerve composition

(**A**) Tibialis nerve cross-section from a *Chat-cre*, A14 (Td-Tomato reporter) mouse (red), counter-stained with a neuron-specific βIII tubulin antibody (grey).

(**B**) When placed into the recording chamber, the majority (75%) of axons revealed by oblique illumination is positive for the cholinergic marker. The asterisk marks a putative sensory (non-cholinergic) axon.

(C) A further enrichment for motor axons in my data results from the diameter bias of the *Thy1*-promotor (left), which excludes most of the sensory axons (right, here revealed by anterograde labeling via an injection of adeno-associated virus into the 4th lumbar dorsal root ganglion, from where some sensory axons project into the tibialis nerve).

3.2.6. Single mitochondrion tracking using new mouse transgenic line *Thy1-MitoKaede* reveals changes in transport characteristics in *SOD^{G93A}* mice

For single mitochondrion tracking, I used transgenic mice which express photo-convertible fluorescent protein, Kaede, selectively in neuronal mitochondria (*Thy1-MitoKaede mice*). The principle of the experiment is shown in **Figure 3.7**. First, I photo-converted a spatially restricted population of mitochondria from green to red fluorescence using 405nm light (**Figure 3.7A**). By imaging the axons either distal or proximal to the site of photo-conversion, I could track the anterograde or retrograde movement of individual red mitochondria amidst their non-photo-converted green counterparts (**Figure 3.7B**). Analysis of single mitochondria movement revealed a decrease in average speed of mitochondria (average speed = total displacement divided by the observation time). The average speed was decreased due to significant changes in stop length and frequency (**Figure 3.8A**). The distribution of stop length showed that the vast majority (~90%) of stops made by mitochondria in WT axons are shorter than 5s and that only ~ 6% of stops are longer that 10s. This fraction is increased in *SOD^{G93A}* axons: here, ~11% of stops were longer than 10s.

In parallel, I performed tracking of single mitochondria in wide-field movies that I obtained for transport rate measurements (**Figure 3.25**). In these movies it is not possible to measure stop length and frequency due to dense mitochondrial labeling in the *Thy1-MitoCFP* line Therefore, the only parameter that I could reliably measure is average speed. Here, I could also detect clear reduction in average speed confirming the data obtained in *Thy1-MitoKaede mice*.

To explore whether these changes in transport are specific to mitochondria I investigated axonal transport of endosomes, another often investigated cargo in axonal transport studies. In order to label endosomes I injected Cholera Toxin Subunit B (CTB) conjugated to the fluorescent dye Alexa-594 into the triangularis sterni muscle *in vivo*. The CTB-dye complex is endocytosed into the axons at NMJs and transported retrogradely. By imaging intercostal axons 24h after injection, I found that transport of CTB-labeled

vesicles was affected in a similar manner as mitochondrial transport. This suggests a possible general transport deficit of organelles in *SOD*^{G93A} mice (**Figure 3.8B**).

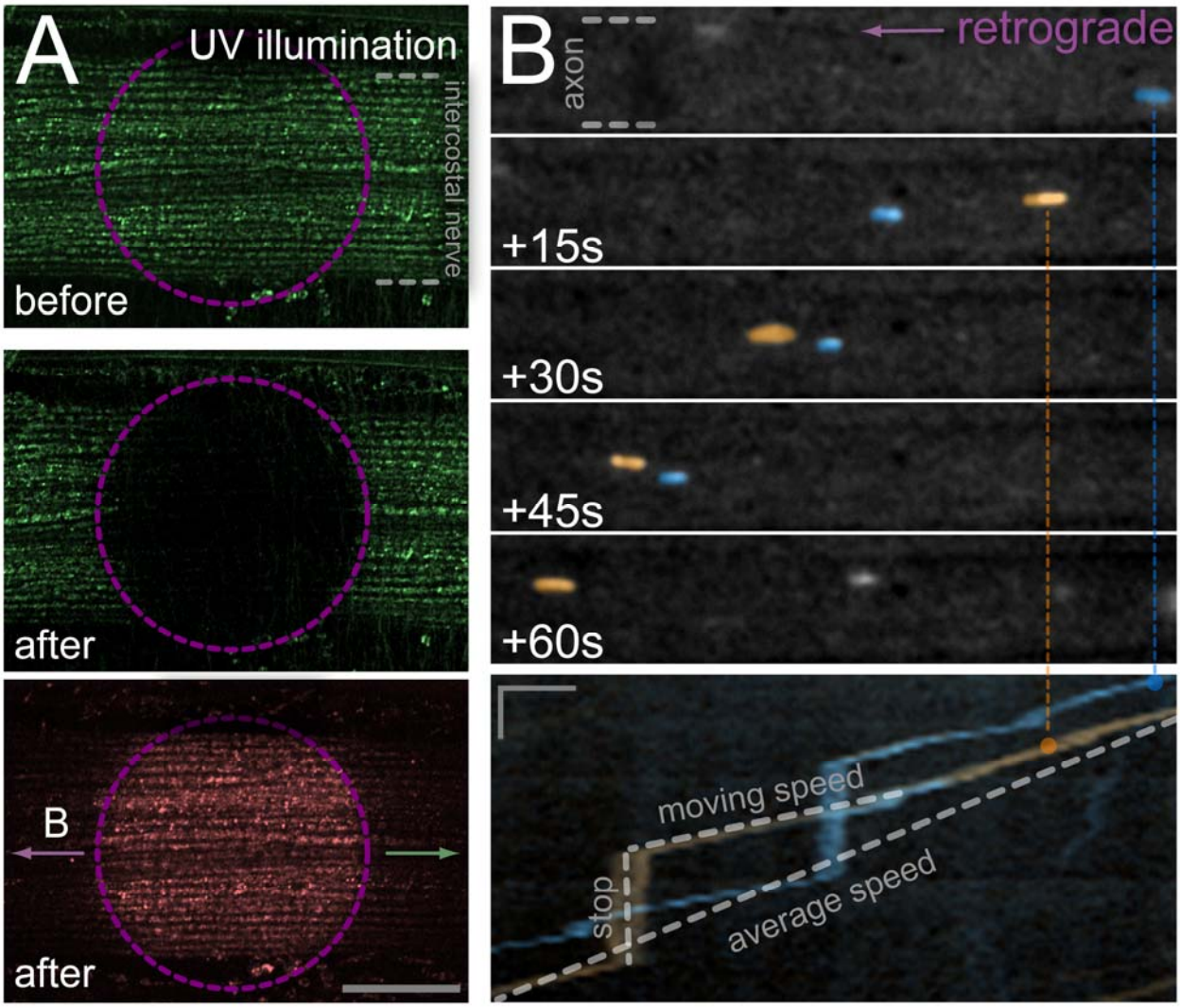

Figure 3.7 – Single mitochondria tracking in *Thy1-mitoKaede* mice

(**A**) Intercostal nerve in a *Thy1-mitoKaede* mouse before (**top**, green channel) and after (**middle**, green channel; **bottom**, red channel) localized photo-conversion (UV-exposed area outlined in magenta).

(**B**) **Top**, time-lapse images of photo-converted mitochondria (pseudo-coloured blue and brown). **Bottom**, corresponding kymograph.

Scale bars, 100μm in (**A**); 10s in y and 10μm in x in (**B**).

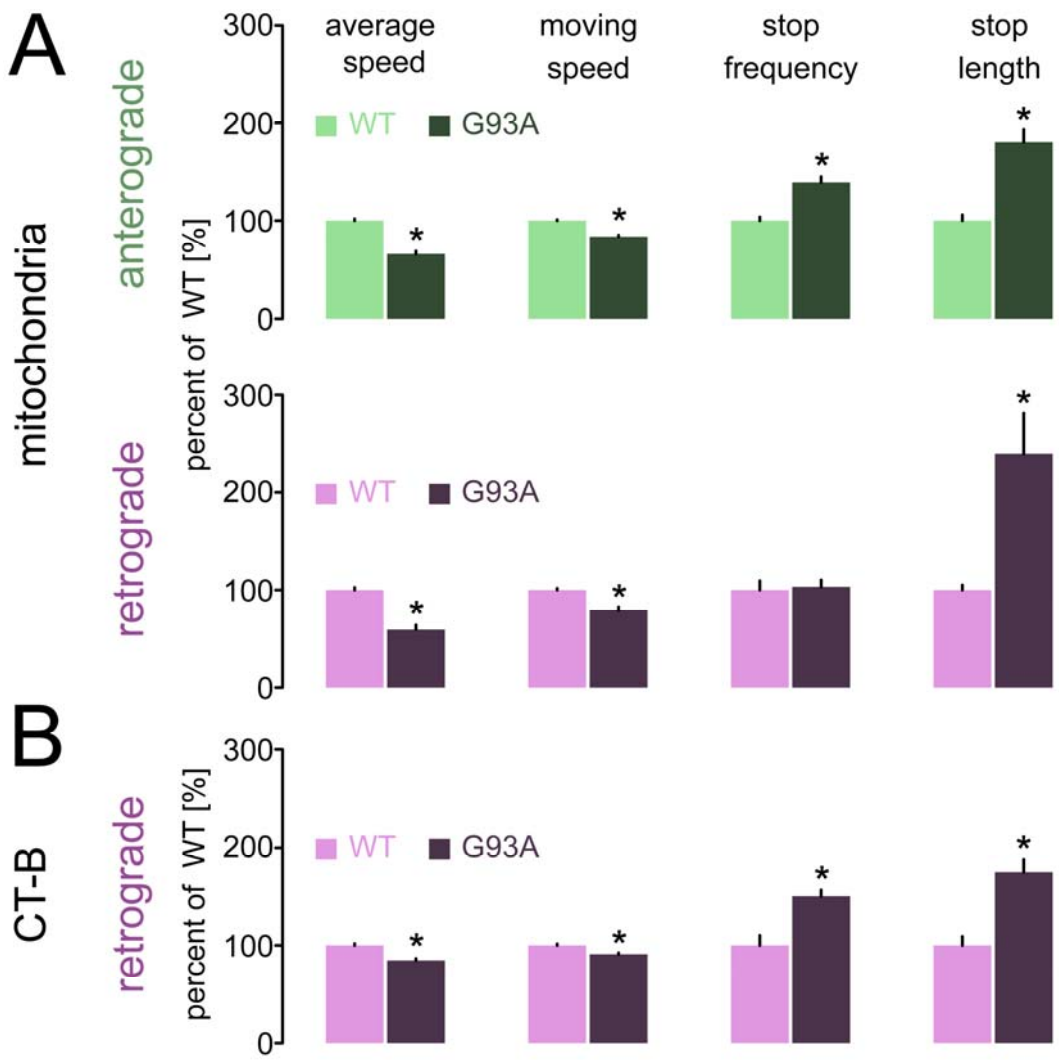

Figure 3.8 – Reduced speed and increased stop length of mitochondria and vesicles in *SOD*^{G93A} mice

(**A**) Transport characteristics of individual mitochondria (n = 195-386 mitochondria; n ≥ 29 axons; n = 4 mice) at 4 months of age. Values are expressed as mean percentage ± S.E.M. of WT control.

(**B**) Single-cargo transport characteristics of individual CTB-labelled vesicles (n = 384-386 vesicles; n ≥ 24 axons; n = 4 mice) at 4 months of age. Values are expressed as mean percentage ± S.E.M. of WT control.

*, $P < 0.05$

3.2.7. Transport of synaptic vesicles precursors in *SOD^{G93A}* mice

I also imaged transport of synaptic vesicles precursors using *Thy1-synaptophysin7 YFP*, *SOD^{G93A}* double transgenic mice. However, imaging transport in triangularis sterni explant preparations derived from these mice turned out to be difficult for several reasons. First, in these mice YFP aggregates are detectable with increasing age. Therefore, it is impossible to distinguish between aggregates and normal, physiologically occurring vesicles. Second, resolving transport and tracking of individual vesicles proves to be very challenging because of their small size (~50 nm) and dim labeling. Additionally, high background prevented reliable assessment of vesicle transport. Therefore, transport was quantified as total number of moving YFP-positive objects per minute per micron of axon length. The measurements at 4 months of age showed a trend towards a reduction (84% ± 17% of moving synaptophysin-positive particles in 4 months old SOD^{G93A} *vs.* littermate controls set to 100%; mean ± S.E.M.), but this was not statistically significant, and one of four experiments failed to show the effect (**Figure 3.9**).

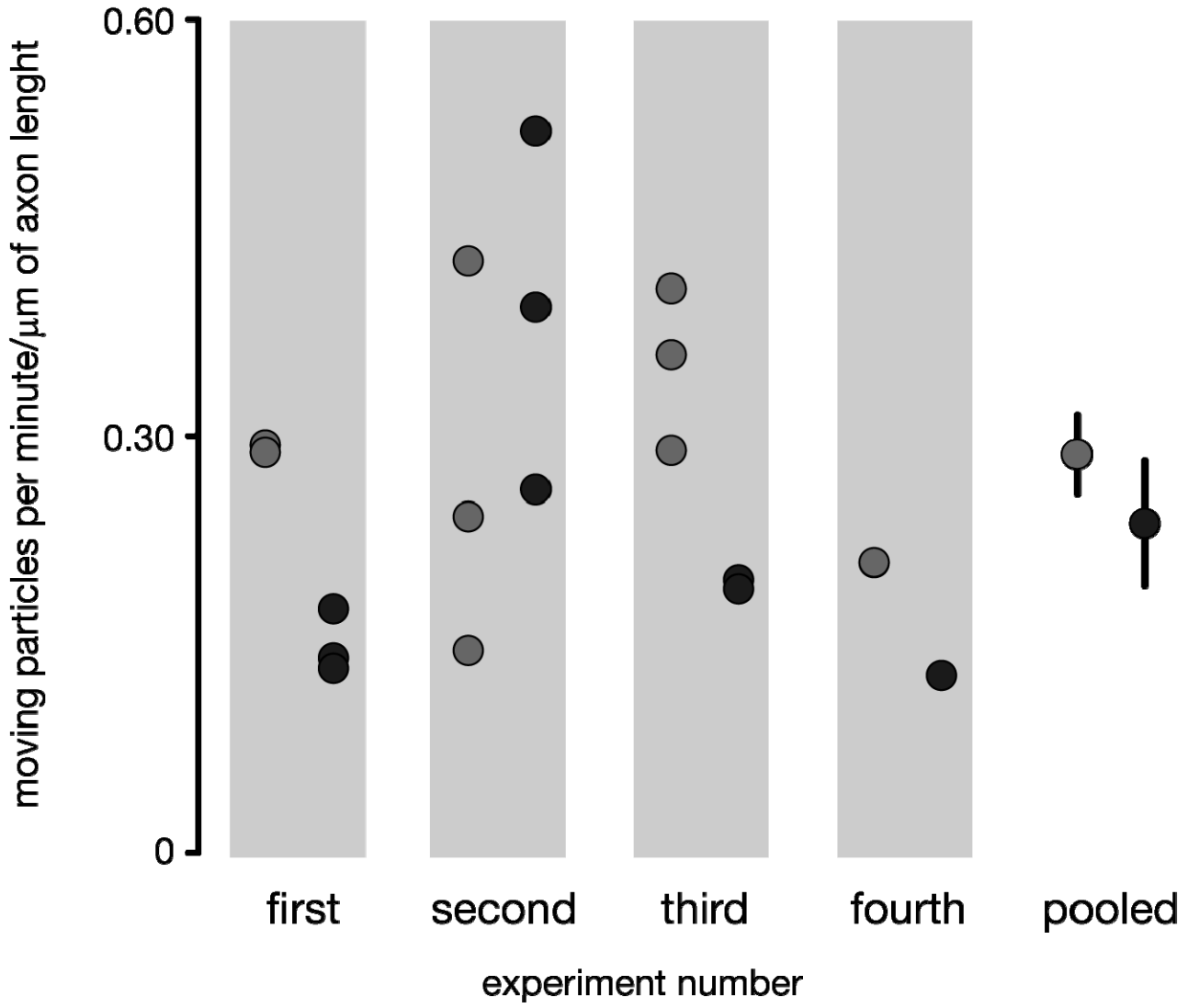

Figure 3.9 – Transport of synaptic vesicles precursors in *SOD^{G93A}* mice

Transport of synaptic vesicles precursors was measured in four independent experiments and average values of several axons for each animal are represented as individual data points (WT black circles, *SOD^{G93A}* grey circles). Pooling all the data together showed no difference between *SOD^{G93A}* and WT mice at 4 months of age (n = 143 axons and n = 9 mice for WT; n = 122 axons and n = 9 for *SOD^{G93A}*). Error bars (S.E.M.).

3.2.8. Transport deficits precede disease onset in *SOD*^{G93A} mice

To investigate when during the disease course transport deficits first appear, I measured mitochondrial flux in *SOD*^{G93A} mice between 10 days and 4 months after birth. Deficits were detectable as early as postnatal day (P) 20 for anterograde transport and P40 for retrograde transport (**Figure 3.10**). To confirm that the transport deficits found in *SOD*^{G93A} mice are not due to the insertion site of the transgene in this mouse line, we compared them to a very similar model of ALS, *SOD*^{G37R} mice (Wong et al., 1995). Also in this model, which has similar disease onset, transport deficits were evident at presymptomatic stages (2 months of age; **Figure 3.10**).

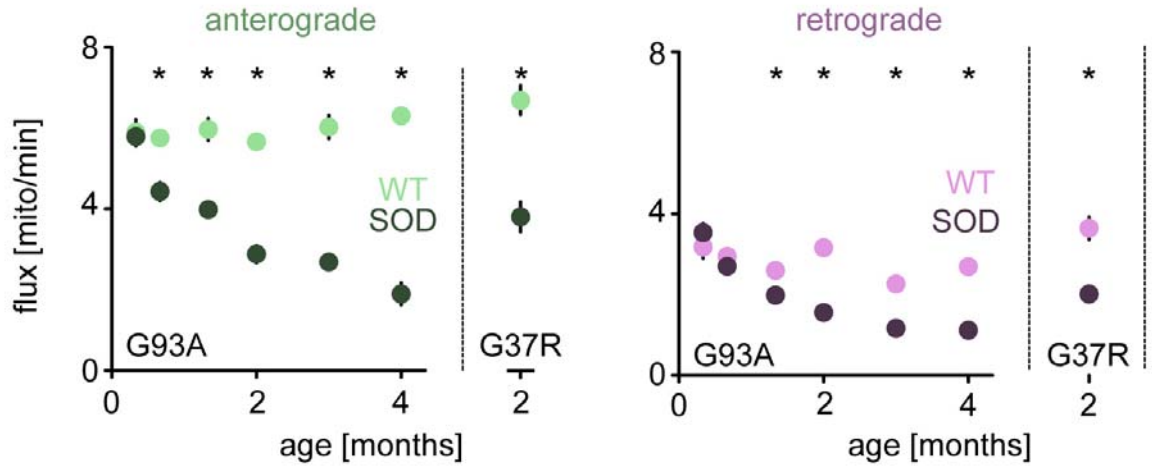

Figure 3.10 – Early onset of transport deficit in intercostal axons of *SOD*^{G93A} mice

Mitochondrial flux in intercostal of *SOD*^{G93A} and WT mice (n > 30 axons, n ≥ 4 mice per time-point) as well as in intercostals nerves of *SOD*^{G37R} mice (n = 45 axons, n = 2 mice). Error bars (S.E.M.) smaller than data symbols in most cases.

*, $P < 0.05$

3.2.9. Mitochondrial density in intercostal axons over disease course in *SOD^{G93A}* mice

The mitochondrial density is reduced in motor axons and synapses in *SOD^{G93A}* mice at 4 moths of age (**Figure 3.3**). However, transport deficits emerge much earlier during disease course (**Figure 3.10**). To further investigate relationship between these two transports and density, I measured the mitochondrial density over the disease course in intercostal axons of *SOD^{G93A}* mice (**Figure 3.11**). The results show that the drop in density is first evident at two months of age indicating that the neurons can maintain normal mitochondrial density for certain period of time despite profound transport deficits. This result suggests existence of compensatory mechanisms in motor axons.

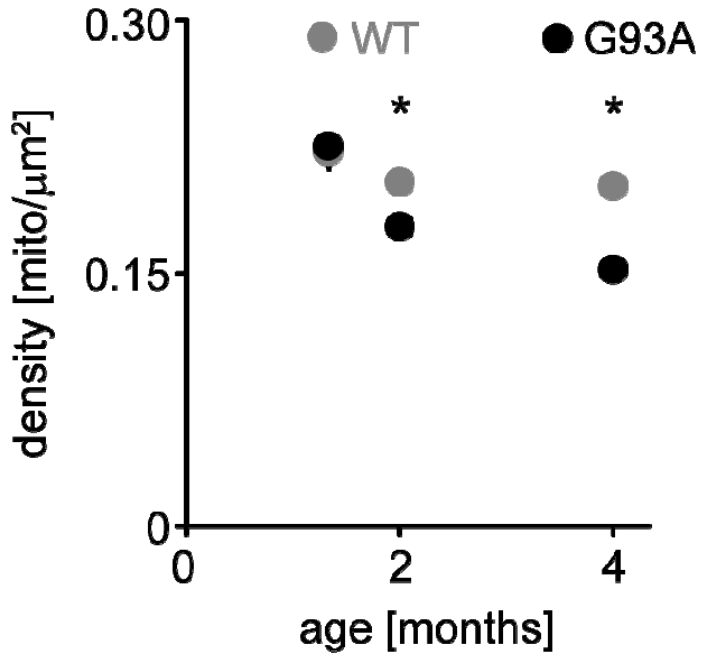

Figure 3.11 – Time-course of mitochondrial density in intercostal nerve axons

Time-course of mitochondrial density in intercostal nerve axons of WT (grey circles) and *SOD^{G93A}* mice (black circles).The 4 months time-point corresponds to data shown in **Fig 3.3B**. Values are expressed as mean ± S.E.M. Error bars (S.E.M.) are smaller than data symbols in most cases.

*, $P<0.05$.

3.2.10. Anterograde transport deficits precede deficit in retrograde transport in individual axons in *SOD^{G93A}* mice

The mean transport values suggest emergence of anterograde deficit first in the disease course (**Figure 3.10**). Still, it is possible that some of the axons are affected simultaneously or in reverse order by transport deficits (i.e. first retrograde followed by anterograde deficit). Moreover, there could be a group of axons not affected by transport deficits at all. To better understand these changes, I examined the correlation of anterograde with retrograde transport within individual axons. The results showed that also in individual axons, anterograde transport deficits precede retrograde transport changes in SOD^{G93A} mice (**Figure 3.12**). No transport deficits are detectable at P10 (**upper panel**). However, at P20, a population of axons in *SOD^{G93A}* mice (black diamonds) shows a deficit in anterograde transport, while retrograde flux still appears normal (**middle panel**). At P40, the majority of axons in *SOD^{G93A}* mice (black diamonds) is affected by anterograde and retrograde transport deficit (**lower panel**).

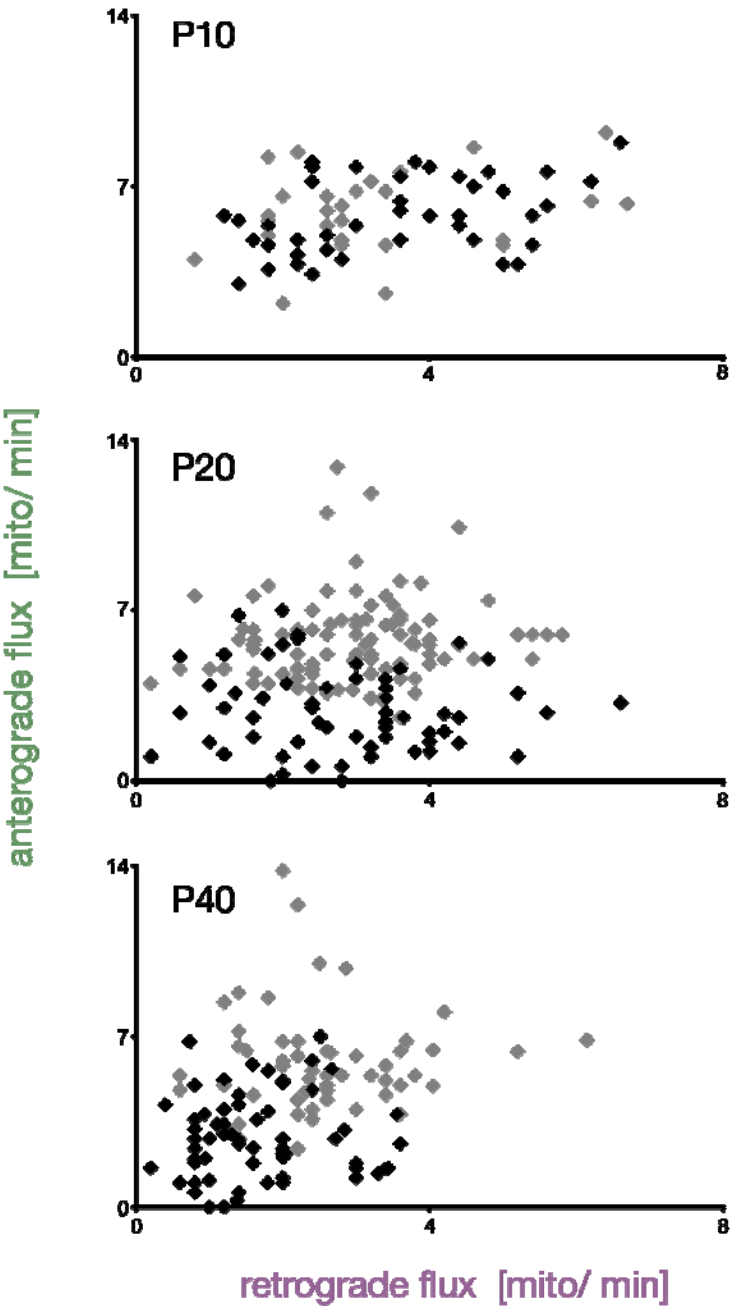

Figure 3.12 – Correlation of anterograde and retrograde transport in intercostal axons of *SOD^{G93A}* mice

Anterograde *vs.* retrograde mitochondrial flux in individual axons of WT (gray diamonds) and *SOD^{G93A}* mice (black diamonds) at P10 (**upper panel**), P20 (**middle panel**) and P40 (**lower panel**).

3.2.11. Axonal transport deficits affect all axons irrespective of their diameter

To investigate whether axons diameter confers a susceptibility for transport deficits, I also plotted total transport (anterograde plus retrograde) against axon diameter at different time points (P40, P60 and P120) (**Figure 3.13**). Such plots did not revealed correlation between total transport (or transport deficits) and axon diameter.

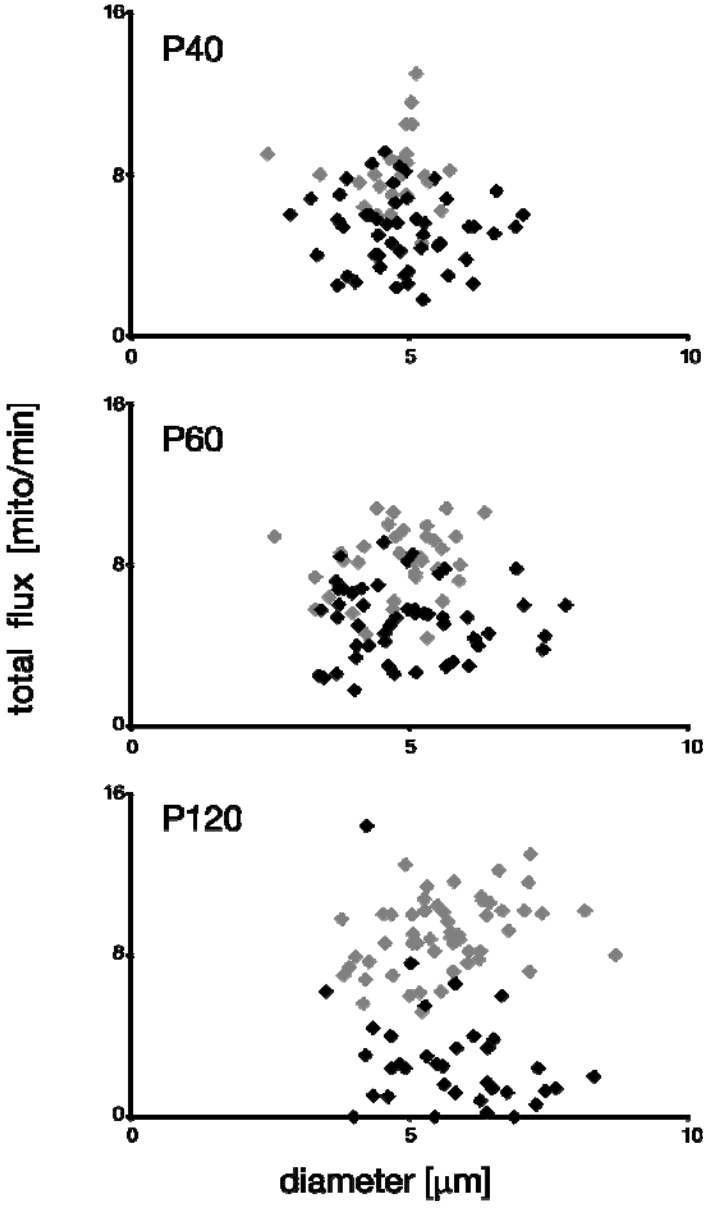

Figure 3.13

Correlation of total transport and diameter of intercostal axons in *SOD^{G93A}* mice

Total transport plotted against diameter of individual axons of WT (gray diamonds) and *SOD^{G93A}* mice (black diamonds) at P40 (**upper panel**), P60 (**middle panel**) and P120 (**lower panel**)

3.2.12. Early changes in mitochondrial morphology in *SOD^{G93A}* mice

To investigate changes of mitochondrial morphology I measured shape factor (mitochondrial length/width ratio) in *SOD^{G93A}* mice over disease course. Shape factor measurements revealed that mitochondrial morphology in axons was altered as early as P20 (**Figure 3.14**). Correlative analysis of transport and shape factor for single axons revealed that alternations in mitochondrial morphology precede decrease in axonal transport in motor axons in SOD^{G93A} mice. Note the population of axons in *SOD^{G93A}* mice (black diamonds) with low shape factor but still normal transport at P20 (**Figure 3.15**).

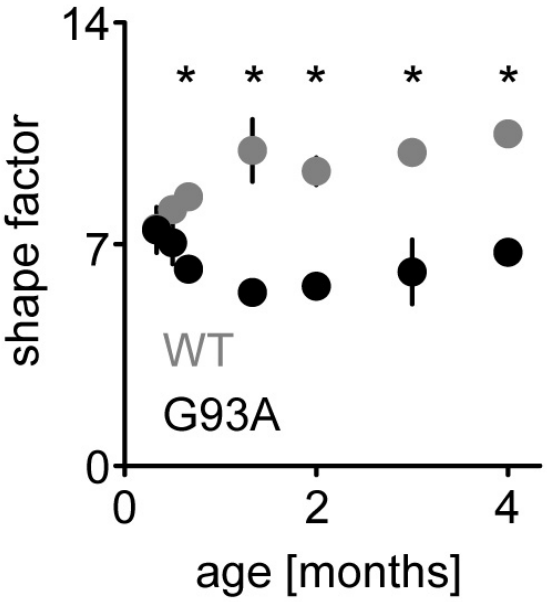

Figure 3.14 – Early changes in mitochondrial morphology in intercostal axons of *SOD^{G93A}* mice

Mitochondrial shape factor in intercostal axons of *SOD^{G93A}* (black circles) and WT (grey circles) mice (n > 20 axons, n ≥ 2 mice per time-point and phenotype). Error bars (S.E.M.) smaller than data symbols in most cases.

*, P<0.05.

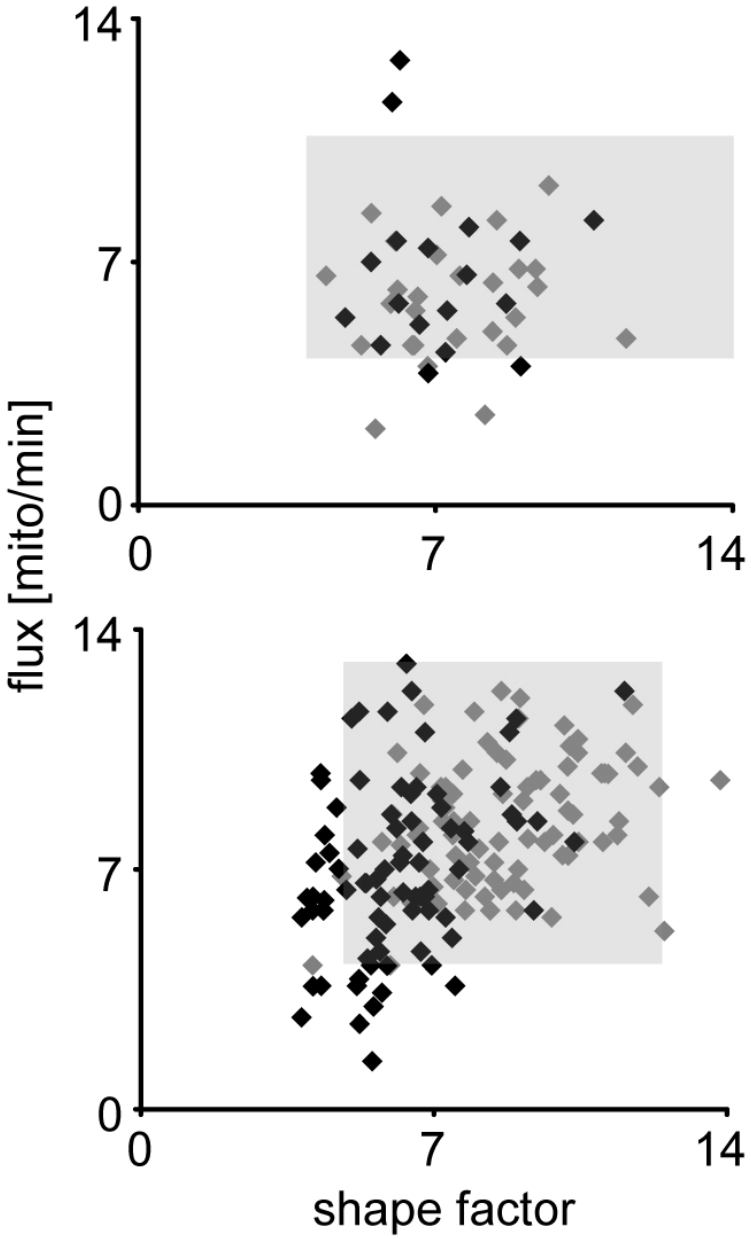

Figure 3.15 – Changes in mitochondrial morphology precede onset of transport deficit in intercostal axons of *SOD^{G93A} mice*

Correlation of mitochondrial shape factor with total (anterograde plus retrograde) mitochondrial transport in intercostal axons of *SOD^{G93A}* mice (black diamonds) at 10 days after birth (**top;** n > 24 axons, n > 3 animals) and 20 days after birth (**bottom;** n > 80 axons, n > 6 animals). Grey areas are representing the spread (mean ± 2 × standard deviations) of WT shape factor and transport values (grey diamonds).

3.2.13. Shape factor and volume of moving mitochondria in *SOD*^{G93A} mice

To explore whether transported mitochondria in *SOD*^{G93A} mice are also affected by shape changes I measured the shape factor of the moving mitochondria at 2 months of age. The measurements showed lower shape factor values in *SOD*^{G93A} mice (**Figure 3.16A**). Similarly, average volume of moving mitochondria was reduced (**Figure 3.15B**).

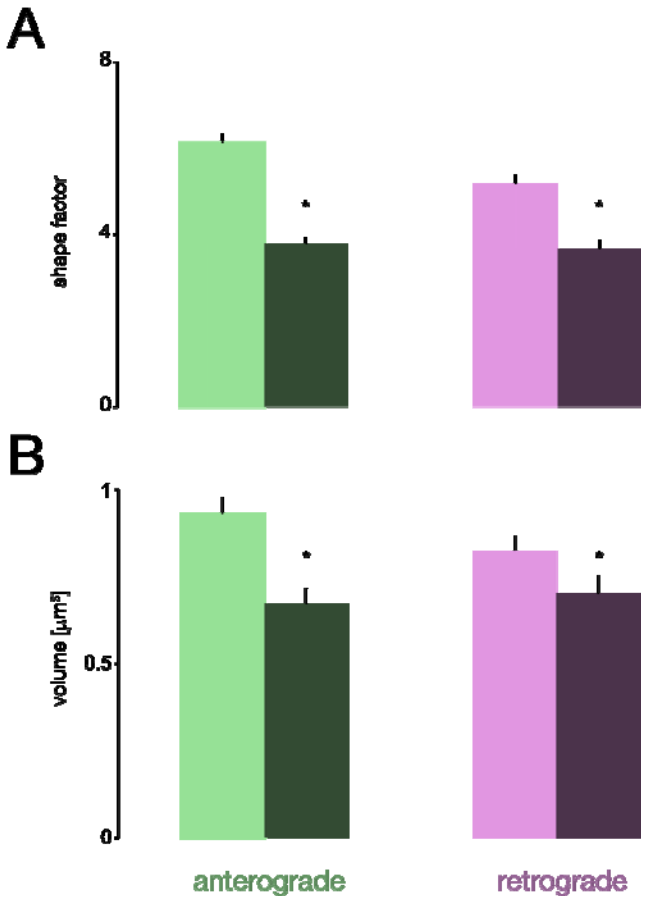

Figure 3.16 – Morphology and volume of moving mitochondria

(**A**) Moving mitochondria in *SOD*^{G93A} mice have decreased shape factor at 2 months of age (n = 2 mice and n = 96-193 mitochondria per phenotype and direction).

(**B**) Reduced volume of moving mitochondria in *SOD*^{G93A} mice (n = 2 mice and n = 121-270 mitochondria per phenotype and direction).

Error bars (S.E.M.) *, P<0.05.

3.2.14. Motor neurons can support complex arbors despite transport deficits in SOD^{G93A} mice

To investigate what are the consequences of early transport deficit for motor neurons and their arbors, I took advantage of *Thy1-YFP^{H}* mice, which due to subset labeling of few motor neurons permit reconstructions of entire motor units. I first measured mitochondrial transport in individual axons, which were fluorescently labeled with cytoplasmic YFP in *SOD^{G93A}, Thy1-MitoCFP*, *Thy1-YFP^{H}* triple-transgenic mice, in the triangularis sterni explant preparation. I then reconstructed the distal arbors and NMJs of such axons by high-resolution confocal microscopy. Remarkably, motor neurons with severely compromised transport and reduced mitochondrial density still support arbors that terminate in normal appearing neuromuscular synapses (**Figure 3.17**). In a control experiment I measured transport in YFP expressing axons and their non-YFP expressing neighboring axons in *Thy1-YFP^{H}* mice. High expression of YFP in subset of motor neurons in *Thy1-YFP^{H}* mice had no influence on mitochondrial transport at 50 days after birth and 4 months (120 days) after birth (**Figure 3.18**). However, YFP positive axons show reduced transport at 6 months of age, preventing use of these mice for studies in SOD mutants with later disease onset or aging studies.

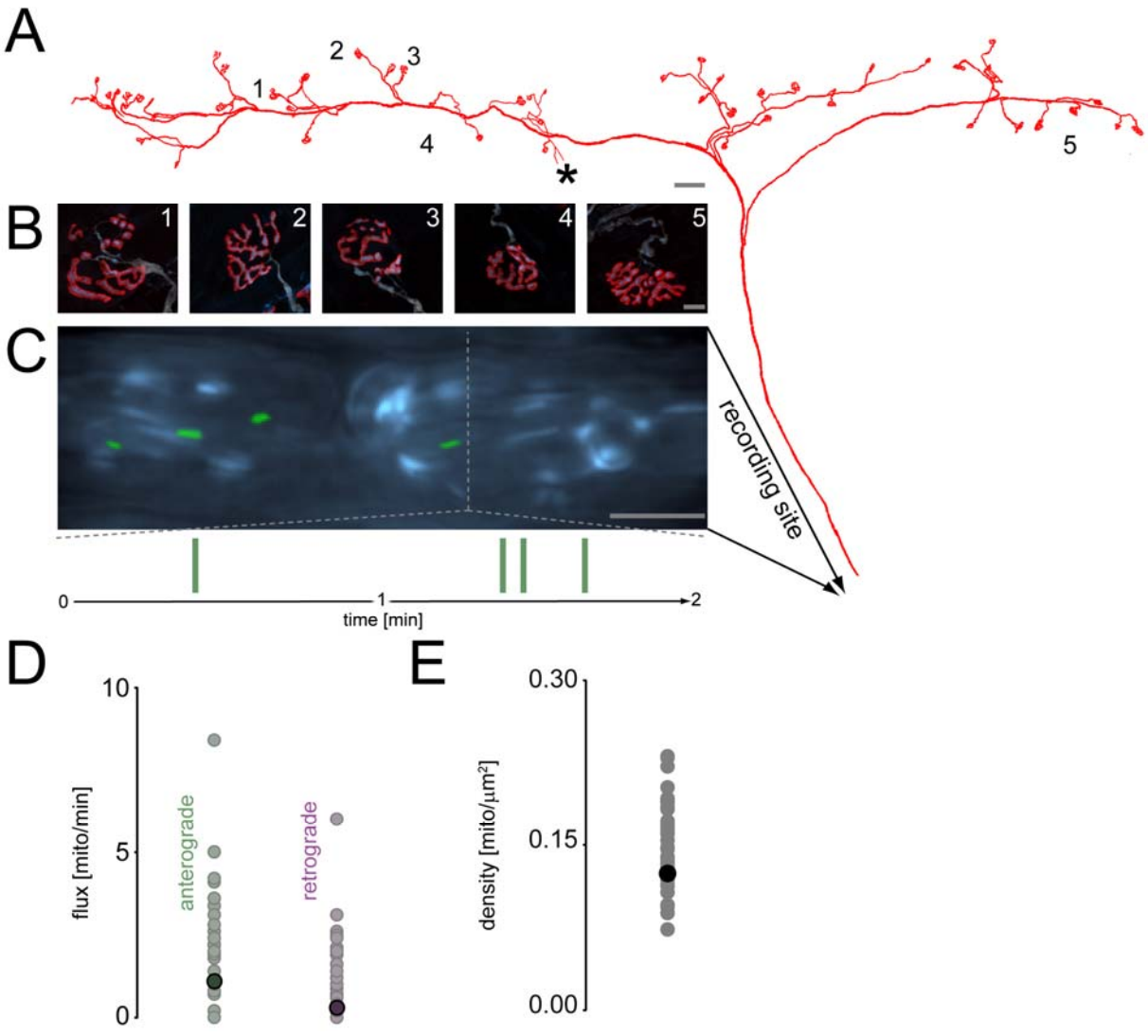
A
1
2
3
4
5
*
B
1
2
3
4
5
C
recording site
0
1
2
time [min]
D
flux [mito/min]
10
5
0
anterograde
retrograde
E
density [mito/µm²]
0.30
0.15
0.00

Figure 3.17 – Motor neurons can support complex arbors despite transport deficits in *SOD^{G93A}* mice

(**A**) Manual tracing of a motor unit in a triple-transgenic *SOD^{G93A}, Thy1-mitoCFP, Thy1-YFP^{H}* mouse (4 months of age), based on a tiled confocal reconstruction. Numbers indicate NMJs shown at higher magnification in **B**. This motor unit maintained normal appearing NMJs. Sprouts are marked by asterisk.

(**B**) Selection of NMJs showing that the axon (gray) fully covers the postsynaptic membrane (labeled with BTX, red; mitochondria shown in cyan).

(**C**) Wide-field image of the reconstructed axon was generated by averaging 50 frames of a time-lapse movie. Stationary mitochondria are shown in cyan. Moving mitochondria from the 1st, 25th and 50th frames of the movie are superimposed as pseudo-coloured masks (green, anterograde moving mitochondria and magenta, retrograde moving mitochondria). **Bottom panel** shows an "event diagram" indicating the time when moving mitochondria crossed an arbitrarily placed line (highlighted in gray in the panel above) over 2 minutes of time-lapse imaging (green, anterograde movement; magenta, retrograde movement).

(**D**) Mitochondrial flux of reconstructed axon (filled circle) plotted against the distribution of transport fluxes found in a population of *SOD^{G93A}, Thy1-mitoCFP* mice (pastel colored circles; data correspond to **Fig 3.4B**).

(**E**) Mitochondrial density in reconstructed axon (filled circle) compared to the distribution found in a population of *SOD^{G93A}, Thy1-mitoCFP* mice (grey circles; data correspond to **Fig. 3.3B**).

Scale bars, 100 µm in (**A**), 10 µm in (**B**), 5 µm in (**C**).

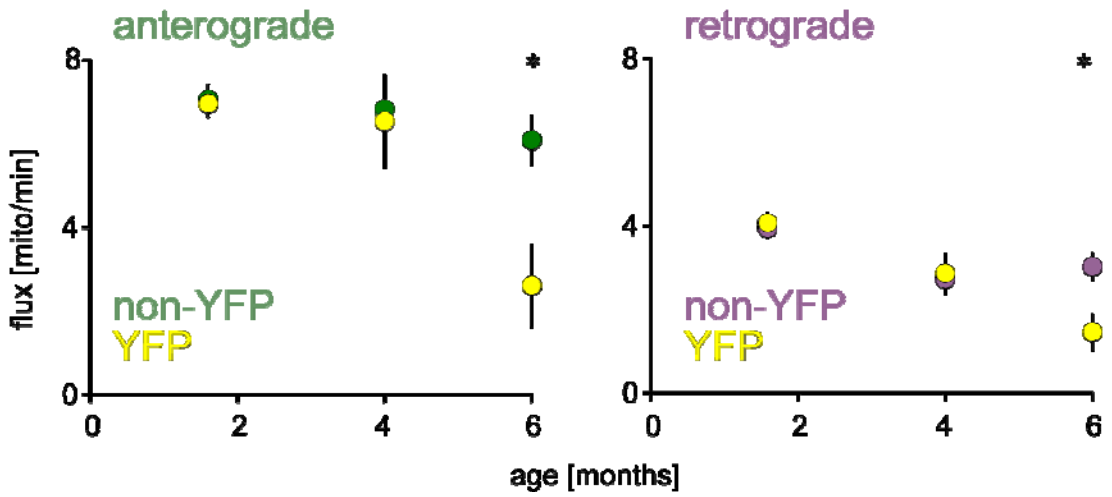

Figure 3.18 – Time-course of transport in intercostal axons over-expressing YFP

Mitochondrial flux in YFP expressing axons and non-YFP expressing neighboring axons in intercostal nerve at 50 days after birth (n =32 axons per phenotype, n = 10 mice total), 4 months (120 days) after birth (n = 9 axons per phenotype, n = 4 mice total) and 6 months after birth n = 32 axons per phenotype, n = 4 mice total).

Error bars (S.E.M.) *, P<0.05.

3.2.15. Capacity to increase axonal transport is not exhausted in *SOD*^{G93A} mice

Next, I wanted to better understand the nature of the transport deficits observed in *SOD*^{G93A} mice. It is reasonable to assume that axons in *SOD*^{G93A} mice are already transporting at maximum levels which are determined by SOD toxicity induced damage to the transport machinery. That would mean that in situations when WT axons respond with increase in transport such response would be absent in *SOD*^{G93A} mice. To investigate, whether axons in *SOD*^{G93A} mice are still capable of increasing their mitochondrial transport I performed complete transections of intercostal nerves. It is known that axotomy induces increase in mitochondrial transport in the proximal stump of the axon that is evident already 6h and persists up to 3 week after the axotomy (Misgeld et al., 2007). I cut the nerves that innervate triangularis sterni muscle *in vivo* at 2 months of age (**Figure 3.19**) and measured axonal transport of mitochondria 24h and 7 days after complete transection in acutely

explanted preparations in several places related to the axotomy: above the lesion ("cut"), in the neighboring intercostal nerve ("neighbor") and in the contralateral intercostal nerve as ("uncut") control (**Figure 3.19**).

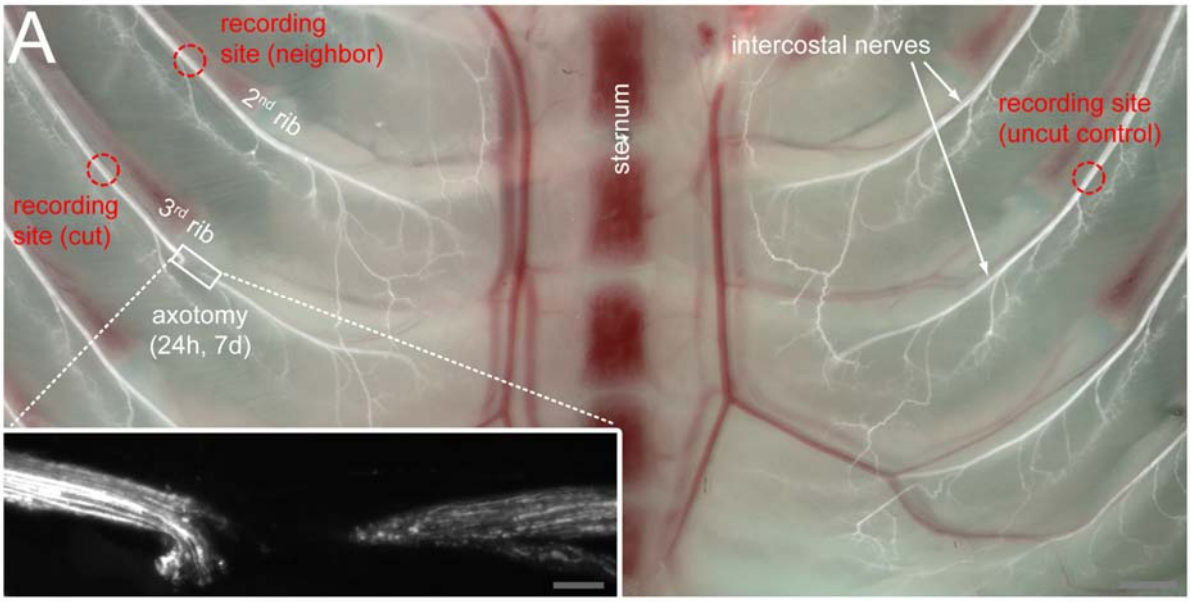

Figure 3.19 – Principle of axotomy experiment in triangularis sterni explant

Wide field image of triangularis sterni explant 24h after complete transection of one intercostal nerve (insert shows higher magnification of cut site). Recording sites in cut nerve (cut), neighbouring nerve (neighbour) and contralateral control (uncut control) are marked with red circles. Intercostal nerves are shown in white.

An increase in anterograde and retrograde transport above the lesion in WT axons was present already after 24h (63% increase for anterograde and 50% increase for retrograde transport) and it further increased after 7 days (98% anterograde, 61% retrograde). Interestingly, an increase in mitochondrial transport was also observed in *SOD*^{G93A} axons. After 24h, anterograde transport increased from 64% of the WT level to 85%, while retrograde increased from 42% of WT transport to 89% (this is increase of 34% in anterograde and 111% in retrograde transport compared to the transport in *SOD*^{G93A} uncut axons). This effect was even more profound 7 days after cut, when anterograde transport reached 143% of WT levels and retrograde 121% (this is increase of 125% in

anterograde and 189% in retrograde transport compared to the transport in *SOD*^{G93A} uncut axons; **Figure 3.20A**). To my surprise, I also observed an increase in the uncut "neighbor" nerve - remarkably, here I found a difference in response between WT and *SOD*^{G93A} mice. In the neighbouring nerve of WT mice, anterograde and retrograde transport were increased in a similar pattern albeit to a lesser degree compared to the cut nerve (44% and 52% increase for anterograde after 24h and 7 days, respectively, and 30% and 49% increase for retrograde after 24h and 7 days respectively). However, in *SOD*^{G93A} axons no increase in anterograde transport was observed, while retrograde transport showed only a slight and transient increase 24h after cut (**Figure 3.20B**). After 24h, anterograde transport in neighboring nerve was 67% of WT transport (65% in uncut control) and retrograde increased from 42% of WT transport to 66% of WT transport. Seven days after cut anterograde transport was still unchanged (59% of WT control) and retrograde had decreased again to 52% of WT transport (**Figure 3.20B**).

Taken together, the results of the axotomy experiment clearly show that capacity to increase transport is preserved in axons in *SOD*^{G93A} mice.

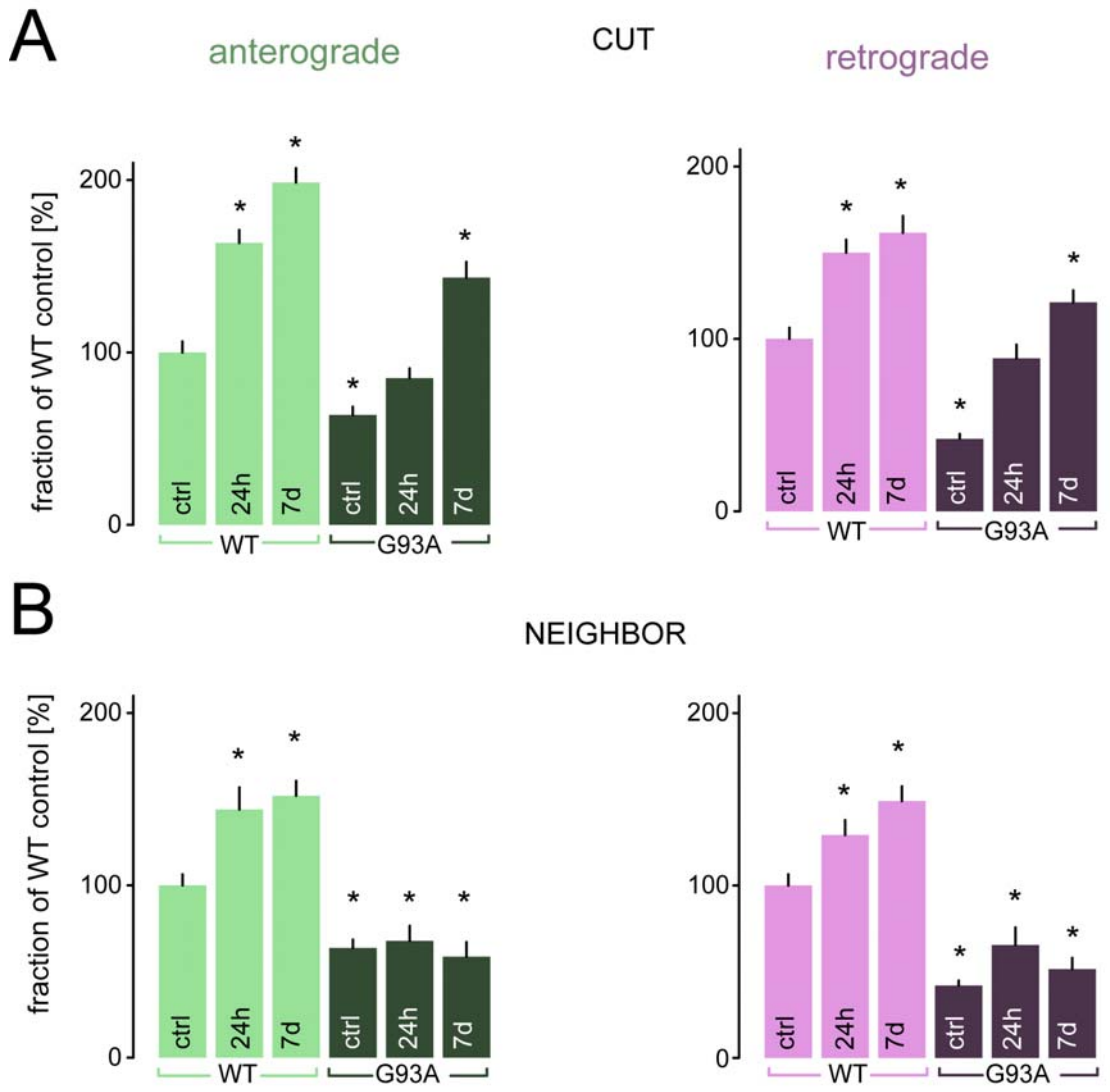

Figure 3.20 – Intercostal axons in *SOD^{G93A}* mice still can increase their transport in response to axotomy

(**A**) Relative change in anterograde (**left**) and retrograde (**right**) mitochondrial flux in cut nerve at 24h and 7 days after complete transection of an intercostal nerve in SOD^{G93A} and WT mice. Increase is expressed as mean percentage ± S.E.M. of transport flux in contra-lateral uncut WT control (ctrl).

(**B**) Relative change in anterograde (**left**) and retrograde (**right**) mitochondrial flux in neighboring nerve at 24h and 7 days after complete transection of intercostal nerve in SOD^{G93A} and WT mice. Values are expressed as mean percentage ± S.E.M. of transport flux in contra-lateral uncut WT control (ctrl).

*, $P < 0.05$ *vs*. WT ctrl

3.2.16. Sham operated animals do not show an increase in transport

To confirm that the observed increase in transport after axotomy is indeed axotomy-specific, I have performed sham operations. I measured axonal transport of mitochondria 24h after operation in acutely explanted preparations from operated (where a complete transection was performed) and sham operated animals. No effect of the sham operation was observed, confirming that the increase in transport is axotomy-specific (**Figure 3.21**)

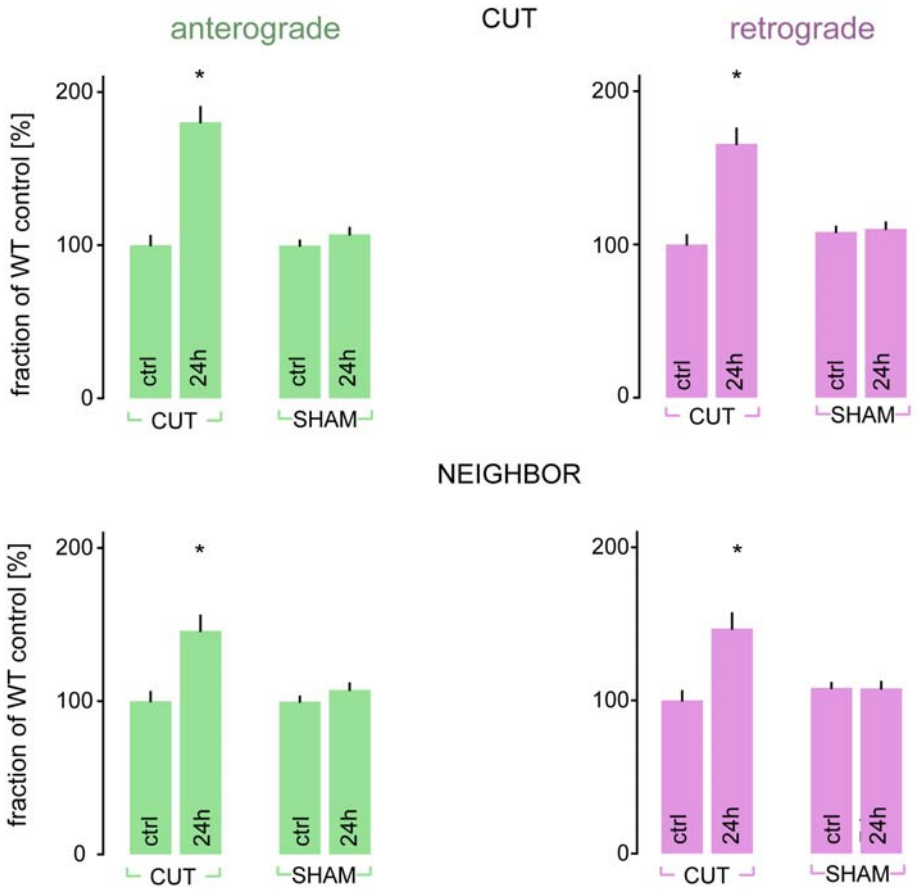

Figure 3.21 – Sham operation does not affect mitochondrial transport

Relative change in anterograde (**left**) and retrograde (**right**) mitochondrial flux in operated animals and sham operated animals at 24h after in WT mice. Values are expressed as mean percentage ± S.E.M. of transport flux in contra-lateral uncut control (ctrl).

*, $P < 0.05$ *vs*. ctrl

3.2.17. Increase in transport after axotomy in SOD^{G93A} mice is accompanied by changes in transport characteristics of individual mitochondria

Single cargo analysis 7 days after cut revealed changes in transport characteristics of mitochondria (**Figure 3.22**). Average speed for anterograde and retrograde moving mitochondria was slightly increased in WT axons due to decrease in stop length and frequency. However, moving speed was not changed. In *SOD^{G93A}* mice similar changes were observed with an increase in average speed due to a profound decrease in stop length and frequency. Hence, axotomy can not only increase flux rates in *SOD^{G93A}* axons, but also alter the transport parameters of single particles to resemble normal values.

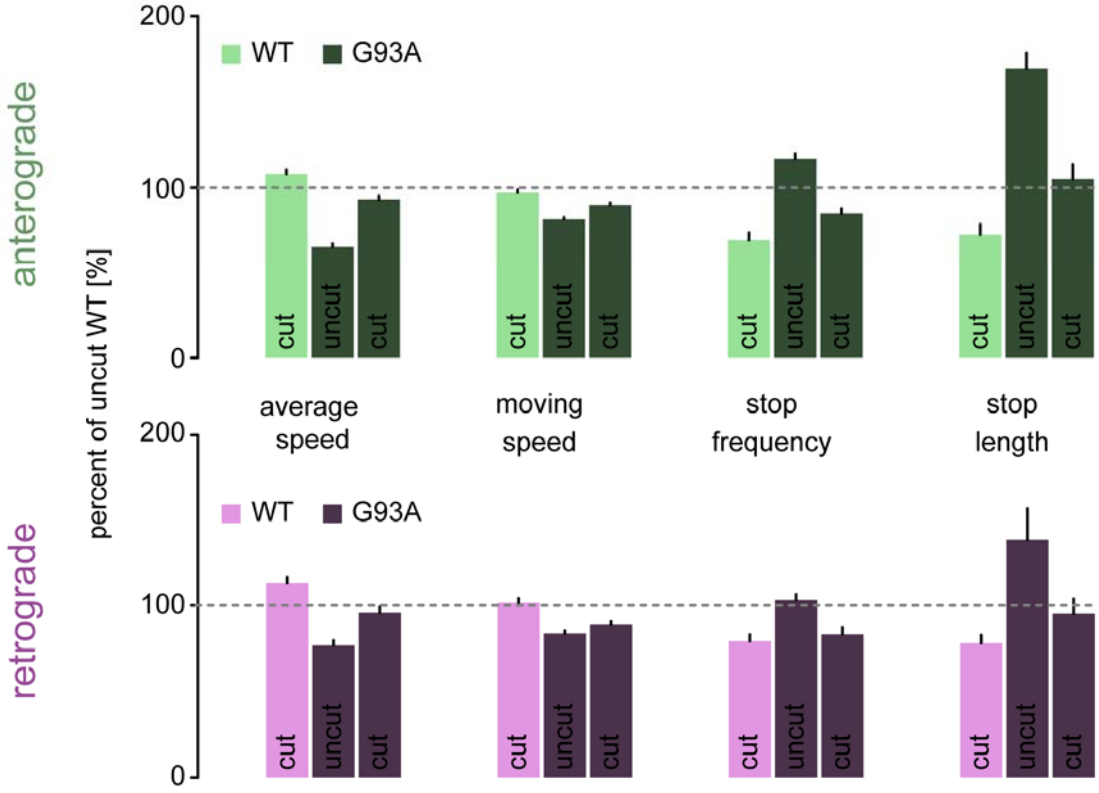

Figure 3.22 – Changes in transport characteristics of individual mitochondria in response to axotomy in intercostal axons in *SOD^{G93A}* mice

Single-cargo transport characteristics of individual mitochondria (n = 80-251 mitochondria; n ≥ 17 axons; n ≥ 4 mice) at 2 month. Values are expressed as mean percentage ± S.E.M. of WT control (dashed line).

3.3. Axonal transport in *SOD*^{G85A} mice

3.3.1. Disease course, clinical symptoms and denervation in *SOD*^{G85R} *mice*

After this detailed investigation of transport of mitochondria and CTB-labeled endosomes in the *SOD*^{G93A} mouse model, I wanted to investigate another ALS mouse model - my expectation being that in all ALS models the transport alterations described for *SOD*^{G93A} and *SOD*^{G37R} mice would be present if transport disruptions indeed mediate ALS-related axon degeneration. I chose a model based on the *SOD*^{G85R} mutation, which has a later disease onset followed by a rather "explosive" disease course. These mice start losing weight about 9 month after birth (**Figure 3.23A**). Subsequently, during the preterminal phase of the disease, they also develop muscle weakness (**Figure 3.23A**) coincident with denervation of muscle fibers (**Figure 3.23B**)

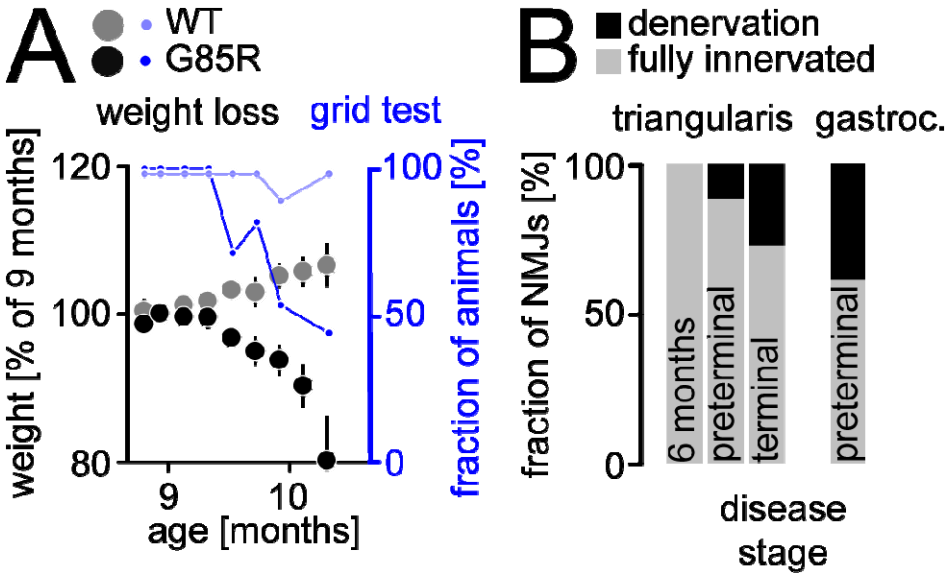

Figure 3.23 – Time-course of clinical symptoms and denervation in *SOD*^{G85R} *mice*

(A) Time-course of body weight (in % of weight at 9 months of age, mean ± S.E.M) and grid test performance (expressed as % of mice with normal grid test) of *SOD*^{G85R} and wild-type (WT) mice (n > 10 mice per genotype and time-point).

(B) Time-course of denervation in triangularis sterni and gastrocnemius muscles of *SOD*^{G85R} mice (n > 250 synapses, n > 3 mice).

3.3.2. Axonal degeneration but no transport deficits are observed in *SOD^{G85R}* mice

Mitochondrial transport measurements in triangularis sterni muscle in *SOD^{G85R}, Thy1-MitoCFP* mice revealed normal anterograde and retrograde flux at 6 months of age (**Figure 3.26A**). At six months animals still do not show disease symptoms. This was surprising result, and in contrast to early and profound transport deficit observed in *SOD^{G93A}* mice. Transport appeared normal even in the preterminal stage of the disease, when signs of axon degeneration, such as axon fragments, are readily detectable in the intercostal and tibialis nerves that I imaged (**Figure 24 A and B**), Retrograde transport of endosomal vesicles labelled by peripheral injection of CTB showed no abnormalities (**Figure 3.24C**). Similarly, tracking of individual mitochondria revealed no changes in average speed (see next section; due to the long disease-course of the SOD^{G85R} model and the apparent normality of transport flux and CTB vesicle transport, we decided to forgo crossing SOD^{G85R} mice with *Thy1*-mitoKaede mice and chose to track single mitochondria in *Thy1-MitoCFP* mice instead.).

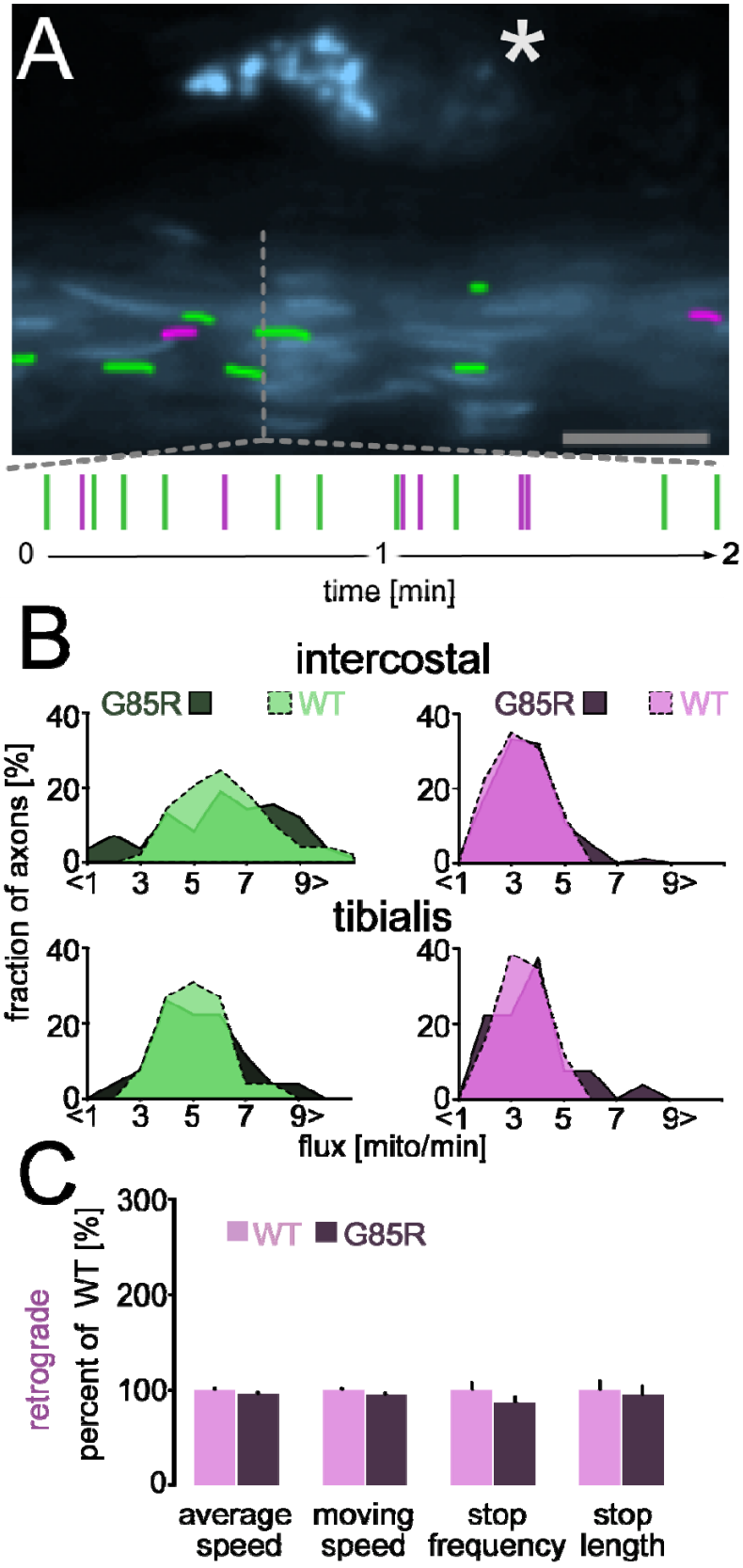

Figure 3.24

Axonal degeneration but no transport deficits are observed in *SOD*^{G85R} mice

(**A**) Wide-field image of an intercostal axon generated and labeled as described for **Fig. 3A**. Asterisk, axonal fragment

(**B**) Mitochondrial flux rates in intercostal and tibialis nerves (n > 40 axons, n ≥ 3 mice).

(**C**) Transport characteristics of individual CTB-labelled vesicles for *SOD*^{G85R} at preterminal stage (n = 301 vesicles; n = 16 axons; n = 3 mice); Values are expressed as mean percentage ± S.E.M. of WT control.

Scale bar, 5µm in (**A**).

3.3.3. Mitochondrial speed in *SOD^{G93A}*, *SOD^{G85R}* and *SOD^{WT}* mice

The tracking of single mitochondria in wide-field movies obtained for transport rate measurements in intercostal and tibialis nerves revealed reduction in average speed in *SOD^{G93A}* and *SOD^{WT}* mice (**Figure 3.25**). No changes in average speed were detected in *SOD^{G85R}* at preterminal stage (**Figure 3.25**).

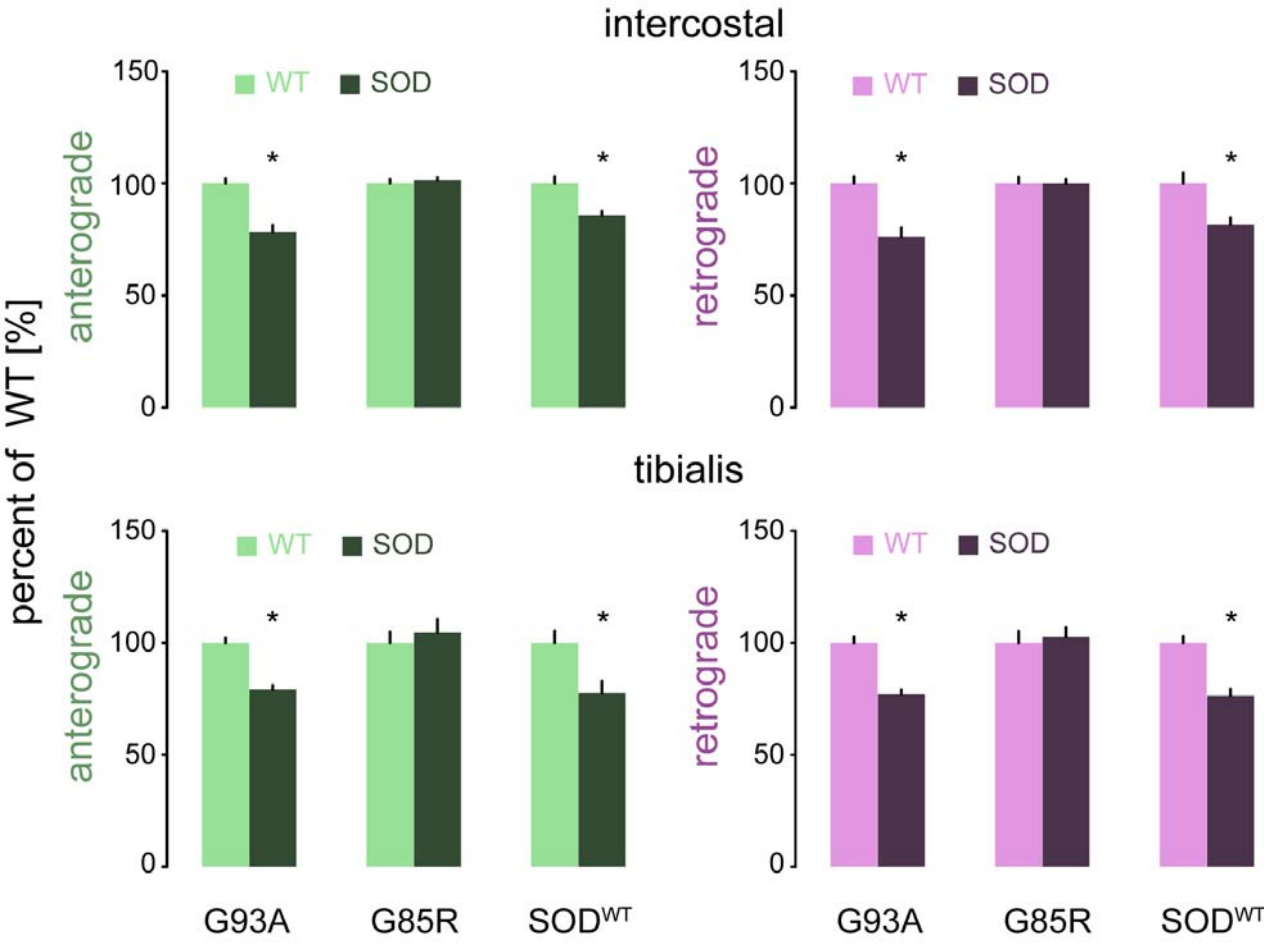

Figure 3.25 – Mitochondrial speed in *SOD^{G93A}*, *SOD^{G85R}* and *SOD^{WT}* mice

Average anterograde (left, green) and retrograde (right, magenta) speed of transported mitochondria measured in movies obtained from *Thy1-mitoCFP*, *SOD* double-transgenic mice for *SOD^{G93A}* (4 months), *SOD^{G85R}* (preterminal) and *SOD^{WT}* (4 months). **Top**, data for intercostal nerve axons; **bottom**; tibialis nerve.Values are expressed as mean ± S.E.M; n = 57-340 mitochondria.

*; P<0.05.

3.3.4. Time course of mitochondrial transport in *SOD^{G85R}* mice

The surprising finding that transport of mitochondria and CTB-labelled endosomes at the preterminal stage in intercostal axons was normal in *SOD^{G85R}*, mice prompted me to investigate mitochondrial transport across the disease course Only at the very late disease stage (terminal) I detected a slight reduction in anterograde transport (**Figure 3.26A**) - which together with the results obtained at preterminal stage allows to estimate that at most a mitochondrial transport deficit in the *SOD^{G85R}* mice persist for two weeks (the time it normally takes for an animal to die once it has reached the preterminal stage). This estimate is in sharp contrast to the deficit that lasts several months found in *SOD^{G93A}*. However, likely even this short survival time in *SOD^{G85R}* is an overestimate for single axons, as the terminal measurement is probably contaminated by axons that are already degenerating and therefore might not have transport anymore. Consistent with normal transport, measurements of mitochondrial density in axons of intercostal and tibialis nerves in *SOD^{G85R}* mice showed no differences at preterminal stage (**Figure 3.26B**). Further, to confirm that the transport of other cargoes is also normal I performed an analysis of transport characteristics of CTB labelled endosomes in the tibialis nerve. Although the tibialis nerve innervates the gastrocnemius muscle, which is more affected at the preterminal stage, analysis showed no change in transport characteristics (**Figure 3.26C**).

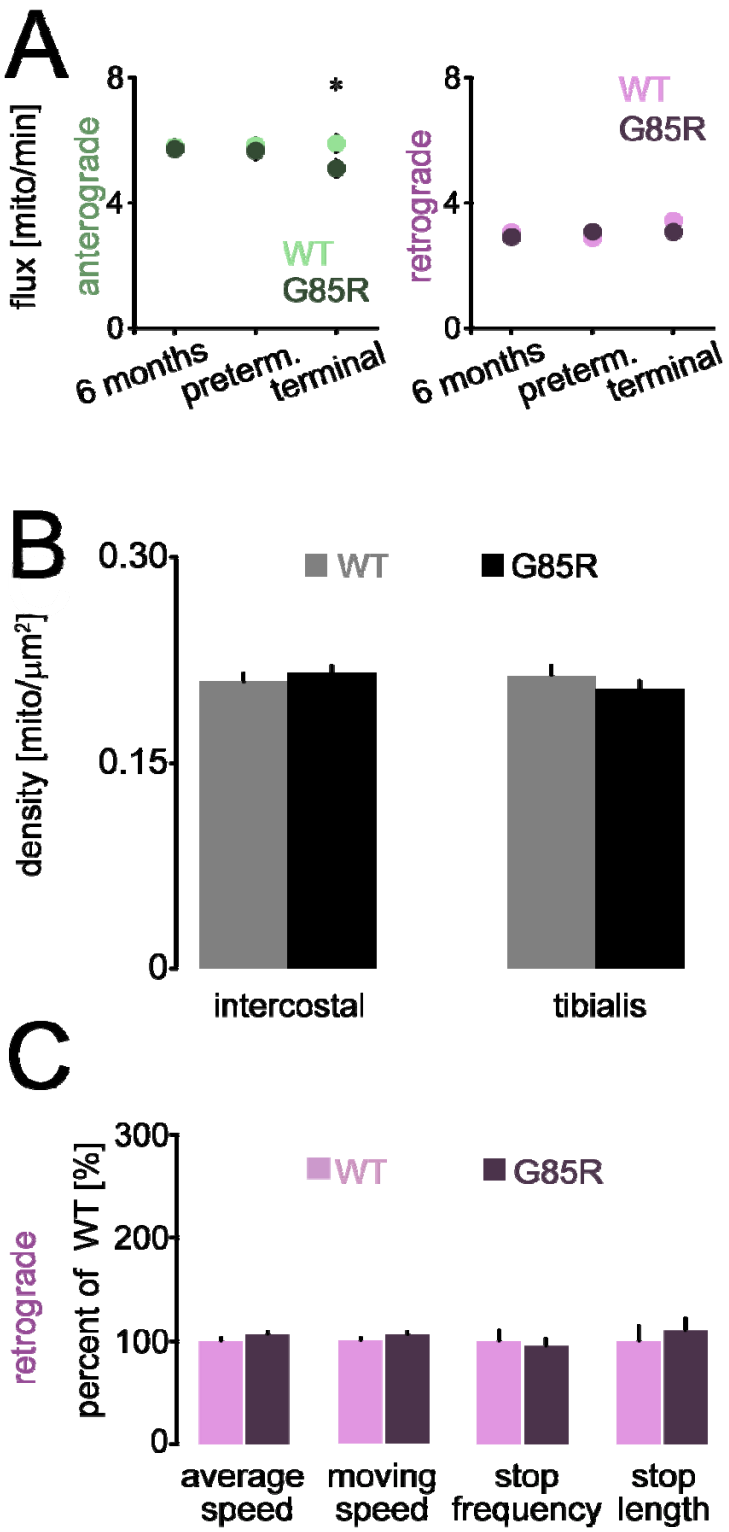

Figure 3.26 – Mitochondrial transport during disease time course, mitochondrial density and transport of CTB labelled endosomes in tibialis nerve in *SOD^{G85R}* mice

(A) Mitochondrial flux rates in intercostal nerve during disease course in *SOD^{G85R}* mice (n > 30 axons, n ≥ 3 mice).

(B) Mitochondrial density in intercostal and tibialis nerves of *SOD^{G85R}* mice (**C**) Single-cargo transport characteristics of individual CTB-labelled vesicles for *SOD^{G85R}* at preterminal stage (n = 301 vesicles; n = 16 axons; n = 3 mice);

Values are expressed as mean percentage ± S.E.M. of WT control. Error bars (S.E.M.) smaller than data symbols in most cases. Scale bar, 5µm in **(A)**.

3.3.5. Mitochondrial transport in *G85R SOD-YFP* mice

I also measured transport in *G85R SOD-YFP* mice kindly provided by Dr. Horwich from Yale University. Although it was previously reported that these mice have disease onset at 9 months of age (Wang et al., 2009), in animals that we obtained we could not observe a clear ALS-like phenotype at the expected times and could not stage them accordingly. Still, as our genotyping confirmed the presence of the *SOD* transgene, I measured transport in three animals total at different time-points. No differences were observed between the animals and pooled together, mitochondrial fluxes appeared normal in *G85R SOD-YFP* mice (anterograde: 6.6 ± 0.6 mito/min; retrograde: 2.5 ± 0.2 mito/min) (**Figure 3.27**). More extensive studies of this second SOD^{G85R} allele are in preparation in collaboration with the Yale group.

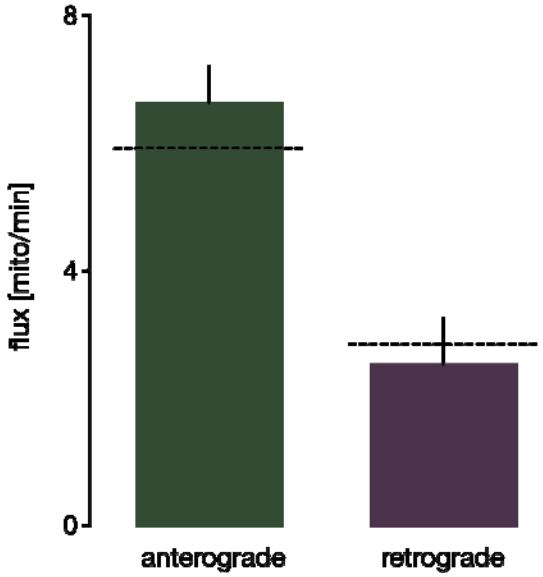

Figure 3.27 – Mitochondrial transport in *G85R SOD-YFP*

Mitochondrial flux in *G85R SOD-YFP* mice (n = 3 mice and n = 24 axons). Dashed lines indicate average value for WT mice.

3.4. Axonal transport in *SOD^{WT}* mice

3.4.1. Disease course, clinical symptoms and denervation in *SOD^{WT}* mice

SOD^{WT} mice over-express a WT human SOD protein and are commonly used as control mice in ALS studies (Gurney et al., 1994). As expected, I detected no weight loss, functional deficits or signs of denervation in these mice when I examined them at 4 months of age (**Figure 3.28 A and B**). As reported previously (Jaarsma et al., 2000), at 1 year of age the animals start showing a mild neurological phenotype, that appears mostly in the form of a broadened ataxic-appearing gait. At this time also mild (<10%) denervation is found in triangularis sterni and gastrocnemius muscles.

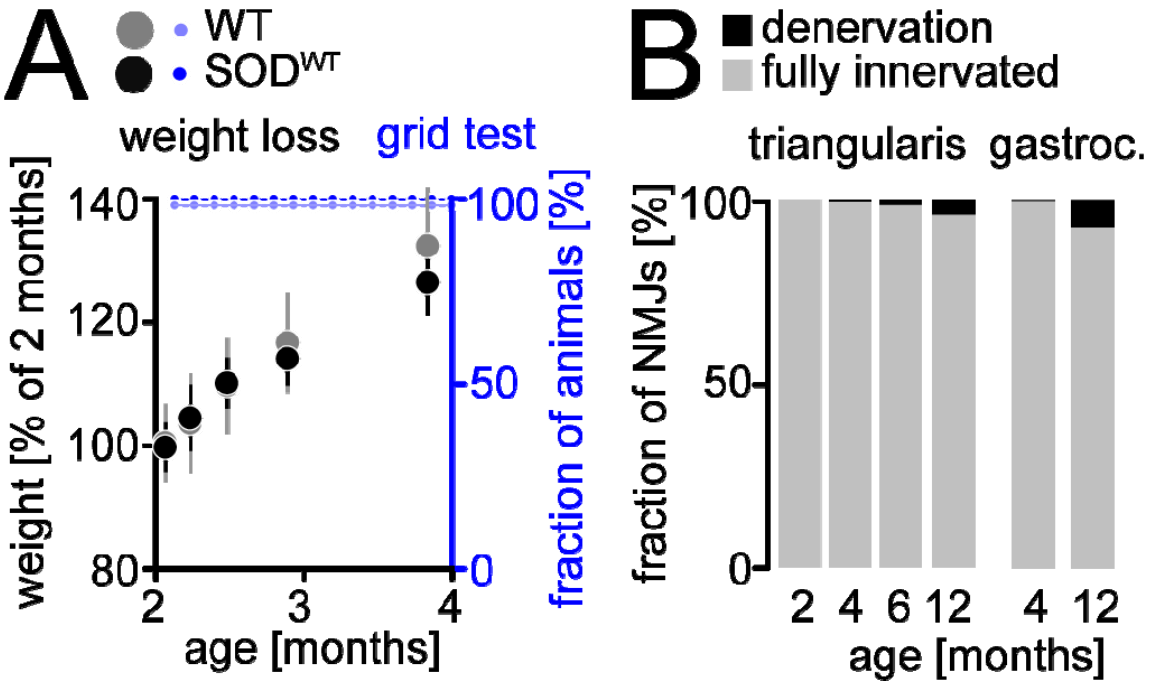

Figure 3.28 – Time-course of body weight and grid test performance of *SOD^{WT}* and WT mice

(**A**) Time-course of body weight (in % of weight 2 months in **A**, mean ± S.E.M) and grid test performance (expressed as % of mice with normal test; n > 10 mice per group).

(**B**) Time-course of denervation in triangularis sterni and gastrocnemius muscles (n > 250 synapses, n > 3 mice).

3.4.2. Axonal transport deficits are observed in *SOD^{WT}* mice

Surprisingly, however, anterograde and retrograde mitochondrial flux in triangularis sterni explants of *SOD^{WT}*, *Thy1-MitoCFP* mice was significantly reduced already 2 months after birth (**Figure 3.29**). This deficit was progressive and reached levels in intercostal and tibialis nerves comparable to *SOD^{G93A}* and *SOD^{G37R}* mice by 4 months and persisted for up to 1 year (**Figure 3.29** and **Figure 3.30 A** and **B**). Similarly, *SOD^{WT}* axons showed slowed transport of mitochondria and CTB-labeled particles (**Figure 3.30E** and **Figure 3.25**). Mitochondrial density was reduced both in intercostal and tibialis nerves at 4 months (**Figure 3.31**). Thus, over-expression of non-mutated human SOD suffices to induce early transport deficits. These deficits, however, do not cause overt motor neuron degeneration for several months – only at 12 months did I detected mild denervation (<4% in triangularis; <8% in gastrocnemius muscle; **Figure 3.28** see also Jaarsma et al., 2000).

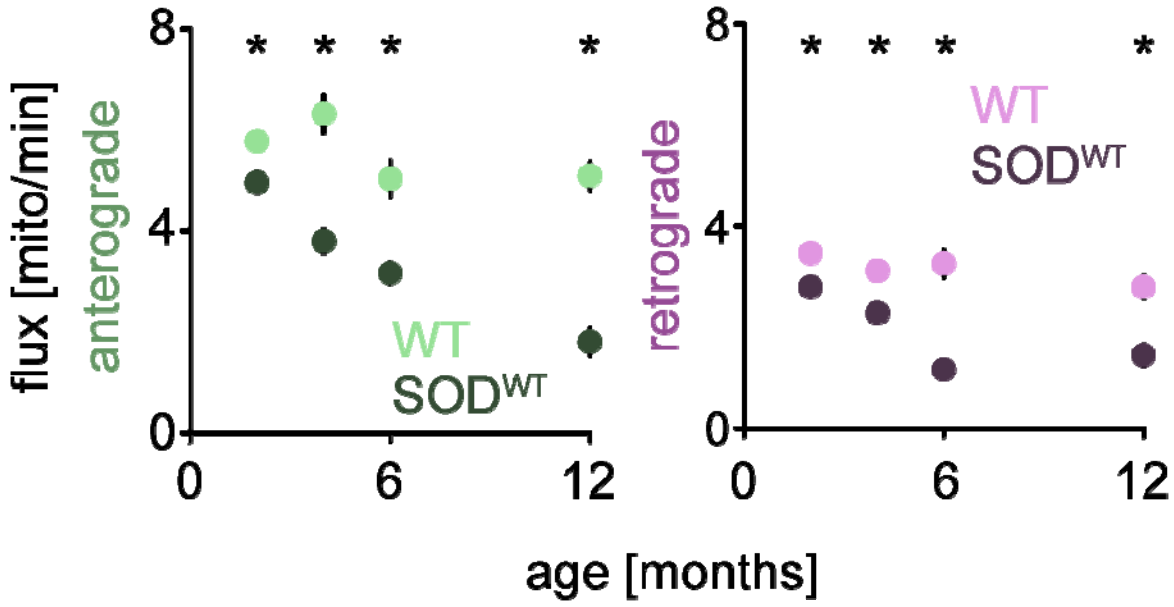

Figure 3.29 – Time course of transport deficit in intercostal axons of *SOD^{G93A}* mice

Mitochondrial flux in intercostal of *SOD^{G93A}* and WT mice (n > 30 axons, n ≥ 4 mice per time-point), as well as in intercostals nerves of *SOD^{G37R}* mice (n = 45 axons, n = 2 mice). Error bars (S.E.M.) smaller than data symbols in most cases.

*, P < 0.05.

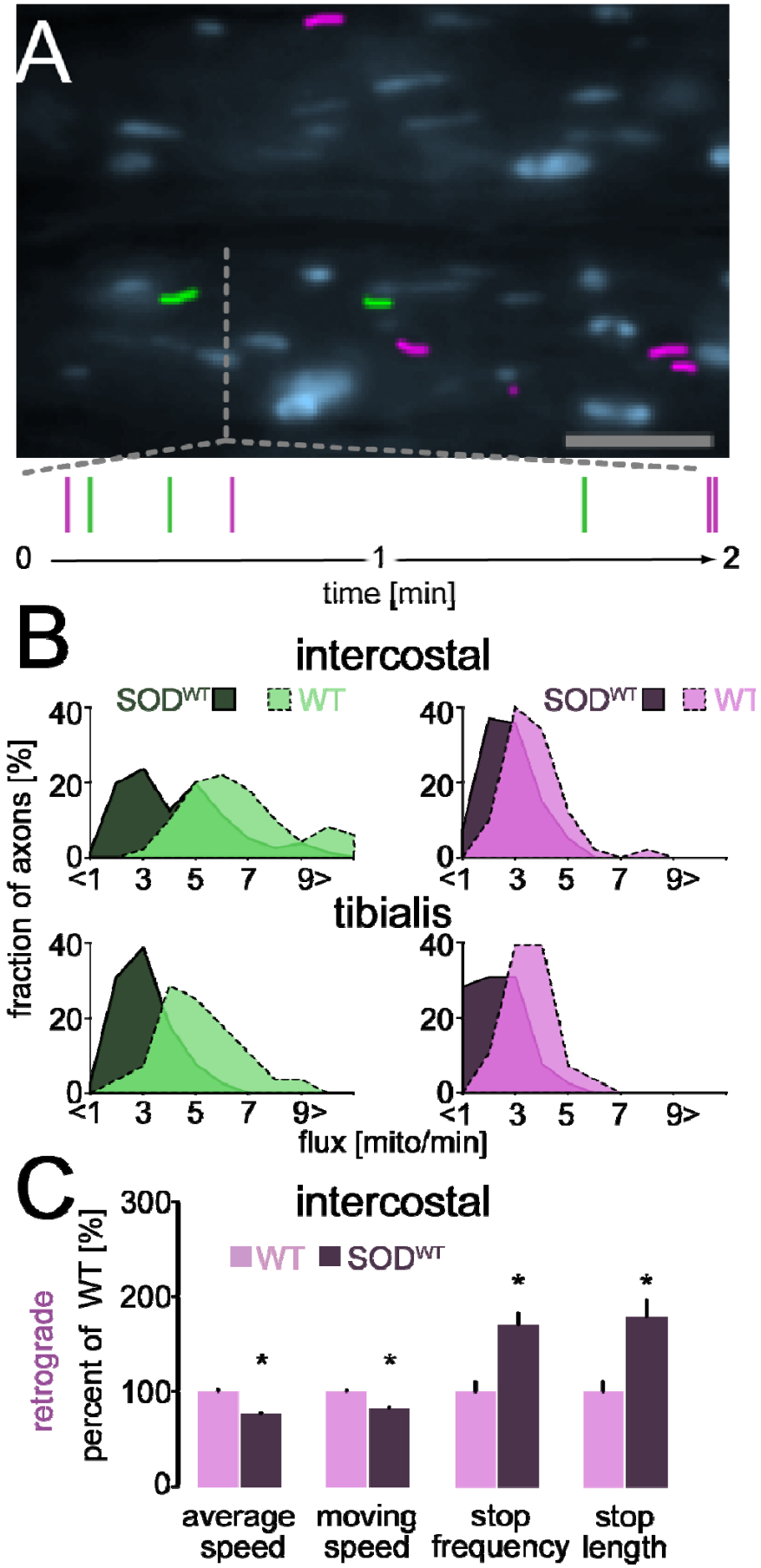
A
0
1
2
time [min]
B
intercostal
SOD^WT
WT
SOD^WT
WT
40
20
0
<1
3
5
7
9>
fraction of axons [%]
tibialis
flux [mito/min]
C
intercostal
WT
SOD^WT
retrograde
percent of WT [%]
300
200
100
0
*
average speed
moving speed
stop frequency
stop length

Figure 3.30 – Axonal transport deficits and degeneration are dissociated in *SOD^{WT}* mice

(**A**) Wide-field image of an intercostal axon generated and labeled as described for **Fig. 1A**.

(**B**) Mitochondrial flux rates in intercostal nerves (n > 40 axons, n ≥ 3 mice).

(**C**) Single-cargo transport characteristics of individual CTB-labelled vesicles for *SOD^{WT}* at 6 months (n = 280 vesicles; n = 23 axons; n = 3 mice).

Values are expressed as mean percentage ± S.E.M. of WT control. Error bars (S.E.M.) smaller than data symbols in most cases. Scale bar, 5μm in (**C**). *, P<0.05.

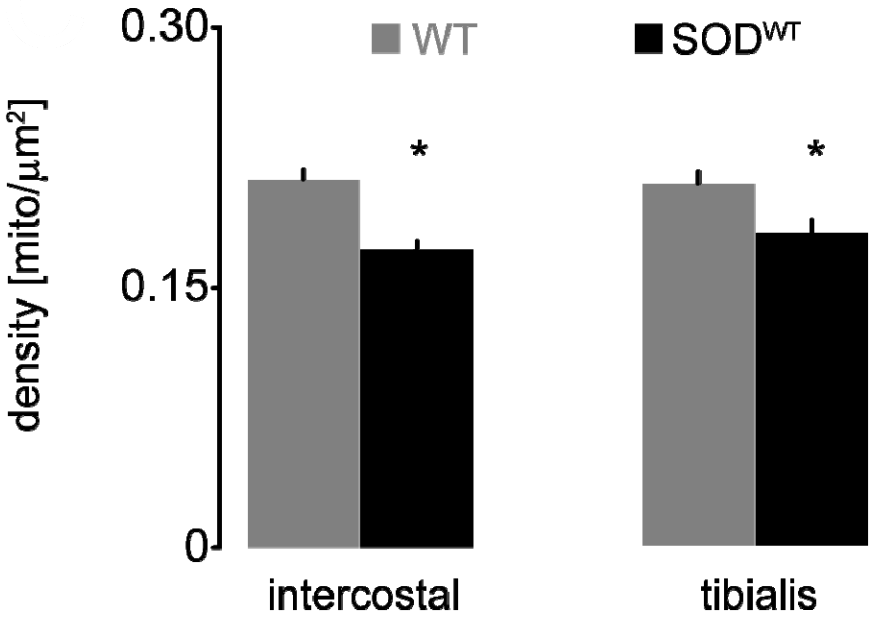

Figure 3.31 – Quantification of mitochondrial density in intercostal and tibialis nerve axons

Mitochondrial density in intercostal and tibialis nerve (n > 25 axons, n ≥ 3 mice for each condition) of 4-month old WT and *SOD^{WT}* mice.

Values are expressed as mean ± S.E.M. *, P<0.05.

4. DISCUSSION

Axonal transport deficits have been reported in many neurodegenerative conditions, including Alzheimer's disease, Huntington's disease and ALS, and are widely assumed to be an immediate cause of neurodegeneration. In my PhD thesis, I used imaging techniques to directly address the relationship between organelle transport and axon degeneration in a set of established ALS animal models, based on different mutations in the SOD gene that cause fALS in humans. The results of this study show that axonal transport deficits and degeneration can evolve independently refuting the hypothesis that disturbances of fast organelle transport are a general and immediately causative step in the emergence of motor neuron degeneration. This conclusion is based on the following results:

(I) *Axonal transport deficits do not cause immediate axon loss*: In the most commonly used SOD-ALS model (*SOD^{G93A}* mice) transport deficits are already present as early as 3 weeks after birth. However, despite these transport deficits, motor axons can survive and maintain complex arbors for several months before axonal degeneration sets in.

(II) *Axonal transport deficits are not sufficient to cause axon loss*: In mice that express a non-mutated human SOD protein (*SOD^{WT}* mice; the standard "negative" control in SOD-ALS studies), we found comparable transport deficits as in *SOD^{G93A}* mice – but only very limited and late loss of axons.

(III) *Axonal transport deficits are not necessary for axon loss:* In the *SOD^{G85R}* mice, another commonly used ALS model, I found no transport deficits until imminent death of the animals due to extensive axonal degeneration.

This study raises a number of important questions for ALS research but also for the neurodegeneration field in general. For example, it is a common practice in studying neurodegenerative diseases to draw general conclusion from results obtained in only one overexpression animal model - not uncommonly one with early disease onset and therefore particularly high expression levels of mutated protein. Particularly, in the SOD-ALS field such practise seems common. This notion is supported by the results of a

survey of SOD-ALS publications from the past 4 years that I did: The results of my survey showed that 96% (24 of 25) of the recent papers used the aggressive *SOD^{G93A}* model and that 56% of the papers are solely on these *SOD^{G93A}* mice. Only 25% of the papers have investigated *SOD^{WT}* mice as control and only 28% at least one more mutant in addition to *SOD^{G93A}*. The data presented in this study clearly indicate the necessity to use various mutants in parallel and appropriate controls (over time to match unavoidable differences in expression levels) in SOD-ALS studies. Our lab is proposing the use of one active and one inactive mutant as minimum and preferably of lines with lower expression levels than *SOD^{G93A}*. Further, time-course data from mice expressing non-mutated SOD (*SOD^{WT}*) should be used as controls. In this way, it is possible to search for patterns and alternation common to different SOD mutants, which induce essentially the same ALS-like phenotype, and absent from the disease-unrelated control.

As these suggestion deviates from the common practice, I would like to give a short retrospective of how this study, from which these recommendations emerged, developed. Originally, our goal was to mechanistically dissect axonal transport in the most commonly used model of ALS, the *SOD^{G93A}* mouse. In this choice, we were influenced by the predominance of this model in the literature. This is the reason why the largest part of the data in this PhD thesis is on the *SOD^{G93A}* model. However, later during the project I discovered a similar transport and mitochondrial phenotype in *SOD^{WT}* and the lack of such a phenotype in *SOD^{G85R}* mice. These findings changed our initial view on the relation between transport deficits and axon degeneration and hence our project plan. We decided to deepen our comparison of the different mouse models and delay publication of our results until we could obtain a complete picture of transport deficits in SOD-based ALS models. In between, a study by the Schiavo lab appeared (Bilsland et al., 2010), reporting early transport deficits in *SOD^{G93A}* mice, but interpreting these deficits as a very important step in ALS pathogenesis. No other SOD mutants were investigated in this study. Our interpretation differs sharply from the Bilsland study.

The discussion is divided into six parts. In the first part, I will discuss the transport deficit in *SOD^{G93A}* mice and the possible underlying mechanisms. Special attention in this part is on the differences in results between my study and previous studies on axonal

transport in ALS. The second part is the discussion of the axotomy experiments. This part is followed by the discussion of changes in mitochondrial morphology observed in *SOD*^{G93A} mice, which are often cited as general ALS hallmarks. However, I will give arguments, supported by the results on *SOD*^{WT} and *SOD*^{G85R} that these changes could be overexpression artefacts and not ALS-related. Similarly, in parts on the axonal transport in *SOD*^{WT} and *SOD*^{G85R} mice, arguments in favour of independent evolvement of axonal transport and axonal degeneration will be discussed. The final part of the discussion is summarizing the main findings, their significance and conclusions of this PhD thesis.

4.1. Axonal transport deficits in *SOD*^{G93A} mice

This is the first study to my knowledge that clearly shows mitochondrial transport flux deficit in mature axons in *SOD*^{G93A} mice. Indeed, the results of the present study show that motor axons in intercostal and tibialis nerves in *SOD*^{G93A} mice at 4 months of age have a reduced mitochondrial transport. Investigation of transport in the purely sensory saphenous nerve at the same age suggested that these transport deficits were specific for motor axons as would be expected for the motor neuron disease ALS. At 4 months of age *SOD*^{G93A} mice also show clinical signs of the disease, such as weight loss and muscle weakness. Consistent with reduced transport, the density of mitochondria is reduced in motor axons and synapses in *SOD*^{G93A} mice. Previous studies have also shown reduced density of organelles in mouse models of ALS, suggesting that reduced organelle density is a consequence of transport impairments (Pun et al., 2006; Shan et al., 2010). However, organelle density should be taken with caution as readout for axonal transport. The density could also be affected by reduced biogenesis, catabolic processes or local fusion/fission processes (Batlevi and La Spada, 2011; Detmer and Chan, 2007). Here, direct time-course measurements of axonal transport and mitochondrial density in axons and synapses support the link between transport and density. At the same time, as we did neither observe fusions in significant numbers, nor a change in the anterograde-to-retrograde ratio in *SOD*^{G93A} mice, we do not have any direct evidence that would support a contribution of other processes than transport to the reduced peripheral density. To the

possibility of reduced biogenesis, my data do not make a point - indeed it would be interesting to "search for" the missing mitochondria: If reduced transport alone explains reduced density, a "pile up" in proximal parts of the cell would be expected, while reduced biogenesis would predict a general paucity of organelles throughout the cell.

To better understand the mechanisms underlying the transport deficit observed in *SOD^{G93A}* mice, I developed two assays that allow analysis of the movement of individual cargoes transported in motor axons *in situ*. The first assay is based on *Thy1-MitoKaede* mice, a new transgenic line recently developed in our lab. The second assay allows investigation of another cargo, namely the endosomes.

In *Thy1-MitoKaede* mice it is possible to reliably track individual photo-converted mitochondria among their non-photo-converted counterparts over long distances in axons. The results of such tracking experiments showed that transport in *SOD^{G93A}* mice is characterized by changes in transport characteristics of individual mitochondria. Transported mitochondria in *SOD^{G93A}* mice have a reduced average speed mainly due to increased stop length and frequency. Based on these results, it is attractive to propose a model where such local events (increase in stop length and frequency) could affect axonal transport flux. In long motor axons, a movement pattern with frequent and long stops could mean that fewer mitochondria reach the distal parts of axons per unit of time (i.e. reduced mitochondrial flux), even if we assume that the same number of mitochondria is sent off from the cell body in *SOD^{G93A}* and WT mice. This view is also supported by the fact that changes in transport characteristics correlate with an observed increase in transport after axotomy in *SOD^{G93A}* and WT mice (**Figure 3.22**; page 88; for details see discussion chapter on “Capacity of motor axons to increase transport in *SOD^{G93A}* mice is not exhausted”; page 107). Furthermore, I observed that in *SOD^{G93A}* axons a larger fraction of moving mitochondria (~ 11% in both anterograde and retrograde direction) make considerably longer stops (> 10s). Some of these mitochondria even remained immobile during the whole recording period. It is possible that these mitochondria stopped permanently and/or that they are degraded by local autophagy (Wang et al., 2011b). Such events would further contribute to the reduction in transport flux.

Second, I asked whether the observed transport defects are specific to mitochondria by investigating transport of other cargos. As experiments with *Thy1-synaptophysin7-YFP* were not reproducible and hard to interpret, I established an assay to investigate the transport of endosomes. I injected **c**holera **t**oxin, subunit **B** (CTB) conjugated to the fluorescent dye Alexa-594 into the triangularis sterni muscle *in vivo*. The CTB-dye complex is taken up by neuromuscular synapses and incorporated into vesicles, likely of endosomal nature (Shogomori and Futerman, 2001), which are then transported retrogradely to the cell body. By imaging intercostal axons 24h after injection, I found that transport of CTB-labeled vesicles was affected in a similar manner as mitochondrial transport. This suggests a general transport deficit of organelles in *SOD*^{G93A} mice, even though generalizing beyond the cargoes examined is dangerous, given the large number and diversity of organelles and proteins transported in axons.

The fact that anterograde and retrograde transport of cargos are affected in a similar manner suggests that both kinesin and dynein motor proteins are affected in the motor axons of *SOD*^{G93A} mice. In support of such an interpretation is a recent study, which shows that mutant SOD interacts with dynein and slows down transport in pre-symptomatic *SOD*^{G93A} mice (Shi et al., 2010). Alternatively, or additionally, microtubules as main tracks for axonal transport of mitochondria could be functionally or structurally modified in *SOD*^{G93A} mice. Indeed, it was shown that alternations in microtubules associated proteins (MAPs) precede ultra-structural changes in ALS (Farah et al., 2003; Binet and Meininger, 1988). These alternations could influence the polymerization of microtubules or change their stability and therefore impair transport of mitochondria and other cargoes. A recent study reported abnormal i.e. increased microtubule dynamics measured by tubulin turnover in *SOD*^{G93A} mice and neuroprotective effects of microtubule stabilization (Fanara et al., 2007). Transgenic mice with labeled polymerizing tip of microtubules (*Thy1-EB3-YFP* mice) that were recently developed in our lab (Kleele et al., in preparation), now allow direct analysis of microtubules dynamics *in vivo* and could therefore provide further insight in the mechanisms underlying transport disruptions. However, preliminary results of my initial experiments in *SOD*^{G93A}, *Thy1-EB3-YFP* mice show no obvious changes in mitochondrial dynamics in motor axons.

On the cellular level, signs of degeneration, namely denervation of muscle fibers, are first evident around 3 months of age in *SOD^{G93A}* mice. Systematic analysis of mitochondrial transport in *SOD^{G93A}* mice showed that transport deficits are already present as early as 3 weeks after birth, which is approximately 2-3 months before disease onset marked by weight loss and muscle weakness. This suggests that motor neurons can survive significant transport deficit (at least of mitochondria) without synapse or axon loss over long periods of time. This conclusion is further supported by results of individual motor unit reconstruction by high resolution confocal microscopy. In triple transgenic *SOD^{G93A}, Thy1-MitoCFP*, *Thy1-YFP^{H}* mice, due to the subset labeling pattern in *Thy1-YFP^{H}* line, I was able to directly correlate mitochondrial transport and density with axonal morphology. Remarkably, motor neurons with severely compromised transport and reduced density of mitochondria still support peripheral arbors that terminate in normal appearing NMJs. In a control experiment I measured transport in YFP expressing axons and their non-YFP expressing neighboring axons in *Thy1-YFP^{H}* mice. High expression of YFP in subset of motor neurons in *Thy1-YFP^{H}* mice had no influence on mitochondrial transport at 50 days after birth and 4 months (120 days) after birth. However, YFP positive axons show reduced transport at 6 months of age, preventing use of these mice for studies in SOD mutants with later disease onset or in aging studies (for discussion see discussion chapter on “Axonal transport in *SOD^{WT}* mice”; page 112). This is not the first report of abnormalities in axons of the *Thy1-YFP^{H}* line. For example, the group of Michael Coleman has shown that spheroids form in the dorsal columns of older mice of this strain (Bridge et al., 2009). My new observations now further limit the usefulness of the popular *Thy1-YFP^{H}* and show that overexpression of a biologically largely "inert" protein alone suffices to induce transport deficits comparable in degree to what is seen in ALS models.

Several *in vivo* and *in vitro* studies have demonstrated that axonal transport of organelles is disrupted in ALS animal models (De Vos et al., 2007; Bilsland et al., 2010). These studies propose transport deficit to be a key and immediate cause of degeneration. In contrast, results of this study in *SOD^{G93A}* mice show a temporal disassociation between the onset of transport deficits and the onset of degeneration. Possible explanation for the discrepancy between the present study and previous *in vitro* studies could be in the methods used. Cell culture systems are made by culturing primary

motor neurons derived from transgenic mice or by transfecting embryonic rat cortical neurons with plasmids carrying human mutant SOD (Kieran et al., 2005; De Vos et al., 2007). Obviously in such systems it is not easy to study the temporal sequence of events that normally stretch over long periods of time in vivo. Moreover, in these systems, neurons are not fully differentiated or myelinated and therefore have different properties than *in vivo*. Undifferentiated neurons could have a different cytoskeleton composition, which would directly affect transport. Indeed, it is known that myelination of axons is required for maturation of the cytoskeleton and that myelin formation affects microtubule stability (Brady et al., 1999; Kirkpatrick et al., 2001). The axon myelination also directly affects mitochondrial motility (Ohno et al., 2011). Finally, the expression levels of mutated SOD after transfection in culture can be very high and therefore could induce overexpression artefacts. A recent *in vivo* study overcame these limitations and it reported, similar to the results of present study, a slowing down of retrogradely transported endosomal cargoes at all stages of disease and increased pausing of mitochondria in SOD^{G93A} mice at the presymptomatic stage (Bilsland et al., 2010). However, remarkably, the Bilsland study reports no decrease in the density of moving mitochondria (a parameter related to mitochondrial flux) in presymptomatic (P36) SOD^{G93A} mice. This is very interesting since these authors used the very *Thy1-mitoCFP* mice that our lab generated and characterized (Misgeld et al., 2007) and that I used in my study. Still, the results from the Bilsland study are in direct conflict to the results presented in this thesis. One possible explanation for this discrepancy could be the imaging technique chosen by Bilsland et al. The imaging frequency in the Bilsland et al. paper is 0.1-0.2Hz, since a slow scanning laser microscope was used. This, in our experience, is insufficient to actually obtain precise transport parameters and would yield lower transport flux simply because many moving mitochondria would pass through the field of view between image acquisitions. Indeed, values reported by Bilsland et al. are very low. Figure 5A of Bilsland et al. suggests a value of approx. 4 moving mitochondria/min - in contrast, Figure 5C indicates ~ 0.55 mitochondria/min (0.4 anterograde + 0.15 retrograde). In contrast, by using imaging at 1Hz on a wide-field microscope I was able to record 8-12 moving mitochondria/min in motor axons, which concords with previously reported

results in our *ex vivo* preparation, as well as in the sciatic nerve *in vivo* (Misgeld et al., 2007;Kerschensteiner et al., 2008).

4.2. Capacity of motor axons to increase transport in *SOD^{G93A}* mice is not exhausted

One of the questions that I tried to answer experimentally in this PhD thesis is if motor axons in *SOD^{G93A}* still have the capacity to increase transport despite their early and profound transport deficits. One possibility would be that axons in *SOD^{G93A}* mice are already transporting at maximum levels which although low, are still sufficient for maintenance of normal appearing arbors (see **Figure 3.17**, page 81). In other words, it is possible that axons simply cannot increase their transport due to the damage caused by the mutant SOD. Mutant SOD could interact with the transport machinery inducing slower and less efficient transport (Shi et al., 2010). In addition, mutant SOD could affect mitochondrial dynamics in the cell body causing fewer mitochondria to be sent out (Magrane et al., 2012). Such scenarios would imply that even if challenged, axons could not increase their transport. To explore this possibility I have performed complete axotomy of intercostal nerves in *SOD^{G93A}* mice. It is known that axotomy induces an increase in mitochondrial transport in the proximal stump of the axon that is evident already at 6h and persists up to 3 week after axotomy (Misgeld et al., 2007). It is though that neurons increase their transport as a part of the regeneration promoting response (Hoffman, 2010).

Surprisingly, axons in *SOD^{G93A}* mice also show an increase in axonal transport after axotomy. 24h after axotomy axons in *SOD^{G93A}* mice increase their total (anterograde plus retrograde) transport by ~50% reaching transport levels comparable to the levels of WT axons. Transport further increases with time after cut. After 7 days, transport in axotomized *SOD^{G93A}* axons exceeds transport in WT axons under normal (uncut) conditions. This suggests that the capacity to increase transport is not exhausted and that the ability to response to injury is preserved in *SOD^{G93A}* axons. Past research reports investigating the effect of axotomy in *SOD^{G93A}* mice were concentrated more on motor

neuron survival and the disease progression. The hope was that axotomy could provoke similar effects as a conditioning lesion. Conditioning lesions can augment neuronal survival and recovery following a subsequent injury. In the PNS, conditioning lesions have been shown to enhance the regeneration rate (Forman et al., 1980) and the extent of axon collateral sprouting (Jenq et al., 1988). However, results of studies in *SOD^{G93A}* mice reported both protective (Kong and Xu, 1999; Franz et al., 2009) and harmful effects of axotomy on motor neuron survival (Mariotti et al., 2002; Sharp et al., 2005). Of interest for this study is a recent report by Mesnard et al. (Mesnard et al., 2011), which shows that axotomized motor neurons in *SOD^{G93A}* and WT displayed similar transcription response to axotomy. Axotomized motor neurons both in WT and *SOD^{G93A}* significantly increased expression of pro-survival/regenerative genes like βII tubulin, GAP-43, Hn1, and BDNF. This result suggests that the response to axotomy is preserved in motor neurons in *SOD^{G93A}* mice. The results of this PhD thesis are adding the increase in mitochondrial transport in the cut nerve to the preserved response.

One interesting result of my axotomy experiment is the unexpected response of neighbouring intercostal nerves (see **Figure 3.20**; page 86), which to my knowledge were so far not examined, neither in WT nor in *SOD^{G93A}* mice. While in WT mice the neighbouring nerve responds with an increase of transport, this response is not detectable in *SOD^{G93A}* mice. (Note: nerves contralateral to a cut or in sham-operated animals do not show a change in transport.) It is of note that cell bodies of neurons that give rise to axons of cut and neighbouring nerve are located in different segments of the spinal cord and that they likely do not contact each other. Therefore, it is reasonable to assume that signal for transport increase comes from the muscle, which undergoes denervation after cut. Possible candidates include neurotrophins for which release after injury has been shown and which can regulate transport (Chada and Hollenbeck, 2004). The lack of response in *SOD^{G93A}* mice suggests impairments in some of these signalling pathways. Alternatively, while signalling might remain functional, the "denervation" stimulus in the mutant might not be strong enough to provoke a response in the neighboring nerve. This explanation would imply that additionally to these "remote" signalling, more local stimuli caused by the axotomy contribute to the response of the axotomized nerve (which is intact in the *SOD^{G93A}* mice). It is clear that further experiments

are needed to indentify the involved signalling pathways and to elucidate the underlying mechanisms. However, we did not pursue this venue of research, as our subsequent results questioned the disease-significance of the *SOD^{G93A}* results.

In line with increased transport, I observed changes in single mitochondria transport characteristics after the axotomy both in WT and *SOD^{G93A}* mice. The most prominent changes after the axotomy were in stop length and frequency, parameters which contribute importantly to the reduced average speed of mitochondria in *SOD^{G93A}* mice. The observed recovery in these parameters after axotomy raise the possibility that putative changes in cytoskeletal tracks or motor proteins underlying transport defects are also in principle reversible.

4.3. Changes of mitochondrial morphology in *SOD^{G93A}* mice

In this study I also tried to address changes in mitochondrial functionality in animal models of ALS. However, it is challenging to assess mitochondrial membrane or redox potential in motor axons *in vivo* or in explant preparation. Therefore I used mitochondrial morphology as a readout for mitochondrial functionality. This is justified by many previous studies in which it was shown by electron microscopy that rounded and swollen mitochondria have altered cristae and therefore are likely functionally impaired (Sun et al., 2007). Direct evidence for a connection between mitochondrial morphology, functionality and ultra-structural changes came from a recent study by Nikić et al., from my thesis labs (Nikić et al., 2011). In this study, the authors used imaging to directly show that swollen appearing mitochondria *in vivo* have an altered mitochondrial potential. Furthermore they used serial section electron microscopy to show ultrastructural alternations at the level of cristae of such mitochondria.

In this study I observed very early change in shape of the stationary axonal mitochondria. These changes are first evident between P15 and P20. Correlation of mitochondrial shape factor and transport in individual axons suggest that the changes in shape factor precede reduction in transport. A possible underlying mechanism could be that mutated *SOD^{G93A}* protein interacts with mitochondria causing functional impairments.

It was shown that mutant *SOD*^{G93A} protein associates with mitochondria and enters the intramembrane space (Liu et al., 2004; Igoudjil et al., 2011). This causes expansion of intermembrane space and leads to problems in mitochondrial function (Manfredi and Xu, 2005). Once morphologically and functionally impaired, mitochondria are likely not able to locally provide ATP or buffer calcium. Also, they could be source of reactive oxygen species (ROS). Insufficient ATP could cause inefficiency of motor proteins (Hirokawa et al., 2010), while high local Ca^{2+} would lead to detachment of motor proteins and cargoes from microtubules (Wang and Schwarz, 2009). Finally, ROS produced in excess from malfunctioning mitochondria could damage microtubules and impair transport. Indeed, swollen mitochondria have higher ROS production in late stage *SOD*^{G93A} mice, as my colleagues and I found using new ROS reporter mice (Breckwoldt et al., in preparation). Still, it is worth nothing that swollen morphology could be an artefact of high expression of mutant SOD and not directly linked to ALS pathogenesis (Bergemalm et al., 2006). Such interpretation is supported by two results of this study. First, *SOD*^{WT} mice show a similar mitochondrial phenotype as *SOD*^{G93A} mice and second *SOD*^{G85R} mice do not show alternations in mitochondrial morphology (for discussion see below).

4.4. Axonal transport in *SOD*^{G85R} mice

Surprisingly, analysis of transport in *SOD*^{G85R} revealed normal transport flux even in the preterminal stage of the disease, when clear signs of axon degeneration were detectable in intercostal and tibialis nerves and when animals show clinical symptoms of the disease. The *SOD*^{G85R} mice express a mutated, but in contrast to *SOD*^{G93A} and *SOD*^{G37R} mice, inactive form of the SOD enzyme. Furthermore, according to the literature, *SOD*^{G85R} mice express mutated protein to levels similar to endogenous mouse SOD (Bruijn et al., 1997). However, our immunohistochemical quantification of *SOD*^{G85R} expression in motor neurons themselves showed similar levels to *SOD*^{WT}, in other words higher than previously reported (see **Figure 3.1**; page 59). These differences could be explained by different methods used (immunohistochemistry in single cells in this study *vs.* whole brain or spinal cord homogenates). Previous studies reported no morphological mitochondrial abnormalities in *SOD*^{G85R} (Bruijn et al., 1997), although association of the mutated enzyme

with spinal mitochondria was reported (Liu et al 2004). Surprisingly, a recent study reported even increase in mitochondrial length in these mice (Vande Velde et al., 2011). Spinal mitochondria in symptomatic *SOD^{G85R}* mice have reduced buffer capacity for Ca^{2+} but respiration rate, ATP synthesis and mitochondrial potential were unaffected (Damiano et al., 2006). Taking these results together it is seems that *SOD^{G85R}* mice in contrast to SOD^{G93A} mice do not show alternations in mitochondrial morphology or function. Changes in mitochondrial morphology are often stated in the literature to be one of the ALS hallmarks. However, these statements are mostly based on studies done in *SOD^{G93A}* or *SOD^{G37R}* mice. Studies on mitochondrial morphology in ALS patients are for obvious reasons rare. One of the most cited papers in the literature is the electron microscopy study of synapses in autopsies from sporadic ALS patients (Sasaki and Iwata, 1996) In this paper authors showed aggregation of structurally altered mitochondria in synapses. However, the data in Sasaki et al study are obtained from autopsies i.e. post-mortem samples form patients who were in terminal stage of the disease. Thus, observed changes in mitochondrial morphology could be part of the final steps of the neurodegenerative processes. Moreover, it is impossible to deduce from such samples if changes in mitochondrial morphology are also present earlier during disease course or in the presymptomatic phase, which would implicate their role in the disease pathogenesis.

No study so far addressed the axonal transport in *SOD^{G85R}* mice *in vivo*, although a transport deficit was suggested based on reduced density of synaptic vesicles at the NMJs, even though the data were not shown (Pun et al., 2006). Previous experiments in cell culture showed that G85R affects mitochondrial transport in a similar way as other mutated forms of SOD protein, i.e. reducing the number of anterograde moving mitochondria and increasing the number of retrograde moving mitochondria (De Vos et al., 2007). The results of the present study now show no transport deficit in *SOD^{G85R}* mice until the terminal stage of the disease, when a slight decrease in anterograde transport was observed. This means that axons can degenerate without long-standing transport deficits and that transport deficits are not a general feature of ALS-like pathology. The lack of transport deficit in another G85R line, the *G85R SOD-YFP* mice, further supports this view, even though limited availability of these mice precluded a comprehensive study.

4.5. Axonal transport in *SOD^{WT}* mice

Axons can thus degenerate without preceding transport deficits, but is the converse also true, i.e. are there models in which axonal transport is disrupted while axons survive? Analysis of *SOD^{WT}* mice suggests that this is indeed possible. *SOD^{WT}* mice over-express a non-mutated form of the human SOD protein and are commonly used as control mice in ALS studies. Transport measurements showed a reduction in mitochondrial transport in these "control" mice already two months after birth. The transport deficit was progressive: by 4 months of age *SOD^{WT}* mice showed a deficit comparable to *SOD^{G93A}* mice and this persisted up to 12 months of age. Here, even more clearly than in *SOD^{G93A}* mice, a temporal disassociation between transport deficit and degeneration was obvious, since only mild denervation was detected at 12 months as previously reported (Jaarsma et al., 2000). This shows once again the remarkable capacity of motor neurons to survive profound transport deficits. However, it is worth noting that these mice do develop a late onset form of neurodegeneration (Dal Canto and Gurney, 1995; Jaarsma et al., 2000). This degeneration does not primarily affect motor neurons, but long projection neurons of the central nervous system, such as the spino-cerebellar or the dorsal column tracts. In contrast, motor neurons are amongst the nerve cells that degenerate late, again dissociating this pathology from ALS. Results obtained in *SOD^{WT}* mice offer the possibility to hypothesise that the observed pathology in *SOD^{G93A}* mice has two components. One which is ALS-related and which initiates explosive axon degeneration, and a second component which is related to over-expression of SOD, no matter whether the protein mutated or not. This component induces transport deficit, affects mitochondrial morphology and (perhaps) accelerates the disease. In support of this hypothesis are the results of a study by Jaarsma et al. 2000, which showed that crossing *SOD^{WT}* mice with *SOD^{G93A}* mice induces earlier disease onset and death. This also suggests that there is a limit to which motor neurons can sustain transport deficits - it seems to perhaps increase their vulnerability to other, ALS-related toxicity mechanisms. The results of the measurements in *Thy1-MitoCFP*, *Thy1-YFP^{H}* further support the view that over expression of proteins can induce transport deficits. In these mice at 6 months of age, YFP-positive axons showed comparable mitochondrial transport deficits to the deficits observed in *SOD^{WT}* and *SOD^{G93A}* mice. This suggests that over-expression of YFP, which does not

have any physiological role in mouse neurons, can induce transport impairments. Therefore, special attention is needed in choosing and characterizing transgenic lines and in running control experiments if protein over-expression is involved.

4.6. General discussion

The aim of this PhD study was to investigate the *in vivo* consequences of reduced organelle transport in ALS mice, which – based on the published literature (De Vos et al., 2007; Bilsland et al., 2010; Magrane et al., 2012; Vande Velde et al., 2011) – was expected to be a general feature of ALS disease models. However, by comparing several different *bona fide* models of SOD-based familial ALS, I found that rather than co-segregating with the ALS-specific mutation, transport disturbances were only present in some SOD-mice (SOD^{G93A} , SOD^{G37R} and SOD^{WT} , but not SOD^{G85R}), irrespective of whether the enzyme carried an ALS mutation or not. These results thus dissociate organelle transport deficits and axon degeneration in animal models of ALS. This conclusion contrasts with widely held assumptions in the field of ALS research, which are based on reduced organelle density in SOD^{G93A} axons (Pun et al., 2006, Vande Velde et al., 2011) and altered organelle motility in SOD^{G93A} axons *in vitro* (De Vos et al., 2007; Magrane et al., 2012) and *in vivo* (Bilsland et al., 2010).

One important distinguishing feature of our study is that we performed a systematic time-course comparison of organelle transport in fully mature motor axons in several ALS models that differ in SOD expression level, enzymatic activity and mutation status. This is of importance as it is well-established from human studies that a vast number of different SOD mutations, which for example differ in their effects on biochemical activity or stability of the enzyme (Dion et al., 2009), lead to essentially the same ALS phenotype. Any cell biological mechanism that is linked to the root-cause of motor neuron degeneration in ALS should therefore probably be similarly affected across the spectrum of disease-related SOD mutations and ideally absent in SOD^{WT} controls. Detailed comparison in this study now shows that organelle transport disruptions do not fulfil this criterion, and hence are not directly related to mutation-specific toxicity of SOD, but seem rather to be caused by excess enzymatic activity, protein expression levels, subcellular mis-localisation or aggregation; however, which combination of these parameters affects transport cannot

be definitively differentiated based on data sets presented here. In contrast to my study, most previous reports on the link between ALS and organelle transport either focussed on only one mutation, performed comparisons *in vitro* or in non-motor neuron cells, or did not include the wild-type over-expression control, SOD^{WT}. Other studies looked only at surrogate markers of transport deficits (such as organelle density; (Vande Velde et al., 2011; Shan et al., 2010; Pun et al., 2006).

In my view, the fact that SOD^{WT} mice maintain essentially normal neuromuscular innervation despite profound and long-lasting transport deficits that are comparable to those observed in SOD^{G93A} and SOD^{G37R} severely weakens the evidence in favor of the hypothesis that disruptions in organelle transport alone could be the pathogenic mechanism in ALS motor neuron degeneration. There is further evidence that argues against a direct role of organelle transport deficits in causing the degenerative phenotype in SOD^{G93A} mice. For example, increasing mitochondrial transport does not yield the expected therapeutic benefit in SOD^{G93A} mice (Zhu and Sheng, 2011). Furthermore, while the fact that mutations in motor proteins can cause a neurodegenerative phenotype is often cited in support of a role for axonal transport in ALS-pathogenesis, mutations in retrograde motor proteins alone do not phenocopy SOD^{G93A} (Perlson et al., 2009). Still, while not primarily pathogenic, the motor axon-specific transport deficits – as seen in SOD^{G93A} or SOD^{G37R} mice – might contribute to the phenotypic variations seen between the diseases caused by differentially mutated SOD. Hence, comparing the phenotypes caused by mutations that affect transport and others that do not (such as SOD^{G85R}) might allow differentiating factors that initiate or just accelerate axon degeneration. Indeed, the observation alone that SOD^{WT} mice have a transport deficit does not strictly refute the possibility that a transport deficit could exist in ALS. Only together with my observations that the SOD^{85R} mice lack a comparable transport deficit does an argument emerge that represents a significant challenge to the idea that ALS is essentially a "transport-o-pathy".

A number of general conclusions emerge from this study: First, in ALS models, the mechanisms that reduce organelle transport appear distinct from those that initiate axon degeneration. Hence, axonal transport of organelles might not be a suitable target to therapeutically prevent the irreversible loss of neurons or axons in ALS, even though in

other neurodegenerative diseases this might clearly be a promising strategy (d'Ydawelle et al., 2011). In any case, my argument strictly applies only to mitochondria and endosome-derived vesicles. While these are the most commonly assayed specific cargoes in the context of ALS-research, it remains possible that disturbed transport of another cargo would better correlate with ALS-related neurodegeneration. For instance, my study does not exclude disturbances in slow axonal transport (Collard et al., 1995; Williamson and Cleveland, 1999) or changes in cargo composition (Perlson et al., 2009) as important steps in ALS pathogenesis, nor does it contradict the view that organelle transport deficits can accelerate axon degeneration, e.g. in the SODG93A model (Jaarsma et al., 2000). Second, our findings underline the phenotypic heterogeneity that characterizes even closely related animal models of neurodegeneration. This emphasizes the need to study several models to differentiate disease-related (e.g. degeneration) from model-related (e.g. transport deficits) events. Third, our study reveals the remarkable capability of motor neurons to survive for long periods of time despite limited axonal transport. Indeed, even in those SOD-overexpression models that affected transport severely, the drop in mitochondrial density was delayed (**Figure 3.10** *vs.* **Figure 3.11;** pages 72 and 73, respectively) suggesting some compensatory mechanism. One part of this compensation could be the time-shifted drop in retrograde transport, which over time reduces the net deficit in organelle number. This would imply a longer residency of individual organelles in the periphery. In the case of mitochondria this could help to buffer a deficit in the supply of energy substrates. However, in the presence of additional stressors (which might well be ALS-related), the accumulation of increasingly dysfunctional mitochondria could well accelerate axonal demise.

5. PUBLICATIONS

Marinković P, Reuter MS, Brill MS, Godinho L, Kerschensteiner M, Misgeld T. **Axonal transport deficits and degeneration evolve independently in mouse models of amyotrophic lateral sclerosis.** *PNAS* (2012)

Marinković P, Godinho L, Misgeld T. **Generation and screening of mice with transgenic neuronal labeling controlled by thy1-regulatory elements**. in *Imaging in Neuroscience: A Laboratory Manual* (2011); CSHL Press, Cold Spring Harbor, NY, USA

Brill MS, Marinković P, Misgeld T. **Sequential photo-bleaching to delineate single Schwann cells at the neuromuscular junction.** *JOVE* (Invited submission). *In preparation*

Breckwoldt B, Pfister F, Williams P, Marinković P, Godinho L, Bareyre FM, Naumann R, Dick TP, Kerschensteiner M and Misgeld T. **In vivo visualisation of fast mitochondrial redox signals during neuronal physiology and pathology.** *In preparation*

Kleele T, Brill MS, Marinković P, Godinho L, Kerschensteiner M, Misgeld T. **EB3 transgenic mice to study microtubule dynamics.** *In preparation*

6. REFERENCES

Alexander GM, Erwin KL, Byers N, Deitch JS, Augelli BJ, Blankenhorn EP, Heiman-Patterson TD (2004) Effect of transgene copy number on survival in the G93A SOD1 transgenic mouse model of ALS. Brain Res Mol Brain Res 130: 7-15.

Bandopadhyay R, de Belleroche J (2010) Pathogenesis of Parkinson's disease: emerging role of molecular chaperones. Trends Mol Med 16: 27-36.

Batlevi Y, La Spada AR (2011) Mitochondrial autophagy in neural function, neurodegenerative disease, neuron cell death, and aging. Neurobiol Dis 43: 46-51.

Beers DR, Henkel JS, Xiao Q, Zhao W, Wang J, Yen AA, Siklos L, McKercher SR, Appel SH (2006) Wild-type microglia extend survival in PU.1 knockout mice with familial amyotrophic lateral sclerosis. Proc Natl Acad Sci U S A 103: 16021-16026.

Bergemalm D, Jonsson PA, Graffmo KS, Andersen PM, Brannstrom T, Rehnmark A, Marklund SL (2006) Overloading of stable and exclusion of unstable human superoxide dismutase-1 variants in mitochondria of murine amyotrophic lateral sclerosis models. J Neurosci 26: 4147-4154.

Bilsland LG, Sahai E, Kelly G, Golding M, Greensmith L, Schiavo G (2010) Deficits in axonal transport precede ALS symptoms in vivo. Proc Natl Acad Sci U S A 107: 20523-20528.

Binet S, Meininger V (1988) Modifications of microtubule proteins in ALS nerve precede detectable histologic and ultrastructural changes. Neurology 38: 1596-1600.

Bogaert E, d'Ydewalle C, Van Den BL (2010) Amyotrophic lateral sclerosis and excitotoxicity: from pathological mechanism to therapeutic target. CNS Neurol Disord Drug Targets 9: 297-304.

Boillee S, Vande VC, Cleveland DW (2006a) ALS: a disease of motor neurons and their nonneuronal neighbors. Neuron 52: 39-59.

Boillee S, Yamanaka K, Lobsiger CS, Copeland NG, Jenkins NA, Kassiotis G, Kollias G, Cleveland DW (2006b) Onset and progression in inherited ALS determined by motor neurons and microglia. Science 312: 1389-1392.

Brady ST (1985) A novel brain ATPase with properties expected for the fast axonal transport motor. Nature 317: 73-75.

Brady ST, Witt AS, Kirkpatrick LL, de Waegh SM, Readhead C, Tu PH, Lee VM (1999) Formation of compact myelin is required for maturation of the axonal cytoskeleton. J Neurosci 19: 7278-7288.

Bridge KE, Berg N, Adalbert R, Babetto E, Dias T, Spillantini MG, Ribchester RR, Coleman MP (2009) Late onset distal axonal swelling in YFP-H transgenic mice. Neurobiol Aging 30: 309-321.

Brooks BR (1994) El Escorial World Federation of Neurology criteria for the diagnosis of amyotrophic lateral sclerosis. Subcommittee on Motor Neuron Diseases/Amyotrophic Lateral Sclerosis of the World Federation of Neurology Research Group on Neuromuscular Diseases and the El Escorial "Clinical limits of amyotrophic lateral sclerosis" workshop contributors. J Neurol Sci 124 Suppl: 96-107.

Bruijn LI, Becher MW, Lee MK, Anderson KL, Jenkins NA, Copeland NG, Sisodia SS, Rothstein JD, Borchelt DR, Price DL, Cleveland DW (1997) ALS-linked SOD1 mutant G85R mediates damage to astrocytes and promotes rapidly progressive disease with SOD1-containing inclusions. Neuron 18: 327-338.

Bruijn LI, Houseweart MK, Kato S, Anderson KL, Anderson SD, Ohama E, Reaume AG, Scott RW, Cleveland DW (1998) Aggregation and motor neuron toxicity of an ALS-linked SOD1 mutant independent from wild-type SOD1. Science 281: 1851-1854.

Buratti E, Brindisi A, Giombi M, Tisminetzky S, Ayala YM, Baralle FE (2005) TDP-43 binds heterogeneous nuclear ribonucleoprotein A/B through its C-terminal tail: an important region for the inhibition of cystic fibrosis transmembrane conductance regulator exon 9 splicing. J Biol Chem 280: 37572-37584.

Cai Q, Davis ML, Sheng ZH (2011) Regulation of axonal mitochondrial transport and its impact on synaptic transmission. Neurosci Res 70: 9-15.

Cai Q, Gerwin C, Sheng ZH (2005) Syntabulin-mediated anterograde transport of mitochondria along neuronal processes. J Cell Biol 170: 959-969.

Cai Q, Zakaria HM, Simone A, Sheng ZH (2012) Spatial Parkin Translocation and Degradation of Damaged Mitochondria via Mitophagy in Live Cortical Neurons. Curr Biol.

Caroni P (1997) Overexpression of growth-associated proteins in the neurons of adult transgenic mice. J Neurosci Methods 71: 3-9.

Chada SR, Hollenbeck PJ (2004) Nerve growth factor signaling regulates motility and docking of axonal mitochondria. Curr Biol 14: 1272-1276.

Chen S, Owens GC, Crossin KL, Edelman DB (2007) Serotonin stimulates mitochondrial transport in hippocampal neurons. Mol Cell Neurosci 36: 472-483.

Chen S, Owens GC, Edelman DB (2008) Dopamine inhibits mitochondrial motility in hippocampal neurons. PLoS ONE 3: e2804.

Chen S, Owens GC, Makarenkova H, Edelman DB (2010) HDAC6 regulates mitochondrial transport in hippocampal neurons. PLoS ONE 5: e10848.

Chen YM, Gerwin C, Sheng ZH (2009) Dynein light chain LC8 regulates syntaphilin-mediated mitochondrial docking in axons. J Neurosci 29: 9429-9438.

Chen YZ, Bennett CL, Huynh HM, Blair IP, Puls I, Irobi J, Dierick I, Abel A, Kennerson ML, Rabin BA, Nicholson GA, Auer-Grumbach M, Wagner K, De Jonghe P, Griffin JW, Fischbeck KH, Timmerman V, Cornblath DR, Chance PF (2004) DNA/RNA helicase gene mutations in a form of juvenile amyotrophic lateral sclerosis (ALS4). Am J Hum Genet 74: 1128-1135.

Chio A, Calvo A, Dossena M, Ghiglione P, Mutani R, Mora G (2009) ALS in Italian professional soccer players: the risk is still present and could be soccer-specific. Amyotroph Lateral Scler 10: 205-209.

Chiu SY (2011) Matching mitochondria to metabolic needs at nodes of ranvier. Neuroscientist 17: 343-350.

Cho KI, Cai Y, Yi H, Yeh A, Aslanukov A, Ferreira PA (2007) Association of the kinesin-binding domain of RanBP2 to KIF5B and KIF5C determines mitochondria localization and function. Traffic 8: 1722-1735.

Clement AM, Nguyen MD, Roberts EA, Garcia ML, Boillee S, Rule M, McMahon AP, Doucette W, Siwek D, Ferrante RJ, Brown RH, Jr., Julien JP, Goldstein LS, Cleveland DW (2003) Wild-type nonneuronal cells extend survival of SOD1 mutant motor neurons in ALS mice. Science 302: 113-117.

Collard JF, Cote F, Julien JP (1995) Defective axonal transport in a transgenic mouse model of amyotrophic lateral sclerosis. Nature 375: 61-64.

Conde C, Caceres A (2009) Microtubule assembly, organization and dynamics in axons and dendrites. Nat Rev Neurosci 10: 319-332.

Crapo JD, Oury T, Rabouille C, Slot JW, Chang LY (1992) Copper,zinc superoxide dismutase is primarily a cytosolic protein in human cells. Proc Natl Acad Sci U S A 89: 10405-10409.

d'Ydewalle C, Krishnan J, Chiheb DM, Van Damme P, Irobi J, Kozikowski AP, Berghe PV, Timmerman V, Robberecht W, Van Den BL (2011) HDAC6 inhibitors reverse axonal loss in a mouse model of mutant HSPB1-induced Charcot-Marie-Tooth disease. Nat Med 17: 968-974.

Dal Canto MC, Gurney ME (1995) Neuropathological changes in two lines of mice carrying a transgene for mutant human Cu,Zn SOD, and in mice overexpressing wild type human SOD: a model of familial amyotrophic lateral sclerosis (FALS). Brain Res 676: 25-40.

Damiano M, Starkov AA, Petri S, Kipiani K, Kiaei M, Mattiazzi M, Flint BM, Manfredi G (2006) Neural mitochondrial Ca2+ capacity impairment precedes the onset of motor symptoms in G93A Cu/Zn-superoxide dismutase mutant mice. J Neurochem 96: 1349-1361.

Davis AF, Clayton DA (1996) In situ localization of mitochondrial DNA replication in intact mammalian cells. J Cell Biol 135: 883-893.

De Vos KJ, Chapman AL, Tennant ME, Manser C, Tudor EL, Lau KF, Brownlees J, Ackerley S, Shaw PJ, McLoughlin DM, Shaw CE, Leigh PN, Miller CC, Grierson AJ (2007) Familial amyotrophic lateral sclerosis-linked SOD1 mutants perturb fast axonal transport to reduce axonal mitochondria content. Hum Mol Genet 16: 2720-2728.

De Vos KJ, Grierson AJ, Ackerley S, Miller CC (2008) Role of axonal transport in neurodegenerative diseases. Annu Rev Neurosci 31: 151-173.

Detmer SA, Chan DC (2007) Functions and dysfunctions of mitochondrial dynamics. Nat Rev Mol Cell Biol 8: 870-879.

Di Giorgio FP, Carrasco MA, Siao MC, Maniatis T, Eggan K (2007) Non-cell autonomous effect of glia on motor neurons in an embryonic stem cell-based ALS model. Nat Neurosci 10: 608-614.

Ding H, Dolan PJ, Johnson GV (2008) Histone deacetylase 6 interacts with the microtubule-associated protein tau. J Neurochem 106: 2119-2130.

Dion PA, Daoud H, Rouleau GA (2009) Genetics of motor neuron disorders: new insights into pathogenic mechanisms. Nat Rev Genet 10: 769-782.

Dixit R, Ross JL, Goldman YE, Holzbaur EL (2008) Differential regulation of dynein and kinesin motor proteins by tau. Science 319: 1086-1089.

Doble A (1996) The pharmacology and mechanism of action of riluzole. Neurology 47: S233-S241.

Durham HD, Roy J, Dong L, Figlewicz DA (1997) Aggregation of mutant Cu/Zn superoxide dismutase proteins in a culture model of ALS. J Neuropathol Exp Neurol 56: 523-530.

Edelstein A, Amodaj N, Hoover K, Vale R, Stuurman N (2010) Computer control of microscopes using microManager. Curr Protoc Mol Biol Chapter 14: Unit14.

Eisen A, Swash M (2001) Clinical neurophysiology of ALS. Clin Neurophysiol 112: 2190-2201.

Fanara P, Banerjee J, Hueck RV, Harper MR, Awada M, Turner H, Husted KH, Brandt R, Hellerstein MK (2007) Stabilization of hyperdynamic microtubules is neuroprotective in amyotrophic lateral sclerosis. J Biol Chem 282: 23465-23472.

Farah CA, Nguyen MD, Julien JP, Leclerc N (2003) Altered levels and distribution of microtubule-associated proteins before disease onset in a mouse model of amyotrophic lateral sclerosis. J Neurochem 84: 77-86.

Feng G, Mellor RH, Bernstein M, Keller-Peck C, Nguyen QT, Wallace M, Nerbonne JM, Lichtman JW, Sanes JR (2000) Imaging neuronal subsets in transgenic mice expressing multiple spectral variants of GFP. Neuron 28: 41-51.

Fischer LR, Culver DG, Tennant P, Davis AA, Wang M, Castellano-Sanchez A, Khan J, Polak MA, Glass JD (2004) Amyotrophic lateral sclerosis is a distal axonopathy: evidence in mice and man. Exp Neurol 185: 232-240.

Forman DS, McQuarrie IG, Labore FW, Wood DK, Stone LS, Braddock CH, Fuchs DA (1980) Time course of the conditioning lesion effect on axonal regeneration. Brain Res 182: 180-185.

Fransson A, Ruusala A, Aspenstrom P (2003) Atypical Rho GTPases have roles in mitochondrial homeostasis and apoptosis. J Biol Chem 278: 6495-6502.

Franz CK, Quach ET, Krudy CA, Federici T, Kliem MA, Snyder BR, Raore B, Boulis NM (2009) A conditioning lesion provides selective protection in a rat model of Amyotrophic Lateral Sclerosis. PLoS ONE 4: e7357.

Fujita T, Maturana AD, Ikuta J, Hamada J, Walchli S, Suzuki T, Sawa H, Wooten MW, Okajima T, Tatematsu K, Tanizawa K, Kuroda S (2007) Axonal guidance protein FEZ1 associates with tubulin and kinesin motor protein to transport mitochondria in neurites of NGF-stimulated PC12 cells. Biochem Biophys Res Commun 361: 605-610.

Fukushima N, Furuta D, Hidaka Y, Moriyama R, Tsujiuchi T (2009) Post-translational modifications of tubulin in the nervous system. J Neurochem 109: 683-693.

Galjart N (2010) Plus-end-tracking proteins and their interactions at microtubule ends. Curr Biol 20: R528-R537.

Gaudette M, Hirano M, Siddique T (2000) Current status of SOD1 mutations in familial amyotrophic lateral sclerosis. Amyotroph Lateral Scler Other Motor Neuron Disord 1: 83-89.

Glater EE, Megeath LJ, Stowers RS, Schwarz TL (2006) Axonal transport of mitochondria requires milton to recruit kinesin heavy chain and is light chain independent. J Cell Biol 173: 545-557.

Gong YH, Parsadanian AS, Andreeva A, Snider WD, Elliott JL (2000) Restricted expression of G86R Cu/Zn superoxide dismutase in astrocytes results in astrocytosis but does not cause motoneuron degeneration. J Neurosci 20: 660-665.

Grafstein B, Forman DS (1980) Intracellular transport in neurons. Physiol Rev 60: 1167-1283.

Greenway MJ, Andersen PM, Russ C, Ennis S, Cashman S, Donaghy C, Patterson V, Swingler R, Kieran D, Prehn J, Morrison KE, Green A, Acharya KR, Brown RH, Jr., Hardiman O (2006) ANG mutations segregate with familial and 'sporadic' amyotrophic lateral sclerosis. Nat Genet 38: 411-413.

Grishin A, Li H, Levitan ES, Zaks-Makhina E (2006) Identification of gamma-aminobutyric acid receptor-interacting factor 1 (TRAK2) as a trafficking factor for the K+ channel Kir2.1. J Biol Chem 281: 30104-30111.

Guo X, Macleod GT, Wellington A, Hu F, Panchumarthi S, Schoenfield M, Marin L, Charlton MP, Atwood HL, Zinsmaier KE (2005) The GTPase dMiro is required for axonal transport of mitochondria to Drosophila synapses. Neuron 47: 379-393.

Gurney ME, Pu H, Chiu AY, Dal Canto MC, Polchow CY, Alexander DD, Caliendo J, Hentati A, Kwon YW, Deng HX, . (1994) Motor neuron degeneration in mice that express a human Cu,Zn superoxide dismutase mutation. Science 264: 1772-1775.

Haass C (2010) Initiation and propagation of neurodegeneration. Nat Med 16: 1201-1204.

Hadano S, Hand CK, Osuga H, Yanagisawa Y, Otomo A, Devon RS, Miyamoto N, Showguchi-Miyata J, Okada Y, Singaraja R, Figlewicz DA, Kwiatkowski T, Hosler BA, Sagie T, Skaug J, Nasir J, Brown RH, Jr., Scherer SW, Rouleau GA, Hayden MR, Ikeda JE (2001) A gene encoding a putative GTPase regulator is mutated in familial amyotrophic lateral sclerosis 2. Nat Genet 29: 166-173.

Hafezparast M, Klocke R, Ruhrberg C, Marquardt A, Ahmad-Annuar A, Bowen S, Lalli G, Witherden AS, Hummerich H, Nicholson S, Morgan PJ, Oozageer R, Priestley JV, Averill S, King VR, Ball S, Peters J, Toda T, Yamamoto A, Hiraoka Y, Augustin M, Korthaus D, Wattler S, Wabnitz P, Dickneite C, Lampel S, Boehme F, Peraus G, Popp A, Rudelius M, Schlegel J, Fuchs H, Hrabe dA, Schiavo G, Shima DT, Russ AP, Stumm G, Martin JE, Fisher EM (2003) Mutations in dynein link motor neuron degeneration to defects in retrograde transport. Science 300: 808-812.

Halpain S, Dehmelt L (2006) The MAP1 family of microtubule-associated proteins. Genome Biol 7: 224.

Hardiman O, van den Berg LH, Kiernan MC (2011) Clinical diagnosis and management of amyotrophic lateral sclerosis. Nat Rev Neurol 7: 639-649.

Heckman CJ, Johnson M, Mottram C, Schuster J (2008) Persistent inward currents in spinal motoneurons and their influence on human motoneuron firing patterns. Neuroscientist 14: 264-275.

Hirokawa N (1982) Cross-linker system between neurofilaments, microtubules, and membranous organelles in frog axons revealed by the quick-freeze, deep-etching method. J Cell Biol 94: 129-142.

Hirokawa N, Niwa S, Tanaka Y (2010) Molecular motors in neurons: transport mechanisms and roles in brain function, development, and disease. Neuron 68: 610-638.

Hirokawa N, Noda Y, Tanaka Y, Niwa S (2009) Kinesin superfamily motor proteins and intracellular transport. Nat Rev Mol Cell Biol 10: 682-696.

Hirokawa N, Pfister KK, Yorifuji H, Wagner MC, Brady ST, Bloom GS (1989) Submolecular domains of bovine brain kinesin identified by electron microscopy and monoclonal antibody decoration. Cell 56: 867-878.

Hoffman PN (2010) A conditioning lesion induces changes in gene expression and axonal transport that enhance regeneration by increasing the intrinsic growth state of axons. Exp Neurol 223: 11-18.

Hollenbeck PJ, Saxton WM (2005) The axonal transport of mitochondria. J Cell Sci 118: 5411-5419.

Hollmann M, Hartley M, Heinemann S (1991) Ca2+ permeability of KA-AMPA--gated glutamate receptor channels depends on subunit composition. Science 252: 851-853.

Horner RD, Kamins KG, Feussner JR, Grambow SC, Hoff-Lindquist J, Harati Y, Mitsumoto H, Pascuzzi R, Spencer PS, Tim R, Howard D, Smith TC, Ryan MA, Coffman CJ, Kasarskis EJ (2003) Occurrence of amyotrophic lateral sclerosis among Gulf War veterans. Neurology 61: 742-749.

Hubbert C, Guardiola A, Shao R, Kawaguchi Y, Ito A, Nixon A, Yoshida M, Wang XF, Yao TP (2002) HDAC6 is a microtubule-associated deacetylase. Nature 417: 455-458.

Igoudjil A, Magrane J, Fischer LR, Kim HJ, Hervias I, Dumont M, Cortez C, Glass JD, Starkov AA, Manfredi G (2011) In vivo pathogenic role of mutant SOD1 localized in the mitochondrial intermembrane space. J Neurosci 31: 15826-15837.

Jaarsma D, Haasdijk ED, Grashorn JA, Hawkins R, van Duijn W, Verspaget HW, London J, Holstege JC (2000) Human Cu/Zn superoxide dismutase (SOD1) overexpression in mice causes mitochondrial vacuolization, axonal degeneration, and premature motoneuron death and accelerates motoneuron disease in mice expressing a familial amyotrophic lateral sclerosis mutant SOD1. Neurobiol Dis 7: 623-643.

Jaarsma D, Teuling E, Haasdijk ED, De Zeeuw CI, Hoogenraad CC (2008) Neuron-specific expression of mutant superoxide dismutase is sufficient to induce amyotrophic lateral sclerosis in transgenic mice. J Neurosci 28: 2075-2088.

Jenq CB, Jenq LL, Bear HM, Coggeshall RE (1988) Conditioning lesions of peripheral nerves change regenerated axon numbers. Brain Res 457: 63-69.

Jonsson PA, Graffmo KS, Andersen PM, Brannstrom T, Lindberg M, Oliveberg M, Marklund SL (2006) Disulphide-reduced superoxide dismutase-1 in CNS of transgenic amyotrophic lateral sclerosis models. Brain 129: 451-464.

Kang JS, Tian JH, Pan PY, Zald P, Li C, Deng C, Sheng ZH (2008) Docking of axonal mitochondria by syntaphilin controls their mobility and affects short-term facilitation. Cell 132: 137-148.

Karki S, Holzbaur EL (1995) Affinity chromatography demonstrates a direct binding between cytoplasmic dynein and the dynactin complex. J Biol Chem 270: 28806-28811.

Kato S (2008) Amyotrophic lateral sclerosis models and human neuropathology: similarities and differences. Acta Neuropathol 115: 97-114.

Keller-Peck CR, Walsh MK, Gan WB, Feng G, Sanes JR, Lichtman JW (2001) Asynchronous synapse elimination in neonatal motor units: studies using GFP transgenic mice. Neuron 31: 381-394.

Kerschensteiner M, Reuter MS, Lichtman JW, Misgeld T (2008) Ex vivo imaging of motor axon dynamics in murine triangularis sterni explants. Nat Protoc 3: 1645-1653.

Khabazian I, Bains JS, Williams DE, Cheung J, Wilson JM, Pasqualotto BA, Pelech SL, Andersen RJ, Wang YT, Liu L, Nagai A, Kim SU, Craig UK, Shaw CA (2002) Isolation of various forms of sterol beta-D-glucoside from the seed of Cycas circinalis: neurotoxicity and implications for ALS-parkinsonism dementia complex. J Neurochem 82: 516-528.

Kieran D, Hafezparast M, Bohnert S, Dick JR, Martin J, Schiavo G, Fisher EM, Greensmith L (2005) A mutation in dynein rescues axonal transport defects and extends the life span of ALS mice. J Cell Biol 169: 561-567.

King SJ, Schroer TA (2000) Dynactin increases the processivity of the cytoplasmic dynein motor. Nat Cell Biol 2: 20-24.

Kirk E, Chin LS, Li L (2006) GRIF1 binds Hrs and is a new regulator of endosomal trafficking. J Cell Sci 119: 4689-4701.

Kirkpatrick LL, Witt AS, Payne HR, Shine HD, Brady ST (2001) Changes in microtubule stability and density in myelin-deficient shiverer mouse CNS axons. J Neurosci 21: 2288-2297.

Kong J, Xu Z (1999) Peripheral axotomy slows motoneuron degeneration in a transgenic mouse line expressing mutant SOD1 G93A. J Comp Neurol 412: 373-380.

Kostic V, Jackson-Lewis V, de Bilbao F, Dubois-Dauphin M, Przedborski S (1997) Bcl-2: prolonging life in a transgenic mouse model of familial amyotrophic lateral sclerosis. Science 277: 559-562.

Kraemer BC, Schuck T, Wheeler JM, Robinson LC, Trojanowski JQ, Lee VM, Schellenberg GD (2010) Loss of murine TDP-43 disrupts motor function and plays an essential role in embryogenesis. Acta Neuropathol 119: 409-419.

Kwiatkowski TJ, Jr., Bosco DA, Leclerc AL, Tamrazian E, Vanderburg CR, Russ C, Davis A, Gilchrist J, Kasarskis EJ, Munsat T, Valdmanis P, Rouleau GA, Hosler BA, Cortelli P, de Jong PJ, Yoshinaga Y, Haines JL, Pericak-Vance MA, Yan J, Ticozzi N, Siddique T, McKenna-Yasek D, Sapp PC, Horvitz HR, Landers JE, Brown RH, Jr. (2009) Mutations in the FUS/TLS gene on chromosome 16 cause familial amyotrophic lateral sclerosis. Science 323: 1205-1208.

LaMonte BH, Wallace KE, Holloway BA, Shelly SS, Ascano J, Tokito M, Van Winkle T, Howland DS, Holzbaur EL (2002) Disruption of dynein/dynactin inhibits axonal transport in motor neurons causing late-onset progressive degeneration. Neuron 34: 715-727.

Lau A, Tymianski M (2010) Glutamate receptors, neurotoxicity and neurodegeneration. Pflugers Arch 460: 525-542.

Lino MM, Schneider C, Caroni P (2002) Accumulation of SOD1 mutants in postnatal motoneurons does not cause motoneuron pathology or motoneuron disease. J Neurosci 22: 4825-4832.

Liu J, Lillo C, Jonsson PA, Vande VC, Ward CM, Miller TM, Subramaniam JR, Rothstein JD, Marklund S, Andersen PM, Brannstrom T, Gredal O, Wong PC, Williams DS, Cleveland DW (2004) Toxicity of familial ALS-linked SOD1 mutants from selective recruitment to spinal mitochondria. Neuron 43: 5-17.

Liu X, Weaver D, Shirihai O, Hajnoczky G (2009) Mitochondrial 'kiss-and-run': interplay between mitochondrial motility and fusion-fission dynamics. EMBO J 28: 3074-3089.

Macaskill AF, Brickley K, Stephenson FA, Kittler JT (2009a) GTPase dependent recruitment of Grif-1 by Miro1 regulates mitochondrial trafficking in hippocampal neurons. Mol Cell Neurosci 40: 301-312.

Macaskill AF, Kittler JT (2010) Control of mitochondrial transport and localization in neurons. Trends Cell Biol 20: 102-112.

Macaskill AF, Rinholm JE, Twelvetrees AE, Arancibia-Carcamo IL, Muir J, Fransson A, Aspenstrom P, Attwell D, Kittler JT (2009b) Miro1 is a calcium sensor for glutamate receptor-dependent localization of mitochondria at synapses. Neuron 61: 541-555.

Mackenzie IR, Bigio EH, Ince PG, Geser F, Neumann M, Cairns NJ, Kwong LK, Forman MS, Ravits J, Stewart H, Eisen A, McClusky L, Kretzschmar HA, Monoranu CM, Highley JR, Kirby J, Siddique T, Shaw PJ, Lee VM, Trojanowski JQ (2007) Pathological TDP-43 distinguishes sporadic amyotrophic lateral sclerosis from amyotrophic lateral sclerosis with SOD1 mutations. Ann Neurol 61: 427-434.

Madisen L, Zwingman TA, Sunkin SM, Oh SW, Zariwala HA, Gu H, Ng LL, Palmiter RD, Hawrylycz MJ, Jones AR, Lein ES, Zeng H (2010) A robust and high-throughput Cre reporting and characterization system for the whole mouse brain. Nat Neurosci 13: 133-140.

Magrane J, Manfredi G (2009) Mitochondrial function, morphology, and axonal transport in amyotrophic lateral sclerosis. Antioxid Redox Signal 11: 1615-1626.

Magrane J, Sahawneh MA, Przedborski S, Estevez AG, Manfredi G (2012) Mitochondrial dynamics and bioenergetic dysfunction is associated with synaptic alterations in mutant SOD1 motor neurons. J Neurosci 32: 229-242.

Manfredi G, Xu Z (2005) Mitochondrial dysfunction and its role in motor neuron degeneration in ALS. Mitochondrion 5: 77-87.

Mantilla CB, Zhan WZ, Sieck GC (2009) Retrograde labeling of phrenic motoneurons by intrapleural injection. J Neurosci Methods 182: 244-249.

Marinkovic, P., Godinho, L., and Misgeld, T. Generation and Screening of Mice with Transgenic Neuronal Labeling Controlled by Thy1 Regulatory Elements. Imaging in Neuroscience: A Laboratory Manual . 2011. Ref Type: In Press

Mariotti R, Cristino L, Bressan C, Boscolo S, Bentivoglio M (2002) Altered reaction of facial motoneurons to axonal damage in the presymptomatic phase of a murine model of familial amyotrophic lateral sclerosis. Neuroscience 115: 331-335.

Mesnard NA, Sanders VM, Jones KJ (2011) Differential gene expression in the axotomized facial motor nucleus of pre-symptomatic SOD1 mice. J Comp Neurol.

Miller KE, Sheetz MP (2004) Axonal mitochondrial transport and potential are correlated. J Cell Sci 117: 2791-2804.

Miller RG, Munsat TL, Swash M, Brooks BR (1999) Consensus guidelines for the design and implementation of clinical trials in ALS. World Federation of Neurology committee on Research. J Neurol Sci 169: 2-12.

Mironov SL (2007) ADP regulates movements of mitochondria in neurons. Biophys J 92: 2944-2952.

Misgeld T, Kerschensteiner M, Bareyre FM, Burgess RW, Lichtman JW (2007) Imaging axonal transport of mitochondria in vivo. Nat Methods 4: 559-561.

Morfini G, Szebenyi G, Elluru R, Ratner N, Brady ST (2002) Glycogen synthase kinase 3 phosphorylates kinesin light chains and negatively regulates kinesin-based motility. EMBO J 21: 281-293.

Nangaku M, Sato-Yoshitake R, Okada Y, Noda Y, Takemura R, Yamazaki H, Hirokawa N (1994) KIF1B, a novel microtubule plus end-directed monomeric motor protein for transport of mitochondria. Cell 79: 1209-1220.

Nikic I, Merkler D, Sorbara C, Brinkoetter M, Kreutzfeldt M, Bareyre FM, Bruck W, Bishop D, Misgeld T, Kerschensteiner M (2011) A reversible form of axon damage in experimental autoimmune encephalomyelitis and multiple sclerosis. Nat Med 17: 495-499.

Nishimura AL, Mitne-Neto M, Silva HC, Richieri-Costa A, Middleton S, Cascio D, Kok F, Oliveira JR, Gillingwater T, Webb J, Skehel P, Zatz M (2004) A mutation in the vesicle-trafficking protein VAPB causes late-onset spinal muscular atrophy and amyotrophic lateral sclerosis. Am J Hum Genet 75: 822-831.

Oberheim NA, Goldman SA, Nedergaard M (2012) Heterogeneity of astrocytic form and function. Methods Mol Biol 814: 23-45.

Ohno N, Kidd GJ, Mahad D, Kiryu-Seo S, Avishai A, Komuro H, Trapp BD (2011) Myelination and axonal electrical activity modulate the distribution and motility of mitochondria at CNS nodes of Ranvier. J Neurosci 31: 7249-7258.

Perlson E, Jeong GB, Ross JL, Dixit R, Wallace KE, Kalb RG, Holzbaur EL (2009) A switch in retrograde signaling from survival to stress in rapid-onset neurodegeneration. J Neurosci 29: 9903-9917.

Pilling AD, Horiuchi D, Lively CM, Saxton WM (2006) Kinesin-1 and Dynein are the primary motors for fast transport of mitochondria in Drosophila motor axons. Mol Biol Cell 17: 2057-2068.

Pramatarova A, Laganiere J, Roussel J, Brisebois K, Rouleau GA (2001) Neuron-specific expression of mutant superoxide dismutase 1 in transgenic mice does not lead to motor impairment. J Neurosci 21: 3369-3374.

Puls I, Jonnakuty C, LaMonte BH, Holzbaur EL, Tokito M, Mann E, Floeter MK, Bidus K, Drayna D, Oh SJ, Brown RH, Jr., Ludlow CL, Fischbeck KH (2003) Mutant dynactin in motor neuron disease. Nat Genet 33: 455-456.

Pun S, Santos AF, Saxena S, Xu L, Caroni P (2006) Selective vulnerability and pruning of phasic motoneuron axons in motoneuron disease alleviated by CNTF. Nat Neurosci 9: 408-419.

Qureshi MM, Hayden D, Urbinelli L, Ferrante K, Newhall K, Myers D, Hilgenberg S, Smart R, Brown RH, Cudkowicz ME (2006) Analysis of factors that modify susceptibility and rate of progression in amyotrophic lateral sclerosis (ALS). Amyotroph Lateral Scler 7: 173-182.

Reid E, Kloos M, Ashley-Koch A, Hughes L, Bevan S, Svenson IK, Graham FL, Gaskell PC, Dearlove A, Pericak-Vance MA, Rubinsztein DC, Marchuk DA (2002) A kinesin heavy chain (KIF5A) mutation in hereditary spastic paraplegia (SPG10). Am J Hum Genet 71: 1189-1194.

Ringholz GM, Appel SH, Bradshaw M, Cooke NA, Mosnik DM, Schulz PE (2005) Prevalence and patterns of cognitive impairment in sporadic ALS. Neurology 65: 586-590.

Riviere JB, Ramalingam S, Lavastre V, Shekarabi M, Holbert S, Lafontaine J, Srour M, Merner N, Rochefort D, Hince P, Gaudet R, Mes-Masson AM, Baets J, Houlden H, Brais B, Nicholson GA, Van Esch H, Nafissi S, De Jonghe P, Reilly MM, Timmerman V, Dion PA, Rouleau GA (2011) KIF1A, an axonal transporter of synaptic vesicles, is mutated in hereditary sensory and autonomic neuropathy type 2. Am J Hum Genet 89: 219-230.

Rosen DR, Siddique T, Patterson D, Figlewicz DA, Sapp P, Hentati A, Donaldson D, Goto J, O'Regan JP, Deng HX, . (1993) Mutations in Cu/Zn superoxide dismutase gene are associated with familial amyotrophic lateral sclerosis. Nature 362: 59-62.

Rothstein JD (2009) Current hypotheses for the underlying biology of amyotrophic lateral sclerosis. Ann Neurol 65 Suppl 1: S3-S9.

Rothstein JD, Martin LJ, Kuncl RW (1992) Decreased glutamate transport by the brain and spinal cord in amyotrophic lateral sclerosis. N Engl J Med 326: 1464-1468.

Rothstein JD, Van Kammen M, Levey AI, Martin LJ, Kuncl RW (1995) Selective loss of glial glutamate transporter GLT-1 in amyotrophic lateral sclerosis. Ann Neurol 38: 73-84.

Santos-Reboucas CB, Pimentel MM (2007) Implication of abnormal epigenetic patterns for human diseases. Eur J Hum Genet 15: 10-17.

Sasaki S, Iwata M (1996) Ultrastructural study of synapses in the anterior horn neurons of patients with amyotrophic lateral sclerosis. Neurosci Lett 204: 53-56.

Schaefer AM, Sanes JR, Lichtman JW (2005) A compensatory subpopulation of motor neurons in a mouse model of amyotrophic lateral sclerosis. J Comp Neurol 490: 209-219.

Schwarzer C, Barnikol-Watanabe S, Thinnes FP, Hilschmann N (2002) Voltage-dependent anion-selective channel (VDAC) interacts with the dynein light chain Tctex1 and the heat-shock protein PBP74. Int J Biochem Cell Biol 34: 1059-1070.

Shan X, Chiang PM, Price DL, Wong PC (2010) Altered distributions of Gemini of coiled bodies and mitochondria in motor neurons of TDP-43 transgenic mice. Proc Natl Acad Sci U S A 107: 16325-16330.

Sharp PS, Dick JR, Greensmith L (2005) The effect of peripheral nerve injury on disease progression in the SOD1(G93A) mouse model of amyotrophic lateral sclerosis. Neuroscience 130: 897-910.

Sheng ZH, Cai Q (2012) Mitochondrial transport in neurons: impact on synaptic homeostasis and neurodegeneration. Nat Rev Neurosci 13: 77-93.

Shi P, Strom AL, Gal J, Zhu H (2010) Effects of ALS-related SOD1 mutants on dynein- and KIF5-mediated retrograde and anterograde axonal transport. Biochim Biophys Acta 1802: 707-716.

Shibata N (2001) Transgenic mouse model for familial amyotrophic lateral sclerosis with superoxide dismutase-1 mutation. Neuropathology 21: 82-92.

Shogomori H, Futerman AH (2001) Cholera toxin is found in detergent-insoluble rafts/domains at the cell surface of hippocampal neurons but is internalized via a raft-independent mechanism. J Biol Chem 276: 9182-9188.

Spillantini MG, Crowther RA, Jakes R, Hasegawa M, Goedert M (1998) alpha-Synuclein in filamentous inclusions of Lewy bodies from Parkinson's disease and dementia with lewy bodies. Proc Natl Acad Sci U S A 95: 6469-6473.

Sreedharan J, Blair IP, Tripathi VB, Hu X, Vance C, Rogelj B, Ackerley S, Durnall JC, Williams KL, Buratti E, Baralle F, de Belleroche J, Mitchell JD, Leigh PN, Al Chalabi A, Miller CC, Nicholson G, Shaw CE (2008) TDP-43 mutations in familial and sporadic amyotrophic lateral sclerosis. Science 319: 1668-1672.

Stamer K, Vogel R, Thies E, Mandelkow E, Mandelkow EM (2002) Tau blocks traffic of organelles, neurofilaments, and APP vesicles in neurons and enhances oxidative stress. J Cell Biol 156: 1051-1063.

Steffan JS, Agrawal N, Pallos J, Rockabrand E, Trotman LC, Slepko N, Illes K, Lukacsovich T, Zhu YZ, Cattaneo E, Pandolfi PP, Thompson LM, Marsh JL (2004) SUMO modification of Huntingtin and Huntington's disease pathology. Science 304: 100-104.

Stepanova T, Slemmer J, Hoogenraad CC, Lansbergen G, Dortland B, De Zeeuw CI, Grosveld F, van Cappellen G, Akhmanova A, Galjart N (2003) Visualization of microtubule growth in cultured neurons via the use of EB3-GFP (end-binding protein 3-green fluorescent protein). J Neurosci 23: 2655-2664.

Stokin GB, Lillo C, Falzone TL, Brusch RG, Rockenstein E, Mount SL, Raman R, Davies P, Masliah E, Williams DS, Goldstein LS (2005) Axonopathy and transport deficits early in the pathogenesis of Alzheimer's disease. Science 307: 1282-1288.

Subramaniam JR, Lyons WE, Liu J, Bartnikas TB, Rothstein J, Price DL, Cleveland DW, Gitlin JD, Wong PC (2002) Mutant SOD1 causes motor neuron disease independent of copper chaperone-mediated copper loading. Nat Neurosci 5: 301-307.

Sun MG, Williams J, Munoz-Pinedo C, Perkins GA, Brown JM, Ellisman MH, Green DR, Frey TG (2007) Correlated three-dimensional light and electron microscopy reveals transformation of mitochondria during apoptosis. Nat Cell Biol 9: 1057-1065.

Szebenyi G, Morfini GA, Babcock A, Gould M, Selkoe K, Stenoien DL, Young M, Faber PW, MacDonald ME, McPhaul MJ, Brady ST (2003) Neuropathogenic forms of huntingtin and androgen receptor inhibit fast axonal transport. Neuron 40: 41-52.

Tanaka K, Sugiura Y, Ichishita R, Mihara K, Oka T (2011) KLP6: a newly identified kinesin that regulates the morphology and transport of mitochondria in neuronal cells. J Cell Sci 124: 2457-2465.

Tanaka Y, Kanai Y, Okada Y, Nonaka S, Takeda S, Harada A, Hirokawa N (1998) Targeted disruption of mouse conventional kinesin heavy chain, kif5B, results in abnormal perinuclear clustering of mitochondria. Cell 93: 1147-1158.

Terada S, Kinjo M, Aihara M, Takei Y, Hirokawa N (2010) Kinesin-1/Hsc70-dependent mechanism of slow axonal transport and its relation to fast axonal transport. EMBO J 29: 843-854.

Thevenaz P, Ruttimann UE, Unser M (1998) A pyramid approach to subpixel registration based on intensity. IEEE Trans Image Process 7: 27-41.

Tollervey JR, Curk T, Rogelj B, Briese M, Cereda M, Kayikci M, Konig J, Hortobagyi T, Nishimura AL, Zupunski V, Patani R, Chandran S, Rot G, Zupan B, Shaw CE, Ule J (2011) Characterizing the RNA targets and position-dependent splicing regulation by TDP-43. Nat Neurosci 14: 452-458.

Trinczek B, Ebneth A, Mandelkow EM, Mandelkow E (1999) Tau regulates the attachment/detachment but not the speed of motors in microtubule-dependent transport of single vesicles and organelles. J Cell Sci 112 (Pt 14): 2355-2367.

Tummala H, Jung C, Tiwari A, Higgins CM, Hayward LJ, Xu Z (2005) Inhibition of chaperone activity is a shared property of several Cu,Zn-superoxide dismutase mutants that cause amyotrophic lateral sclerosis. J Biol Chem 280: 17725-17731.

Umemori H, Linhoff MW, Ornitz DM, Sanes JR (2004) FGF22 and its close relatives are presynaptic organizing molecules in the mammalian brain. Cell 118: 257-270.

Vale RD, Reese TS, Sheetz MP (1985) Identification of a novel force-generating protein, kinesin, involved in microtubule-based motility. Cell 42: 39-50.

Van Damme P, Bogaert E, Dewil M, Hersmus N, Kiraly D, Scheveneels W, Bockx I, Braeken D, Verpoorten N, Verhoeven K, Timmerman V, Herijgers P, Callewaert G, Carmeliet P, Van Den BL, Robberecht W (2007) Astrocytes regulate GluR2 expression in motor neurons and their vulnerability to excitotoxicity. Proc Natl Acad Sci U S A 104: 14825-14830.

Van Damme P, Van Den BL, Van Houtte E, Callewaert G, Robberecht W (2002) GluR2-dependent properties of AMPA receptors determine the selective vulnerability of motor neurons to excitotoxicity. J Neurophysiol 88: 1279-1287.

Vance C, Rogelj B, Hortobagyi T, De Vos KJ, Nishimura AL, Sreedharan J, Hu X, Smith B, Ruddy D, Wright P, Ganesalingam J, Williams KL, Tripathi V, Al Saraj S, Al Chalabi A, Leigh PN, Blair IP, Nicholson G, de Belleroche J, Gallo JM, Miller CC, Shaw CE (2009) Mutations in FUS, an RNA processing protein, cause familial amyotrophic lateral sclerosis type 6. Science 323: 1208-1211.

Vande VC, McDonald KK, Boukhedimi Y, McAlonis-Downes M, Lobsiger CS, Bel HS, Zandona A, Julien JP, Shah SB, Cleveland DW (2011) Misfolded SOD1 associated with motor neuron mitochondria alters mitochondrial shape and distribution prior to clinical onset. PLoS ONE 6: e22031.

Vucic S, Cheah BC, Yiannikas C, Kiernan MC (2011) Cortical excitability distinguishes ALS from mimic disorders. Clin Neurophysiol 122: 1860-1866.

Vucic S, Kiernan MC (2006) Axonal excitability properties in amyotrophic lateral sclerosis. Clin Neurophysiol 117: 1458-1466.

Vucic S, Kiernan MC (2010) Upregulation of persistent sodium conductances in familial ALS. J Neurol Neurosurg Psychiatry 81: 222-227.

Vukosavic S, Stefanis L, Jackson-Lewis V, Guegan C, Romero N, Chen C, Dubois-Dauphin M, Przedborski S (2000) Delaying caspase activation by Bcl-2: A clue to disease retardation in a transgenic mouse model of amyotrophic lateral sclerosis. J Neurosci 20: 9119-9125.

Wang J, Farr GW, Zeiss CJ, Rodriguez-Gil DJ, Wilson JH, Furtak K, Rutkowski DT, Kaufman RJ, Ruse CI, Yates JR, III, Perrin S, Feany MB, Horwich AL (2009) Progressive aggregation despite chaperone associations of a mutant SOD1-YFP in transgenic mice that develop ALS. Proc Natl Acad Sci U S A 106: 1392-1397.

Wang J, Slunt H, Gonzales V, Fromholt D, Coonfield M, Copeland NG, Jenkins NA, Borchelt DR (2003) Copper-binding-site-null SOD1 causes ALS in transgenic mice: aggregates of non-native SOD1 delineate a common feature. Hum Mol Genet 12: 2753-2764.

Wang L, Ho CL, Sun D, Liem RK, Brown A (2000) Rapid movement of axonal neurofilaments interrupted by prolonged pauses. Nat Cell Biol 2: 137-141.

Wang S, Melhem ER, Poptani H, Woo JH (2011a) Neuroimaging in amyotrophic lateral sclerosis. Neurotherapeutics 8: 63-71.

Wang X, Schwarz TL (2009) The mechanism of Ca2+ -dependent regulation of kinesin-mediated mitochondrial motility. Cell 136: 163-174.

Wang X, Winter D, Ashrafi G, Schlehe J, Wong YL, Selkoe D, Rice S, Steen J, LaVoie MJ, Schwarz TL (2011b) PINK1 and Parkin target Miro for phosphorylation and degradation to arrest mitochondrial motility. Cell 147: 893-906.

Wang Y, Pan Y, Price A, Martin LJ (2011c) Generation and characterization of transgenic mice expressing mitochondrial targeted red fluorescent protein selectively in neurons: modeling mitochondriopathy in excitotoxicity and amyotrophic lateral sclerosis. Mol Neurodegener 6: 75.

Watanabe M, Dykes-Hoberg M, Culotta VC, Price DL, Wong PC, Rothstein JD (2001) Histological evidence of protein aggregation in mutant SOD1 transgenic mice and in amyotrophic lateral sclerosis neural tissues. Neurobiol Dis 8: 933-941.

Wegorzewska I, Bell S, Cairns NJ, Miller TM, Baloh RH (2009) TDP-43 mutant transgenic mice develop features of ALS and frontotemporal lobar degeneration. Proc Natl Acad Sci U S A 106: 18809-18814.

Weisiger RA, Fridovich I (1973) Superoxide dismutase. Organelle specificity. J Biol Chem 248: 3582-3592.

Williamson TL, Cleveland DW (1999) Slowing of axonal transport is a very early event in the toxicity of ALS-linked SOD1 mutants to motor neurons. Nat Neurosci 2: 50-56.

Wils H, Kleinberger G, Janssens J, Pereson S, Joris G, Cuijt I, Smits V, Ceuterick-de Groote C, Van Broeckhoven C, Kumar-Singh S (2010) TDP-43 transgenic mice develop spastic paralysis and neuronal inclusions characteristic of ALS and frontotemporal lobar degeneration. Proc Natl Acad Sci U S A 107: 3858-3863.

Wong PC, Pardo CA, Borchelt DR, Lee MK, Copeland NG, Jenkins NA, Sisodia SS, Cleveland DW, Price DL (1995) An adverse property of a familial ALS-linked SOD1 mutation causes motor neuron disease characterized by vacuolar degeneration of mitochondria. Neuron 14: 1105-1116.

Xu YF, Gendron TF, Zhang YJ, Lin WL, D'Alton S, Sheng H, Casey MC, Tong J, Knight J, Yu X, Rademakers R, Boylan K, Hutton M, McGowan E, Dickson DW, Lewis J, Petrucelli L (2010) Wild-type human TDP-43 expression causes TDP-43 phosphorylation, mitochondrial aggregation, motor deficits, and early mortality in transgenic mice. J Neurosci 30: 10851-10859.

Zhang CL, Ho PL, Kintner DB, Sun D, Chiu SY (2010) Activity-dependent regulation of mitochondrial motility by calcium and Na/K-ATPase at nodes of Ranvier of myelinated nerves. J Neurosci 30: 3555-3566.

Zhu YB, Sheng ZH (2011) Increased axonal mitochondrial mobility does not slow ALS-like disease in mutant SOD1 mice. J Biol Chem.